ISTANBUL TECHNICAL UNIVERSITY ★ GRADUATE SCHOOL

THE EFFECT OF DIFFERENT ADDITION RATIO OF RARE EARTH ELEMENT ERBIUM AND EUROPIUM ON MICROSTRUCTURE AND MECHANICAL PROPERTIES OF A356 (Al-7Si-0.3Mg) ALLOY

M.Sc. THESIS

Hayati ŞAHİN

Metallurgy and Materials Engineering Department

Production Metallurgy and Technologies Engineering Programme

DECEMBER 2022

ISTANBUL TECHNICAL UNIVERSITY ★ GRADUATE SCHOOL

THE EFFECT OF DIFFERENT ADDITION RATIO OF RARE EARTH ELEMENT ERBIUM AND EUROPIUM ON MICROSTRUCTURE AND MECHANICAL PROPERTIES OF A356 (Al-7Si-0.3Mg) ALLOY

M.Sc. THESIS

Hayati ŞAHİN
(506181221)

Metallurgy and Materials Engineering Department

Production Metallurgy and Technologies Engineering Programme

Thesis Advisor: Assoc. Prof. Dr. Derya DIŞPINAR

DECEMBER 2022

<u>ISTANBUL TEKNİK ÜNİVERSİTESİ ★ LİSANSÜSTÜ EĞİTİM ENSTİTÜSÜ</u>

NADİR TOPRAK ELEMENTİ ERBİUM VE EUROPYUM'UN FARKLI İLAVE ORANLARININ A356 (Al-7Si-0.3Mg) ALAŞIMININ MİKROYAPI VE MEKANİK ÖZELLİKLERİ ÜZERİNDEKİ ETKİSİ

YÜKSEK LİSANS TEZİ

Hayati ŞAHİN
(506181221)

Metalurji ve Malzeme Mühendisliği Anabilim Dalı

Üretim Metalurjisi ve Teknolojileri Mühendisliği Programı

Tez Danışmanı: Doç. Dr. Derya DIŞPINAR

ARALIK 2022

Hayati ŞAHİN, a M.Sc. student of İTU Graduate School student ID 506181221, successfully defended the thesis/dissertation entitled "THE EFFECT OF DIFFERENT ADDITION RATIO OF RARE EARTH ELEMENT ERBIUM AND EUROPIUM ON MICROSTRUCTURE AND MECHANICAL PROPERTIES OF A356 (Al-7Si-0.3Mg) ALLOY", which he prepared after fulfilling the requirements specified in the associated legislations, before the jury whose signatures are below.

Thesis Advisor :	**Assoc. Prof. Dr. Derya DIŞPINAR** İstanbul Technical University	....
Jury Members :	**Asst. Prof. Cevat Fahir AKSOY** Istanbul Technical University	....
	Assoc. Prof. Dr. Ahmet TURAN Yeditepe University	....

Date of Submission : 6 December 2022
Date of Defense : 14 December 2022

To faithful humans…

FOREWORD

It can be assumed that the foundryman were rude people as a result of their hard work and working conditions. In fact, like the sculptor who shapes the marble, the foundryman who shape the metal are also artists. Maybe that's why we don't have a heart of stone. If you want to melt it, just go above 660ºC.

I would like to express my endless thanks to my beloved family, who always supported me without losing their faith in me during my most difficult times. I don't know where to start with my thanks to Mr. Derya DIŞPINAR. Apart from our professional life, which we continue as first my lecturer, then my consultant, my project manager and now my boss. I take great pleasure in presenting him with endless love and respect as he is my friend, brother and even my closest friend, who has never spared his moral and material support. I learned a lot from him in both business and private life, I am learning and I will continue to learn. Hope to work together for many more years. Thanks to my numerous friends and colleagues who have helped me experience the positive and negative aspects of life.

Finally, since the first day I joined the Istanbul Technical University, I am glad to graduate from this institution, where warm welcomes, free from conflict and jealousy, a helpful and peaceful environment where everyone is interested in their own business. I am very happy that the dear ITU family gave me the opportunity to experience their wonderful culture.

Tot Ziens…

December 2022

Hayati ŞAHİN
(Metallurgy and Materials Engineer)

TABLE OF CONTENTS

Page

ABBREVIATIONS

SDAS	: Secondary Denrite Arm Space
RPT	: Reduced Pressure Test
TPRE	: The twin-Plane Re-entrant Edge
IIT	: Impurity Induced Twinning
Er	: Erbium
Eu	: Europium
XRF	: X-ray Fluorescence
YS	: Yield Strength
UTS	: Ultimate Tensile Strength
SEM	: Scanning Electron Microscope
EDS	: Energy Eispersive X-ray Spectroscopy
MPa	: Megapascal

SYMBOLS

e **:** Percent Elongation at Fracture

^{o}C **:** Celsius

LIST OF TABLES

Page

LIST OF FIGURES

Page

THE EFFECT OF DIFFERENT ADDITION RATIO OF RARE EARTH ELEMENT ERBIUM AND EUROPIUM ON MICROSTRUCTURE AND MECHANICAL PROPERTIES OF A356 (Al-7Si-0.3Mg) ALLOY

SUMMARY

A356 (Al-7Si-0.3Mg) alloy is widely used in automotive, aerospace and defense industries due to its good specific strength, castability, corrosion resistance and weldability. The main microstructural features of Al-Si alloys are primary α-Al dendrites, secondary denrite arm space (SDAS), eutectic Si and intermetallic phases. The size and morphology of primary α-Al, the acicular and coarse plate-like structure of eutectic Si cause poor mechanical properties. α -Al grain refinement and eutectic Si modification techniques are used to improve the mechanical properties of the alloy. Alloying is widely used in industry for grain refinement and modification because of its simple handling and low cost advantages. Ti, B, and their combinations are commonly used as grain refiners, while Na and Sr are used to modify the eutectic Si. It is seen that there are more effective grain refinement and/or modification effects with the addition of rare earth elements in trace amounts. The present work investigates the optimum addition amount of Er and Eu to achieve the best mechanical properties on sand mold casting. Sand casting is one of the most traditional casting methods. It has advantages such as slower solidification and ability to mold complex parts.

Defect free casting begins with starting melt cleanliness, casting speed and well-designed runner systems. Failure of one of these three main components has a significant negative impact on the quality of part. The ASTM B108/B 108M mold is the most common mold used to obtain a tensile specimen. New mold designs were proposed in this work that would provide statistically reproducible results. Filling analyzes of the designs were made in the Anycast software. In order to evaluate the tensile test results of the samples cast with A356 alloy. T6 heat treatment was carried out, and the quality index values were calculated. The reliability of the results was evaluated using survivability plots. Considering these results, V3 mold was casted by tilt casting method in subsequent alloying castings.

Alloying additions were applied in the best mold design and casting method. The effect of adding different amounts of Er and Eu to the A356 alloy was investigated:

- 0.0
- 0.1 Er wt%
- 0.1 Er + 0.1 Eu wt%
- 0.3 Er wt%
- 0.3 Er + 0.1 Eu wt%

T6 heat treatment was applied to examine the heat treatment effect of the same addition rates. To the heat-treated and non-heat-treated samples; OES, XRF, RPT, microstructure, hardness, tensile test, microstructure and SEM tests were employed to the fractured surfaces.

Grain refinement was observed with the addition of Er, while grain coarsening was observed with the addition of Eu. However, while there is no change in the eutectic Si length with the addition of Er, a shortening is observed as the amount of Er increases. Eutectic Si is modified by the addition of Eu. The best eutectic Si aspect ratio was obtained with the addition of Eu with the heat treatment. The mechanical properties were improved with the addition of alloying elements. The best mechanical properties were obtained by heat treatment and the addition of alloying elements. The hardness value decreased with the addition of alloying elements, although the heat treatments increased. In SEM examinations, acicular Fe intermetallic phases in unalloyed structure were observed. With the addition of the alloying element, there wer acicular intermetallic phases containing Er or Er, Eu elements together in accordance with the alloying element. The frequency of intermetallic phases in the structure increased with the addition of alloying element. Although these intermetallic phases shortened after heat treatment, they could not be fully spheroidized.

NADİR TOPRAK ELEMENTİ ERBİUM VE EUROPYUM'UN FARKLI İLAVE ORANLARININ A356 (Al-7Si-0.3Mg) ALAŞIMININ MİKROYAPI VE MEKANİK ÖZELLİKLERİ ÜZERİNDEKİ ETKİSİ

ÖZET

A356 (Al-7Si-0.3Mg) alaşımı, iyi özgül mukavemet, dökülebilirlik, korozyon direnci, kaynaklanabilme özellikleri sayesinde otomotiv, havacılık ve savunma sanayinde yaygın olarak kullanılmaktadır. Ötektik altı Al-Si alaşımlarının başlıca mikroyapısal özellikleri birincil α-Al dendritleri, ikincil denrit kol aralığı (SDAS), ötektik Si ve intermetalik fazlarıdır. Birincil α-Al'nin boyutu ve morfolojisi, ötektik Si'nin iğnemsi ve kaba plaka benzeri yapısı, zayıf mekanik özelliklere sebep olur. Bu yapıların kontrol edilerek istenilen forma getirilmesiyle istenen mekanik özelliklere sahip döküm ürünleri elde etmek mümkündür. Alaşımın mekanik özelliklerini iyileştirmek için α-Al tane inceltmesi ve ötektik Si modifikasyon teknikleri kullanılır. Alaşımlama, basit kullanım ve düşük maliyet avantajları nedeniyle, endüstride tane inceltme ve modifikasyon için yaygın olarak kullanılmaktadır. Ti, B ve kombinasyonları tane inceltici olarak yaygın olarak kullanılırken, Na ve Sr ötektik Si'yi modifiye etmek için kullanılmaktadır. Nadir toprak elementlerinin çok az miktarda ilaveleriyle daha etkili tane inceltme ve/veya modifikasyon etkilerinin olduğu görülmektedir.

Kum kalıba döküm, en geleneksel döküm yöntemlerinden biridir. Daha yavaş katılaşması ve karmaşık parçaların kalıplanabilmesi gibi avantajları söz konusudur.

Bu çalışmada çekme test kalıbı olarak kullanılan ASTM B108/B 108M kalıbının tek dökümden sadece 2 adet numune üretmektedir. İstatistiksel çalışmalarda birden fazla kalıbın dökümüne ihtiyaç duyulmaktadır. Bu durumunda operatör etkisini ve döküm şartlarında (sıcaklık vb.) değişiklik olması muhtemeldir. Aynı zamanda ASTM B108/B 108M kalıbının Anycasting simülasyonuyla dolum analizi incelenmiş bu analiz sırasında kalıp tasarımında sıvı metalin birçok noktada türbülansa uğradığı görülmüştür. İyi bir nihai döküm ürünü elde etmek için iyi sıvı kalitesine sahip metalle başlamak kadar kalıp tasarımının döküm sırasında türbülans yaratmadan kalıbı türbülanssız ve yeni oksit oluşturmadan doldurması gerekmektedir. Bu nüanslar göz önünde bulundurularak farklı kalıp tasarımları ve farklı döküm yöntemleri uygulanmıştır. Kalıp tasarımlarında aynı dökümde, döküm şartları değişmeden 10 adet test silindirik test numunesi üretmek amaçlanmıştır. Simülasyon ve yapılan dökümlerle en iyi tasarımın eğerek dökme (tilt casting) yöntemiyle elde edilmiştir.

Alaşımlama ilaveleri elde edilen en iyi kalıp tasarımı ve döküm yönteminde uygulanmıştır. A356 alaşımına farklı oranlarda Er ve Eu ilavelerinin etkisi araştırılmıştır:

- 0.0
- 0.1 Er wt%
- 0.1 Er + 0.1 Eu wt%
- 0.3 Er wt%

- 0.3 Er + 0.1 Eu wt%

Aynı ilave oranlarının ısıl işlem etkisini incelemek için T6 ısıl işlemi uygulanmıştır. Elde edilen ısıl işlem görmüş ve görmemiş numunelere; OES, XRF, RPT, mikroyapı, sertlik, çekme testi, mikroyapı ve kırık yüzeylere SEM testleri uygulanmıştır.

Optical Emission Spectroscopy (OES) test sonucuyla A356 alaşımının kimyasal kompozisyonun Fe dışında standartlar içindedir. Kullanılan A356 külçeleri ikincil üretim olduğu için Fe değerleri sınır aralığından yüksektir. XRF sonucuyla, Er ve Eu alaşım elementlerinin istenen oranlarda eklendiği görülmüştür.

Sıvı metal temizliği için uygulanan gaz giderme işlemlerinden önce bifilm değeri 71 mm’dir. Gaz giderme işleminden sonra alınan Reduced Presure Test (RPT) numunelerinin kesit yüzeyleri incelenerek döküm için uygun bifilm index değerlerin olan 10 mm’den az değerlere sahip oldukları elde edilmiştir.

Mikroyapı incelemeleri için dağlandıktan sonra numunelere polarize ışık altında tane boyutları ölçümleri yapılmıştır. Isıl işlem görmemiş numunelerde ilavesiz tane boyutu 789 µm’dir. Er ilavesi tane boyutunda küçülmeye sebep olmazken Eu ilavesiyle tane kabalaşması görülmektedir En kaba tane boyutu 0.1 Er + 0.1 Eu wt% ilavesinde 1033 µm’dir. Isıl işlem görmüş numunelerde ilavesiz A356 alaşımının tane boyut ortalaması 950 µm’dir. Er ilavesiyle tane incelmesi gözlemlenirken, Eu ilavesiyle tane kabalaşması olmuştur. En ince tane değeri 0.3 Er ilavesiyle 643 µm, en kaba tane 0.1 Er + 0.1 Eu ilavesiyle 1022 µm’dir.

Ötektik Si morfolojisi incelendiğinde alaşım element ilavesi olmadan 12 µm’dir. Er ilavesiyle ötektik Si boyunda bir değişiklik olmazken Er miktarı arttıkça boyunda kısalma görülmektedir. Ama en iyi ötektik Si boyundaki etkiyi 0.1 Er + 0.1 Eu ilavesiyle 2.4 µm elde edilmiştir. Alaşımlama ilavesi olmadan 9.6 olan ötektik Si en-boy oranı alaşımlama elementlerinin ilavesiyle küçülerek daha küresel bir hale gelmiştir. Ama en iyi ötektik Si 0.1 Er + 0.1 Eu ilavesiyle 2.4 olarak bulunmuştur. T6 ısıl işlemi etkisiyle ötektik Si fazlarının boyutları ve en-boy oranı azalmıştır. Alaşım element ilavesinden önce sırasıyla 5.8 µm ve 1.9’dur. Alaşım elementlerinin ilavesiyle modifikasyon etkisi artmıştır. En iyi modifikasyon 0.1 Er + 0.1 Eu ilavesiyle elde edilmiştir (2.8 µm ve 1.2).

A356 alaşımında yapılan alaşımlama sonrasında ısıl işlemli ve ısıl işlemsiz numunelere çekme testleri uygulanmıştır. Isıl işlemsiz numunelerde alaşım element ilavesi olmadan çekme dayanımı değeri 138 MPa ve % uzaman 1.1’dir. Alaşım element ilavesiyle mekanik özellikler iyileştirilmiştir. En iyi çekme dayanımı değeri 0.1 Er ilavesiyle 177 MPa olarak elde edilirken en iyi uzama değeri 3.7 ile 0.3 Er + 0.1 Eu ilavesinde elde edilmiştir. Isıl işlem sonrası alaşımlama elementi ilavesi olmayan A356 alaşımı 228 MPa çekme dayanımı ve 0.8 % uzama değerine sahiptir. Alaşımlama elementi ilavesiyle mekanik özelliklerde iyileşmeler olmasına rağmen en iyi çekme dayanımı 0.1 Er ilavesiyle elde edilirken en iyi uzama değeri 2.4 ile 0.3 Er + 0.1 Eu ilavesinde elde edilmiştir.

Isıl işlem uygulanmış ve uygulanmamış A356 alaşımına sertlik testi yapılmıştır. Alaşımlama ilavesi olmayan ısıl işlem görmemiş numunenin sertlik değeri 11.5 HRB10’dur. Alaşım elementi ilavesiyle sertlik değerleri değişmektedir. En iyi sertlik değeri 19.5 HRB10 olarak 0.1 Er ilavesinde elde edilmiştir. Isıl işlemle alaşımsız numunenin sertliği 58.5 HRB10 olmasına rağmen alaşımlama elementinin ilavesiyle sertlik değeri sürekli azalmaktadır ve en düşük değer 0.3 Er ilavesiyle 48.5 HRB10 olarak elde edilmiştir.

SEM incelemelerinde alaşım elementi olamayan yapıda iğnemsi Fe intermetalik fazları gözlemlenmiştir. Alaşım elementinin ilavesiyle alaşım elementine uygun olarak Er veya Er, Eu elementlerini birlikte içeren iğnemsi intermetalik fazları bulunmaktadır. Alaşım elementinin ilavesiyle yapıdaki intermetalik fazlarının sıklığında artmıştır. Isıl işlem sonrası bu intermetaliklerin boyu kısalmış olmasına rağmen tam olarak küreselleştirilememiştir.

1. INTRODUCTION

In terms of classification of metals, there are two essential divisions which are “Ferrous” and “Non-Ferrous” alloys. Figure 1.1 illustrates the general overview and information of those metals. The most common pure metals physical properties are shown in Table 1.1.

Table 1.1 : Some physical features of pure metals [2].

Property	Unit	Al	Mg	Ti	Be	Fe	Cu
Atomic number	-	13	12	22	4	26	29
Relative atomic mass	-	26.982	24.305	47.90	9.012	55.847	63.546
Crystall structure	-	fcc	cph	cph	cph	bcc	fcc
a	nm	0.4041	0.3203	0.2950	0.2286	0.2866	0.3615
c	Nm	-	0.5199	0.4653	0.3583	-	-
Meltin point	ºC	660	650	1678	1289	1525	1083
Boiling point	ºC	2520	1090	3289	2472	2862	2563
Relative density (d)	-	2.70	1.74	4.51	1.85	7.87	8.96
Elastic modulus (E)	GPa	70	45	120	295	211	130
Specific modulus (E/d)	-	26	26	26	160	27	14
Mean specific heat 0-100ºC	$Jkg^{-1}K^{-1}$	917	1038	528	2052	456	386
Thermal conductivity 20-100ºC	$Wm^{-1}K^{-1}$	238	156	26	194	78	397
Coeffcient of thermal expansion 0-100ºC	$10^{-6}K^{-1}$	23.5	26.0	8.9	12.0	12.1	17.0
Electrical resistivity at 20ºC	µ.ohm.cm	2.67	4.2	54	3.3	10.1	1.69

Mechanical properties, formability, suitability for machining, weldability and resistance of corrosion are quite important in selecting an alloy. Ashby diagram gives a comparison of strength/density ratios for different materials (Figure 1.2). Table 1.2 also gives information about material indices and relative costs. This information provides essential information for the selection and application of an alloy.

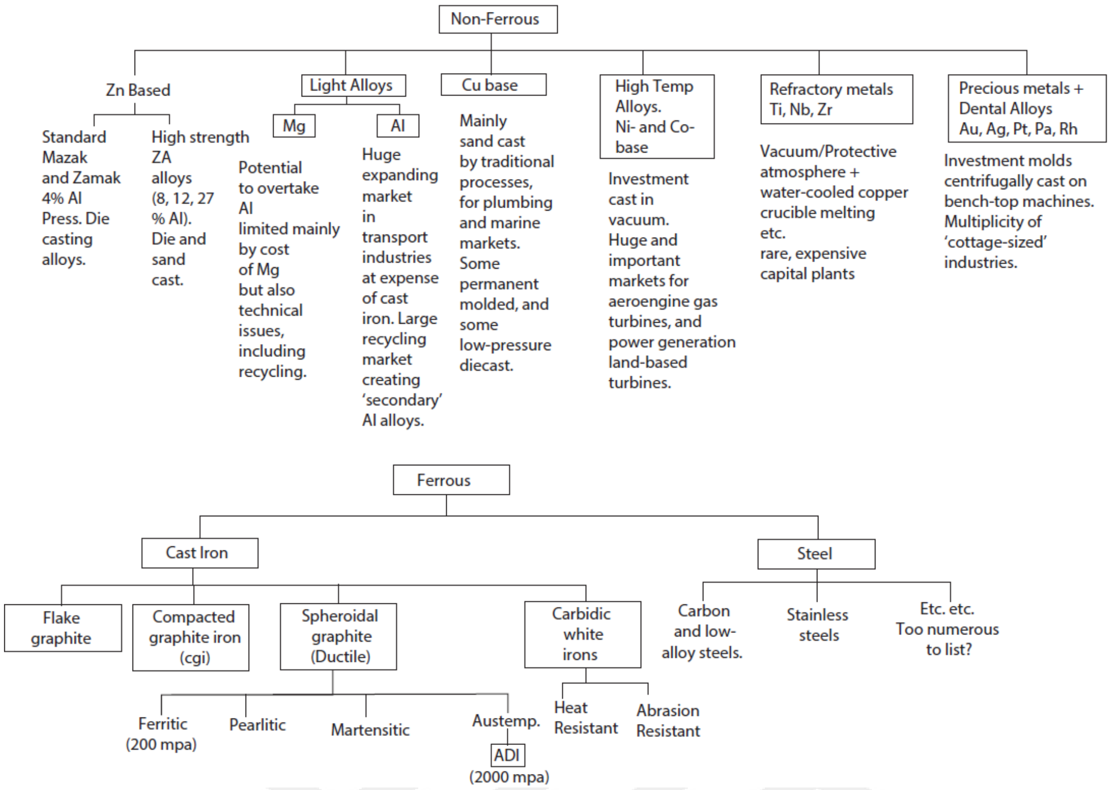

Figure 1.1 : Structure of the metal casting industry [1].

Aluminum is one of the most important non-ferrous alloys due to its high-density strength ratio, widely ways of forming ranging from casting to extrusion, highly recyclable and numerous application areas like can for drinkable products, engine for automotive or many parts of aerospace and defense industry. Table 1.3 illustrates the properties of unalloyed aluminum.

Table 1.2 : Material indexes and relative costs [3].

Material	Properties (relative values)			Material index for stiffness critical design			Material index for strength critical design		Cost of material (relative values)
	Density (ρ)	Modulus (E)	Tensile strength (S_t)	Tension $\frac{E}{\rho}$	Buckling $\frac{E^{1/2}}{\rho}$	Bending $\frac{E^{1/3}}{\rho}$	Tension $\frac{S_t}{\rho}$	Bending $\frac{S_t^{1/2}}{\rho}$	
DQ Steel	1	1	1	26.3	1.83	0.75	40.3	2.26	1
DP Steel	1	1	2.21	26.3	1.83	0.75	88.9	3.36	1.15
AA6111	0.34	0.34	1.13	25.9	3.10	1.53	133.3	7.03	4–5
Mg AZ91	0.23	0.22	0.76	25	3.73	1.97	133.3	8.6	4–5
SS304	1	0.97	1.94	25.3	1.79	0.74	77.7	3.14	6–8
High strength CFRE	0.2	0.67	4.89	89	7.58	3.33	1000	25.4	15–20
GFRE	0.23	0.19	3.04	21.1	3.37	1.83	521.6	16.8	8
SMC	0.24	0.08	0.52	8.5	2.14	1.35	87.7	6.85	1.5

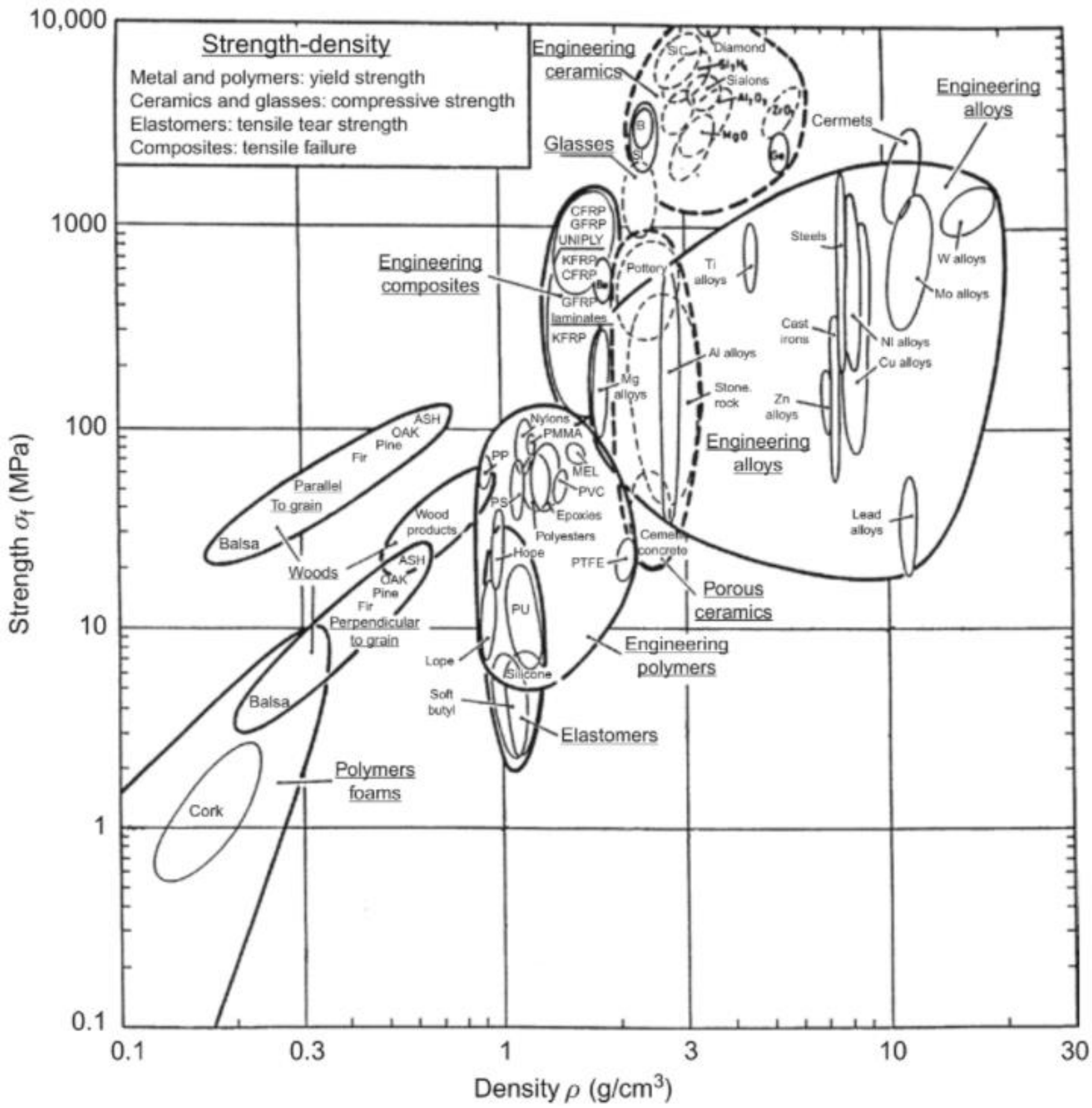

Figure 1.2 : Ashby Diagram for different materials [2].

Table 1.3 : Properties of unalloyed aluminum [4].

Property	Unit	Value	Note
Atomic number		13	
Density	kg.m^{-3}	2.698	
Melting point	ºC	660.45	<1,013 x 10^{-3} bar>
Boiling point	ºC	2056	<1,013 x 10^{-3} bar>
Vapour pressure	Pa	3.7 x 10^{-3}	At 927ºC
Massinternal energy	J.kg^{-1}	3.98 x 10^{5}	
Mass thermal capacity	J.kg^{-1}K^{-1}	897	At 25ºC
Thermal conductivity	W.m^{-1}.K^{-1}	237	At 27ºC
Linear expansion coefficient	10^{-6}K^{-1}	23.1	At 25ºC
Electrical resistivity	10^{-9} Ω.m	26.548	At 25ºC
Magnetic susceptibility		0.6 x 10^{-3}	At 25ºC
Longitudinal elastic modulus	MPa	69,000	
Poisson's ratio		0.33	

1.2 Aluminium Production

Aluminum is the second most produced metal and third most abundant material (Figure 1.3). Total metal production increased with increasing recycling production percentage, even though decreasing percentage of primary aluminum production in the last decades (Figure 1.4).

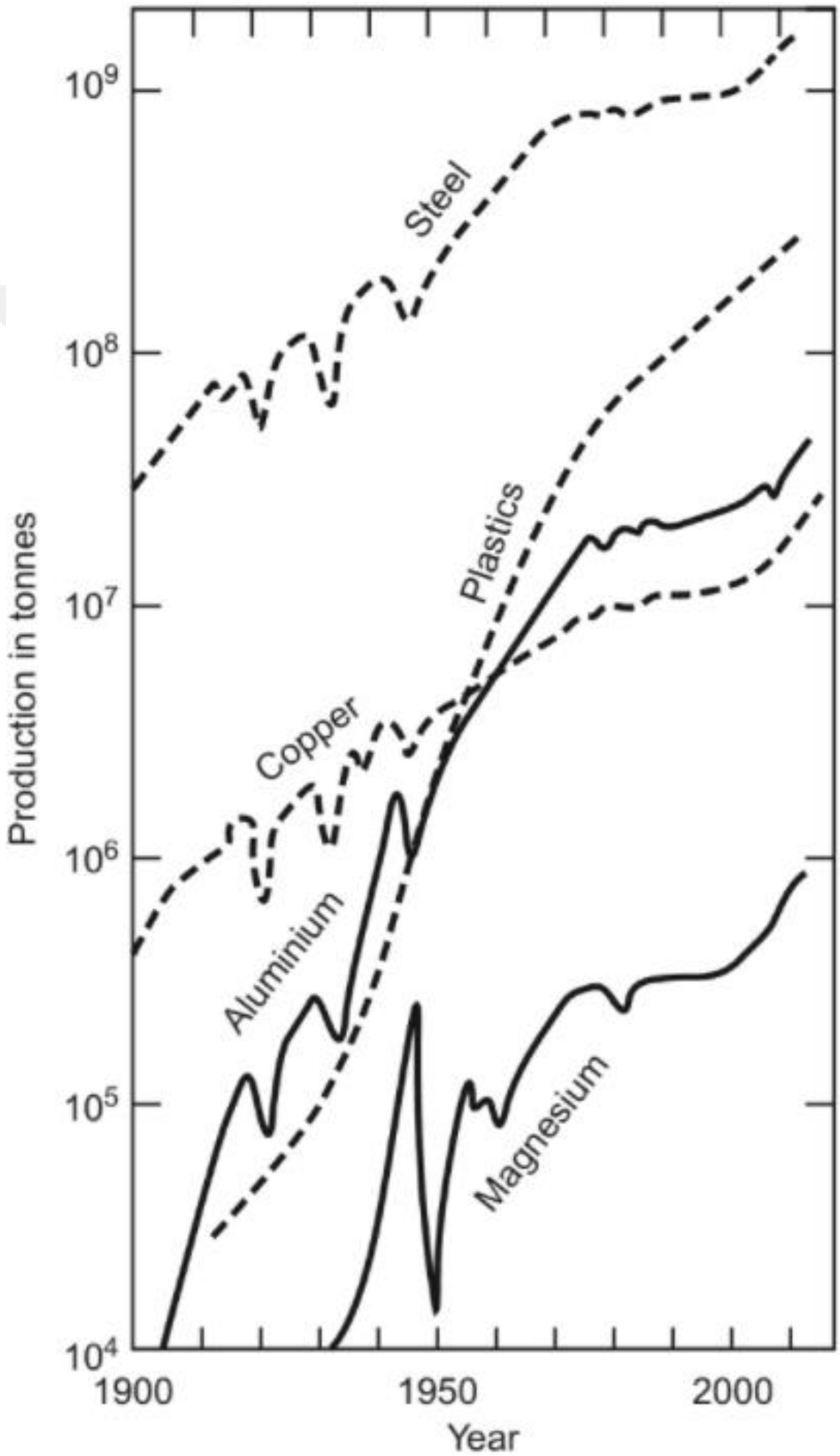

Figure 1.3 : World production numbers for different metals and plastics [1].

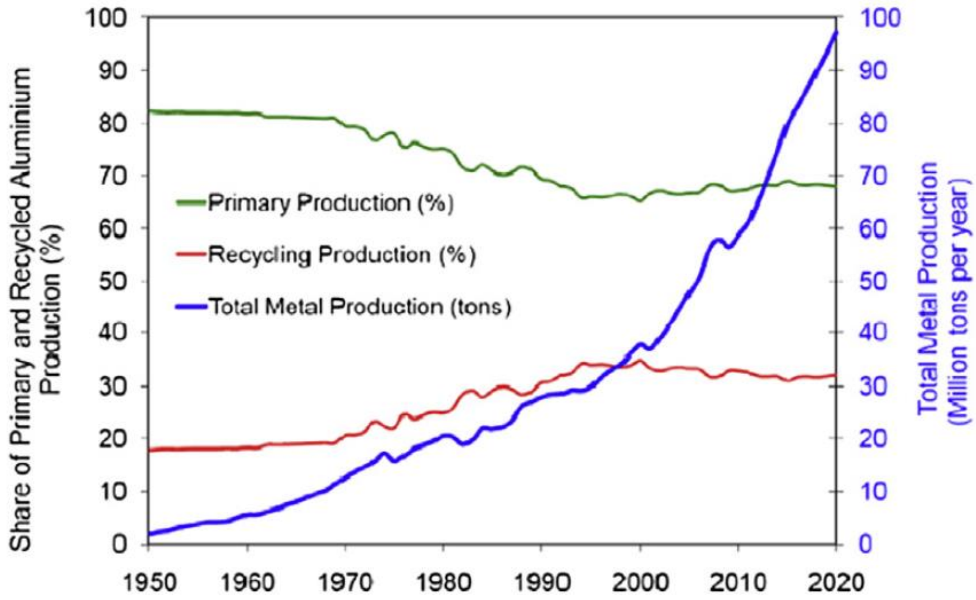

Figure 1.4 : Distribution ratios of primary and secondary production in total aluminum production [4].

Total production of non-ferrous metal casting has been dramatically increasing in Turkey in the last a few years. It was 573 10^3 ton in 2019 (Table 1.4). Figure 1.5 illustrates that producing primary aluminum was quite similar except at 2009. On the other hand, producing secondary aluminum was increasing logarithmically. This is mainly due the high recyclability of aluminum which in turn is an environmentally friendly process.

Table 1.4 : Total metal casting of non-ferrous metal in 1000 t [4].

Country	2015	2016	2017	2018	2019
Austria	140	147	148	163	144
Czech Rep.	116	119	122	124	116
France	357	362	367	441	392
Germany	1221	1248	1206	1176	1146
Italy	900	934	1000	1000	958
Poland	353	349	346	346	356
Spain	146	163	167	153	154
Turkey	380	427	440	547	573
United Kingdom	131	141	152	166	166
Total CAEF	4006	4237	4278	4495	4360

Figure 1.6 is showing the life cycle of aluminum from bauxite mineral to final products using areas which are construction, durable goods, electrical, machinery, packaging, transportation and others. About 180 metric tons bauxite is used to produce 65 metric tons alumina. Only 34 metric tons primary aluminum was gained from that alumina.

Final product was 40 metric tons and it included primary and recycled aluminum. Total 586 metric tons aluminum was used.

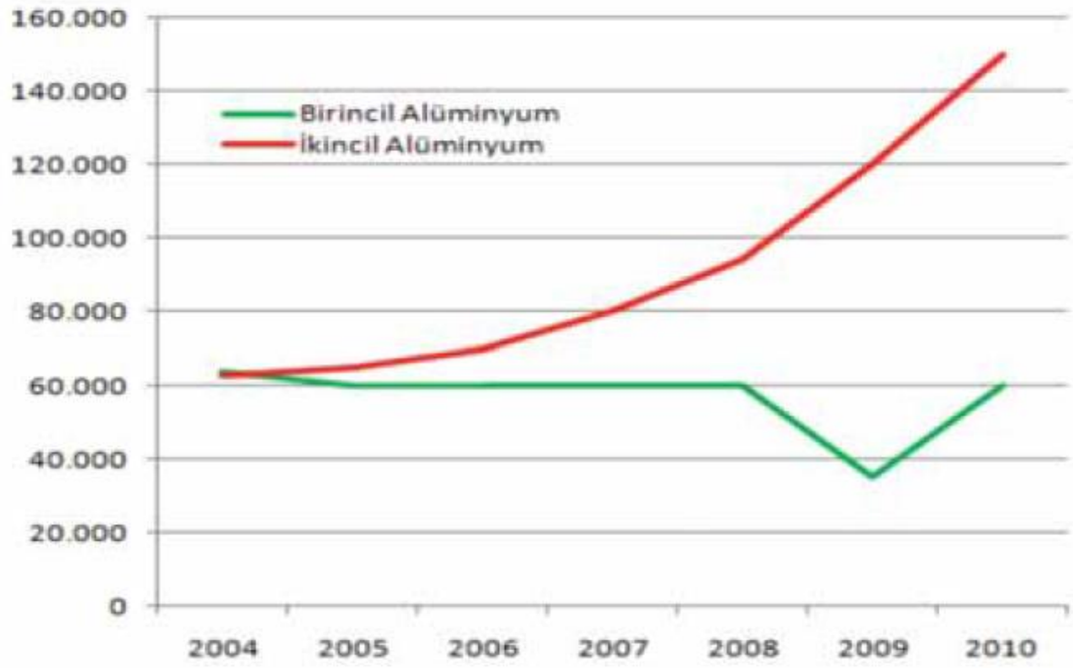

Figure 1.5 : Turkey primary and secondary aluminum production (Ton) [5].

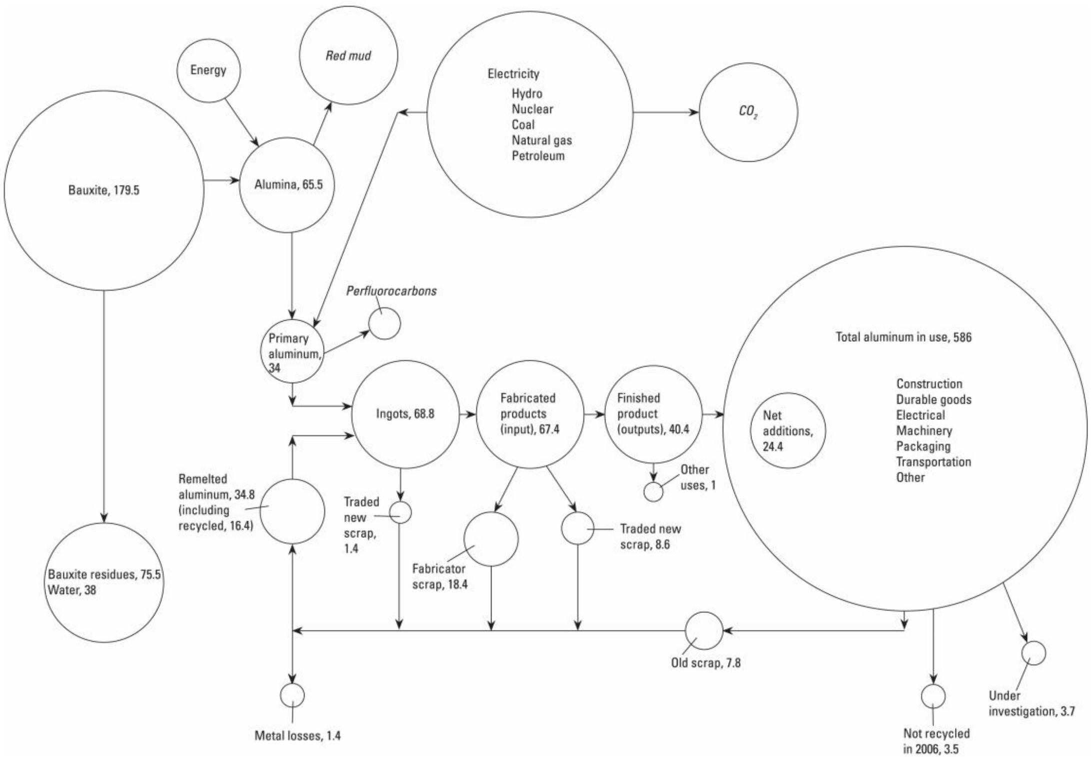

Figure 1.6 : Global life cycle of aluminum [6].

Transportation, consumers and packaging and building and construction include the main areas for consumption of aluminum (Figure 1.7)

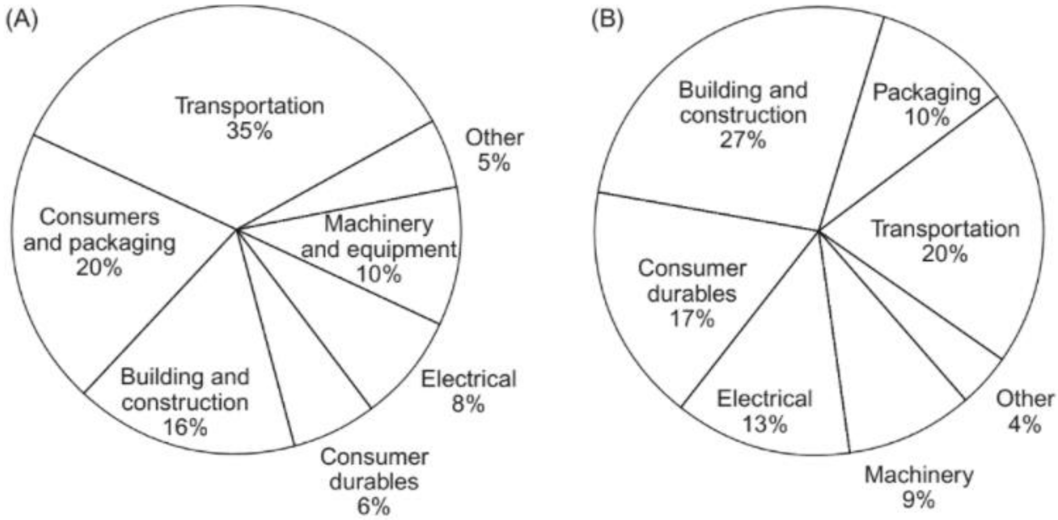

Figure 1.7 : Global aluminium consumption in (A) advanced economies and (B) emerging economies [2].

1.3 Recycling of Aluminium

Aluminum has a positive reputation of recycling. It is most recyclable metal and Figure 1.8 shows its ability, aluminum is two times better than iron/steel.

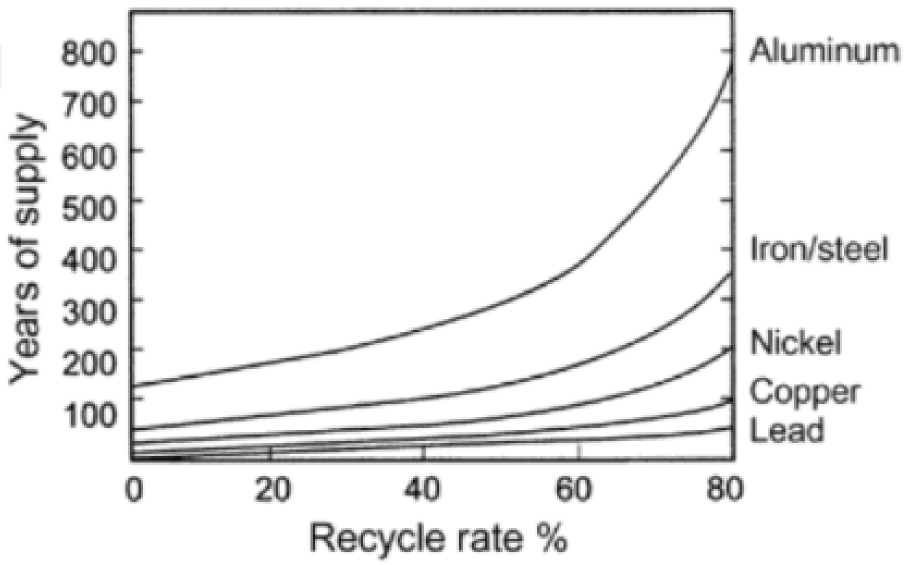

Figure 1.8 : Estimated relationship between recycling rates and remaining years of supply [2].

1.4 Classification of Aluminium

Aluminum alloys are divided into two major categories: casting alloys and wrought alloys. In addition to this, these alloys can also be classified according to their heat treatment capabilities. Figure 1.9 demonstrates the principal types of aluminum alloys.

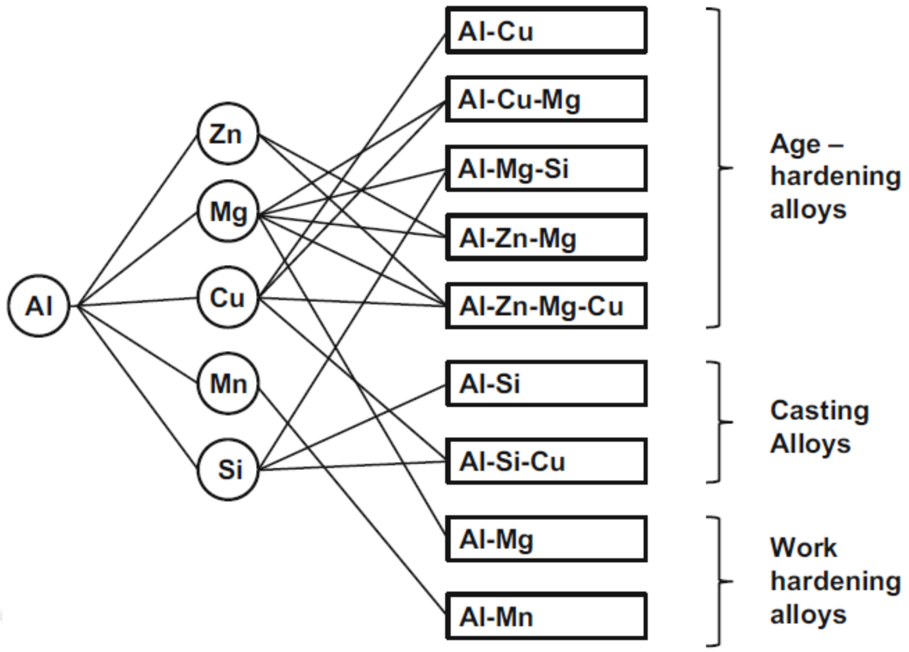

Figure 1.9 : The main types of aluminium alloys [7].

Table 1.5 : Aluminium wrought alloys [4].

Mode of hardening	Series	Alloying element	Content range (wt.%)	Additives	Tensile strength Rm (MPa)
Strain hardenable	1xxx	None		Cu	50-160
	3xxx	Manganese	0.5-1.5	Mg, Cu	100-240
	5xxx	Magnesium	0.5-5	Mn, Cr	100-340
	8xxx	Iron and silicon	Si: 0.3-1 Fe: 0.6-2		130-190
Age hardenable	6xxx	Magnesium and silicon	Mg: 0.5-1.5 Si:0.5-1.5	Cu, Cr	200-300
	2xxx	Copper	2-6	Si, Mg	300-480
	7xxx	Zinc and magnesium	Zn: 5-7 Mg: 1-2		Without Cu 320-350 With Cu 430-600

Table 1.6 : Aluminium casting alloys [4].

Alloy element	Designation	
	AA	EN1780
Unalloyed aluminium >99%	1xx.x	10000
Copper	2xx.x	20000
Silicon + magnesium and/or copper	3xx.x	40000
Silicon (binary aluminium-silicon)	4xx.x	40000
Magnesium (major allyoing element)	5xx.x	50000
Zinc (major alloying element)	7xx.x	70000

There are many different identification systems. The Aluminum Association system has three-digit system for casting alloys and four-digit system for wrought alloys. Table 1.5 and Table 1.6 list wrought alloys and casting alloys classification with the principal alloying elements.

1.5 Casting Aluminium Alloy

Chemical composition and casting proses significantly effects their mechanical properties (yield stress, tensile stress and elongation) and casting characteristics. These effects are shown in Table 1.7 in detail. The detailed chemical compositions of casting alluminum alloys shows in Table 1.8.

Table 1.7 : Compositions of casting aluminium alloys [2].

Association number	LM number	Si	Fe	Cu	Mn	Mg	Zn	Ti	Other
150.1	LM 1			0.10			0.05		99.5 Al
201.0		0.10	0.15	4.0-5.2	0.20-0.50	0.15-0.55		0.15-0.35	Ag 0.40-1.0
	LM 4	4.0-6.0	0.8	2.0-4.0	0.20-0.6	0.15	1.0	0.25	
355.0	LM 16	4.5-5.5	0.6	1.0-1.5	0.50	0.40-0.6	0.35	0.25	
356.0	LM 29	6.5-7.5	0.20	0.20	0.10	0.20-0.40	0.10	0.20	
360.0	LM 9	9.0-10.0	2.0	0.6	0.35	0.40-0.6	0.50		
380.0	LM 24	7.5-9.5	2.0	3.0-4.0		0.50	3.0		
413.0	LM 20	11.0-13-0	2.0	1.0	0.35	0.10	2.0	0.20	
520.0	LM 10	0.25	0.30	0.25	0.15	9.5-10.6	0.15	0.25	

Table 1.8 : Foundry characteristics and mechanical properties of casting aluminium alloys [2].

Association number	LM number	Fludity	Resistance of hot tearing	Corrosion resistance	Weldability	Machining
201.0		C	D	D	C	B
355.0	LM 16	B	B	C	B	C
356.0	LM 25	B	A	B	B	C
360.0	LM 9	A	A	B	B	C
413.0	LM 20	A	A	B	A	C
520.0	LM 10	D	B	A	E	B

1.6 Casting

The casting of metal is an artwork from art and science so the foundryman is a scientist and also an artist. There are many casting methods as gravity diecasting, low pressure die casting, high pressure diecasting and squeeze casting etc. There are many variables that can affect the quality of end product properties. Mold materials, pouring temperature, runner, feeders and gating design, melt treatment such as degassing or flux and inoculation of refiners and modifiers. Fig 1.10 shows different mold materials and their casting time. Different casting methods significantly effect of the microstructure and cause changes in mechanical properties. That impact clearly seen at Table 1.9 squeeze casting yield stress and tensile properties is 50% better than sand casting and elongation is five times better than sand casting [8].

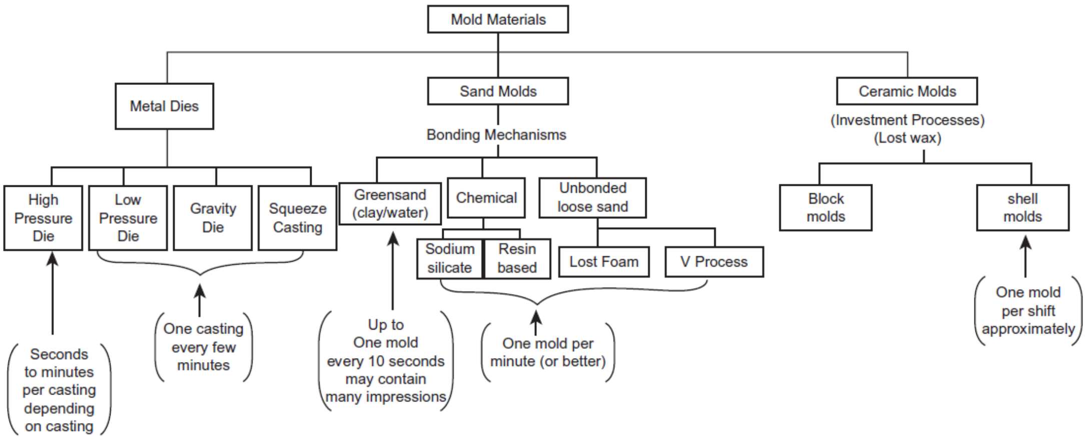

Figure 1.10 : The structure of the casting industry with molding technology [1].

Table 1.9 : Mechanical properties of A357 alloy produced by different casting methods [2].

Process	0.2% Proof stress (MPa)	Tensile strength (MPa)	Elongation (%)
Sand cast	200	226	1.6
Chill cast	248	313	6.9
Squeeze cast	283	347	9.3
Cosworth	242	312	9.8

1.7 Liquid Aluminum Cleanness

Producing final product without any defects based on two main steps. The first is the cleaning of the liquid metal before casting and the second is that it does not produce any turbulence during casting. Turbulence creates a bifilm which causes potential defects or porosity in final product.

Aluminum is located bottom part of EMF series. This is critical in physical properties where one of them is oxidation. Aluminum oxidizes so fast and it creates protective oxide layer. If it stays on the surface, it is protective, but if it becomes entrained into the melt, it generates a defect called a bifilm (Figure 1.11) . The bifilm density is quite similar to liquid aluminum and it generates a disadvantage. Due to similar density of aluminum and its oxide, it floats in liquid aluminum. It would not float to the surface nor sedimate to the bottom. These oxides must be removed in order to obtain a clean liquid metal. Degassing, flux or combination of them are used for cleaning liquid metal. Inoculation of refiners and modifiers are also potential for entrainment bifilm (Figure 1.12) so a cleaning proses should be used after alloying [8].

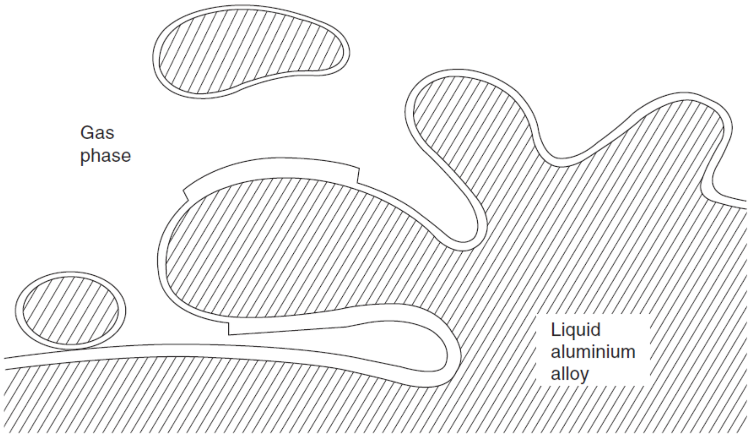

Figure 1.11 : Sketch of bifilm formation by surface turbulence [1].

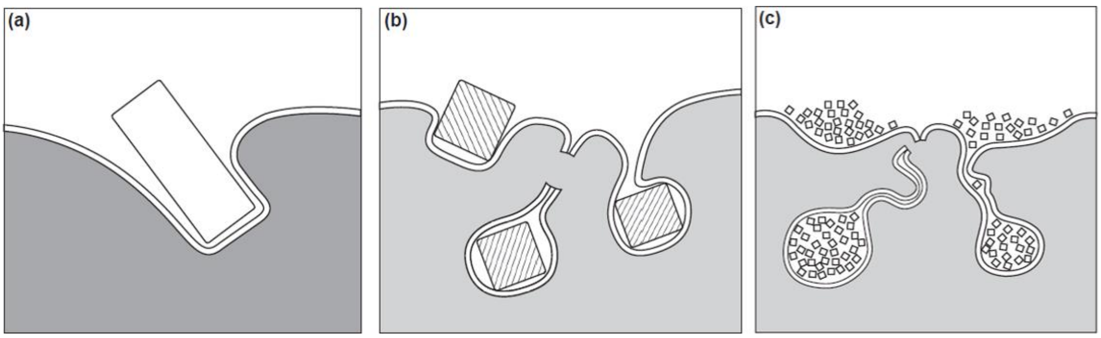

Figure 1.12 : Mixing surface oxide into liquid metal by alloying methods of different sizes (a) big (b) medium and (c) small [1].

It does not produce turbulence, contains two parts. Firstly, not to exceed critical height and velocity of liquid metal. Figure 1.13 demonstrates the liquid metal flow below and above the critical velocity. The critical height and velocities show in Table 1.10.

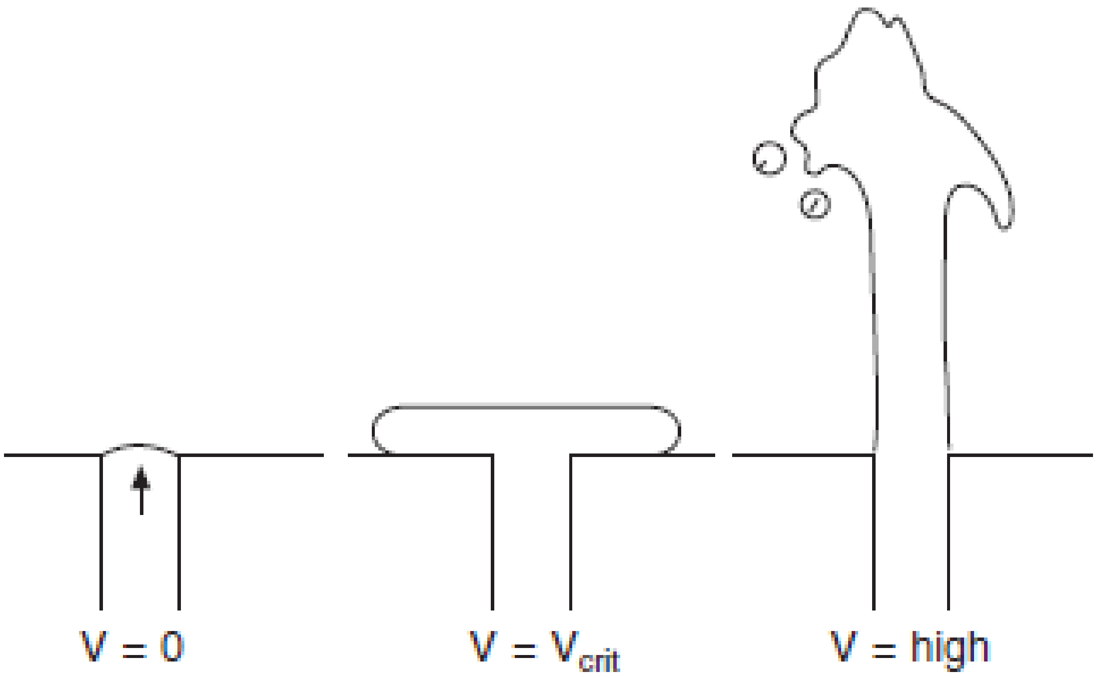

Figure 1.13 : Liquid metal flow at different speeds [1].

Table 1.10 : The critical velocities and height of some liquid metals [1].

Liquid	Density (kgm^{-3})	Surface Tension (Nm^{-1})	Critical Height h (mm)	Critical Velocity (ms^{-1})
Ti	4110	1.65	12.8	0.50
Al	2385	0.914	12.5	0.50
Mg	1590	0.559	16.0	0.42
Fe	7015	1.872	10.4	0.45
Ni	7905	1.778	9.6	0.43
Cu	8000	1.285	8.1	0.40
Zn	6575	0.782	7.0	0.37
Pt	19,000	1.8	6.2	0.35
Au	17,360	1.14	5.2	0.32
Pb	10,678	0.468	4.2	0.29
Hg	13,691	0.498	3.9	0.27
Water	1000	0.072	5.4	0.33

Even though liquid metal flow does not exceed the critical velocity, if mold design is not appropriate it can still produce bifilm. Vertical and horizonal runner shape, gate location (drag or cope), offset, feeder location etc. are critically important to proper design. Figure 1.14 a shows basically poor mold design and Fig 1.14 b shows a more satisfactory mold design [8].

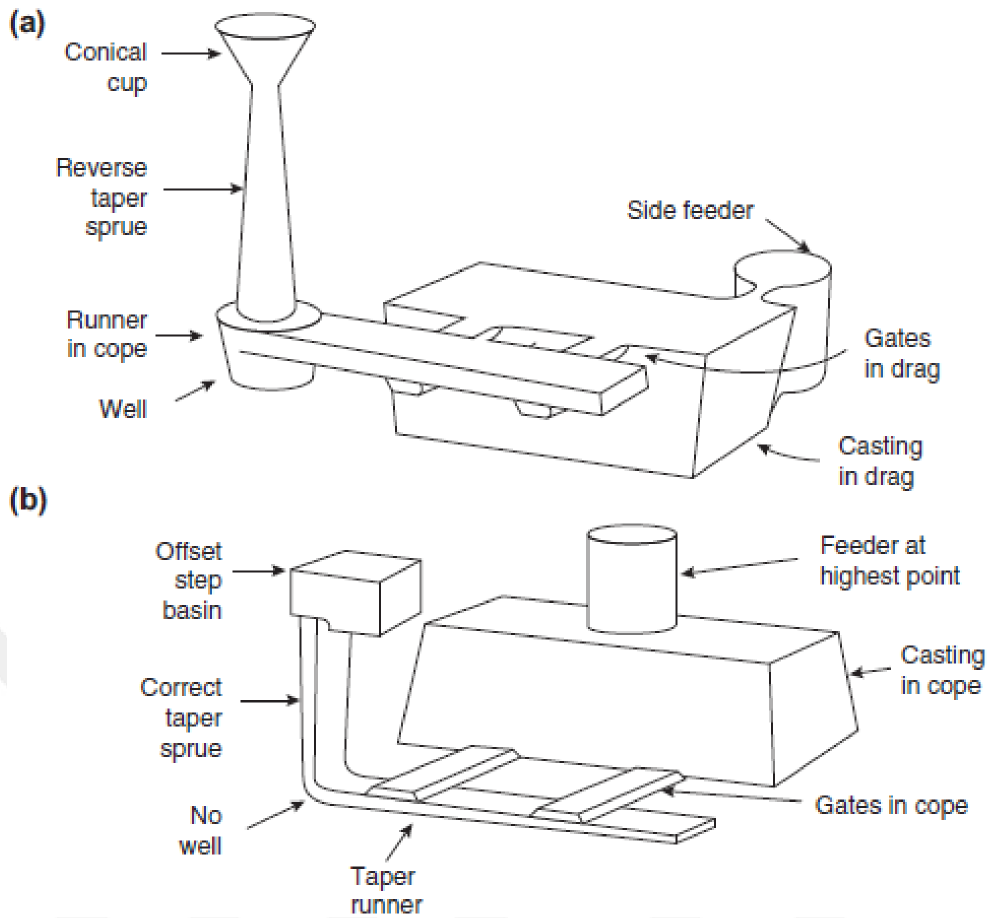

Figure 1.14 : (a) poor sprue, top runner and side feeder system. (b) better sprue, bottom tapper runner and top feeder system [1].

1.8 Determination of Liquid Metal Quality

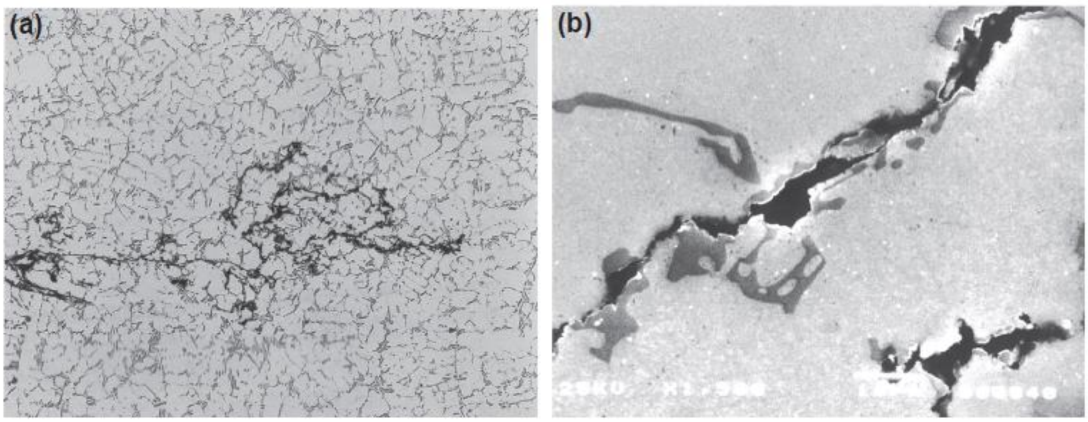

Figure 1.15 : Different bifilm morphologies (a) convoluted and (b) canyon-like [1].

Entrainment surface oxide, i.e. bifilm, is present in the cast part, it can deteriorate the product properties. Fig 1.15 shows convoluted bifilm in microstructure and in the SEM image. Defects or porosity can occur with the unfurling or inflation of the bifilm (Figure 1.16).

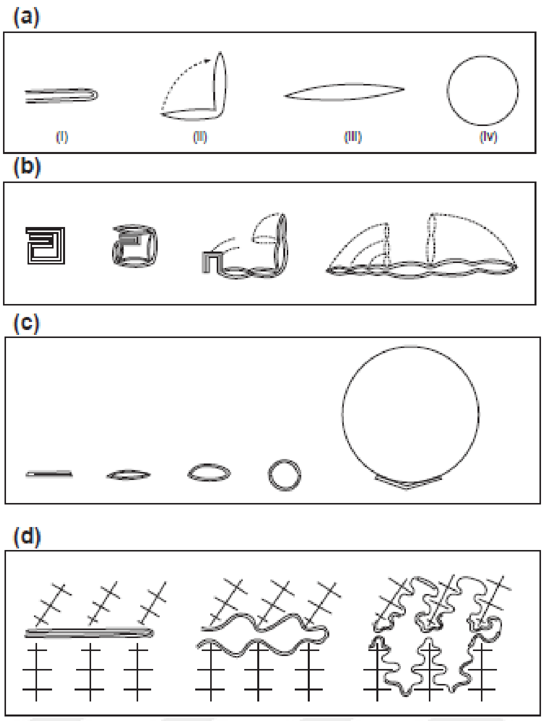

Figure 1.16 : (a-d)Unfurling and inflation stages of bifilms [1].

Determination of liquid metal quality is easy and cheap with Reduced Pressure Test (RPT). Liquid metal is poured into sand or preheated permanent mold. It solidified under vacuum. That RPT sample is sliced vertically (Figure 1.17). Measurement of bifilm index unfurling or inflation bifilms under vacuum with Equation 1. Liquid metal cleanses can relatively compare with that equation before degassing, after inoculation, after degassing and before casting. The effect of these processes on liquid metal cleanings can thus be easily determined [8,9].

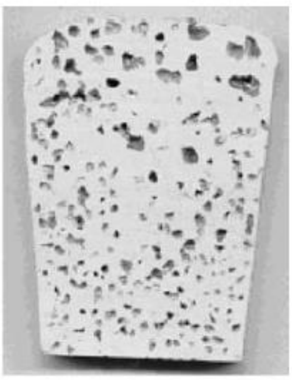

Figure 1.17 : Cross section of RPT sample [9].

$$bifilm\ index = \sum(pore\ length) = L_b \tag{1.1}$$

1.9 The 10 Rules of Castings by Campbel John [1]

John Campbell came out with "The 10 Rules are my personal checklist, ensuring that I have not forgotten any essential aspect of casting manufacture." for 10 rules. That check list is important to obtain appropriate final product. Many of these rules are described in this section, but it maybe more convenient to view them as a list.

Summary of 10 rules:

1. Start with a good quality melt
2. Avoid turbulent entrainment of the surface film on the liquid
3. Avoid laminar entrainment of the surface film on the liquid
4. Avoid bubble entrainment
5. Avoid core blows
6. Avoid shrinkage
7. Avoid convection
8. Reduce segregation
9. Reduce residual stress
10. Provide location point

1.10 Grain Refinement and Modification

The major microstructure features of Al alloys are primary α-Al dendrites, secondary dendrite arm spacing (SDAS), acicular or coarse plate-like eutectic Si (secondary phases) and intermetallic phases in the alloy. These coarse microstructure features determine the mechanical properties.

1.10.1 Grain refinement

Solidification of melted metal starts from mold surface. Adjacent to the mold walls, the heat transfer is so rapid that these grains are finer in those regions. The second region is the columnar grains. This structure is formed due to the heat loss where the growth is in the reverse direction. Center of the mold has equiaxed grains (Figure 1.18). These grains are coarser because of slowed heat loss. It is important to control microstructure as it has direct influence on the mechanical properties. The schematic representation of dendrites joining to form grains is shown in Figure 1.19.

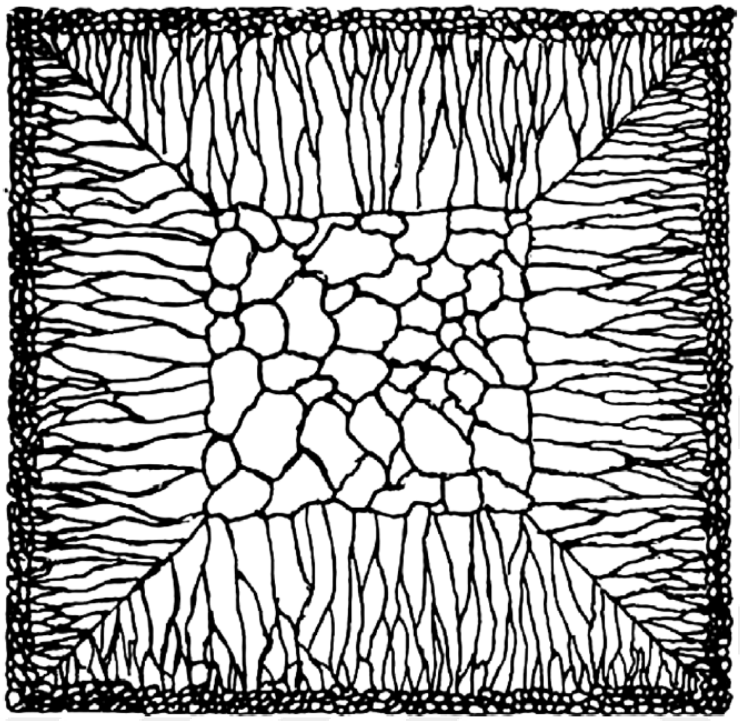

Figure 1.18 : Schematic casting grain structure distribution [2].

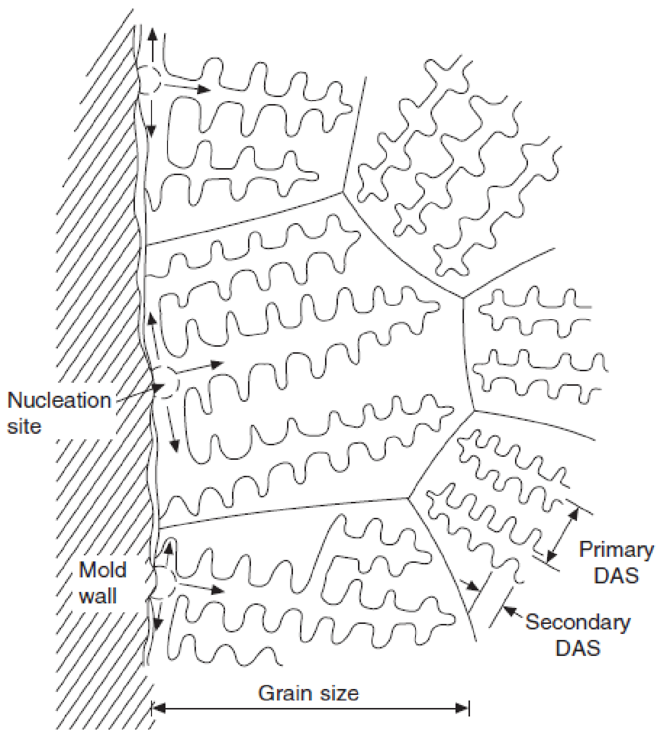

Figure 1.19 : Schematic illustration of grain-forming dendrites [1].

Obtaining of small grains of the casting microstructure provides many advantages. The smaller grain means, larger grain boundaries. When the area of grain boundary is increased, dislocation needs more energy to overcome those obstacles. Due to the finer grain, mechanical properties such as yield stress, ductility, toughness, fatigue resistance are improved. Porosity and size of pores are also reduced with finer grain.

The Al-Ti-B master alloys are the most widely used in the grain refinement of aluminum casting alloys. The purpose of grain refinement is to lower the temperature in the melt. It encourages equiaxed grains and removes columnar growth. Even though there are many theories such as peritectic hulk, duplex, hyper nucleation and phase related theories, none of these theories is not accepted as main theory. These theories are based on two assumptions which are TiB_2 particles poor nucleants for aluminum and peritectic reaction. Fig 1.20 shows the grain refinement effect at the macro size. Therefore, typically B is added to the alloy where TiB_2, AlB_2 and Al_3Ti all together acts as heterogeneous nucleation sites to decrease the grain size.

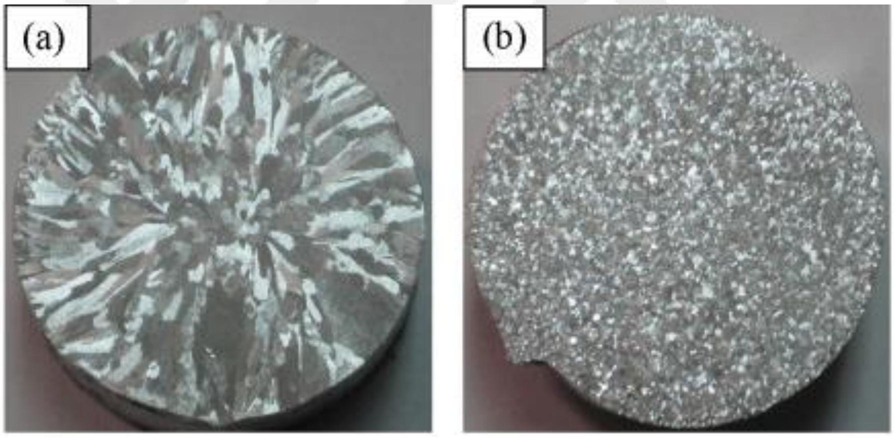

Figure 1.20 : (a)Unalloyed and (b)alloyed macrostructure [1].

The solidification process includes of the nucleation and growth of α-Al and this determines the grain size of aluminum alloy. The nucleation step is obtaining heterogeneous nucleation sites of α-Al by adding grain refiner to aluminum melt. The α-Al grain growth stage is the grain growth restriction by aggregation solution elements or insoluble particles between the grains. Grain size refinement is achieved with high nucleation rate and grain growth restriction. The carbide-borides theory, the peritectic theory, the peritectic hulk theory, the duplex nucleation theory and the solute theory are proposed to explain the grain refinement mechanism with the grain refiner [10].

The carbide-borides theory was proposed by Cibula. The carbide or boride particles promote the heterogeneous nucleation of α-Al in solidification process of aluminum alloy. These particles with high melting point and small size acted as α-Al nucleation sites [10].

Nevertheless, Fan et al., Gruzleski et al. and Zhou et al. proposed that the insoluble particles such as TiB2 could not act as nucleation sites of α-Al in the absence of other soluble elements. When Al-Ti-B grain refiner was added, a more effective grain refinement effect was obtained in aluminum alloy [11-13].

In the peritectic theory, it was argued that the grain refinement obtained by the refiner was achieved by the peritectic reaction [10,14-15]. However, the reliability of these reactions is questioned [10].

The peritectic hulk theory was put forward by Backerud et al [16]. In this theory, $TiAl_3$ was thought to be surrounded by the hulk form TiB2, so the dissolution rate decreased with hulk. The peritectic reaction took place when the Ti composition reached the critical value. Nevertheless, Fan et al. and Mohanty et al [11-12] argued that the main grain refinement mechanism of grain refiner was not the peritectic reaction. Since $TiAl_3$ particles are not stable in molten aluminum alloy, Ti amount provided by refiner is less than peritectic reaction requirement.

According to the duplex nucleation mechanism, nucleation consisted of two steps. The first step was the aggregation of $TiAl_3$ on the TiB_2 surface. In the second step, α-Al nucleates in the region consisting of TiB_2 and $TiAl_3$. Jones proposed the hypernucleation theory which is similar with the duplex nucleation mechanism [16]. However, Horsfield et al. suspected that the Ti source on the surface of TiB_2 was not certain, also Schumacher et al. argued that the duplex nucleation mechanism was not accuracy [17-18].

In the solute theory, solute element such as Ti and nucleation particles were suggested to be important for grain refinement in aluminum alloy. Heterogeneous nucleation was promoted by structural supercooling caused by the solute element, and solute element segregation near the solid-liquid interface limited the grain growth of aluminum alloy [19].

Zhang et al. proposed that the addition of rare earth element promoted the grain refinement. The $TiAl_3$ was wrapped by the rare earth and decreased the surface energy of $TiAl_3$, this indicated that the peritectic reaction was accelerated [20].

The schematic of different nucleation theories was shown in Figure 1.21, while the positive and negative viewpoints of these theories were shown in Table 1.11.

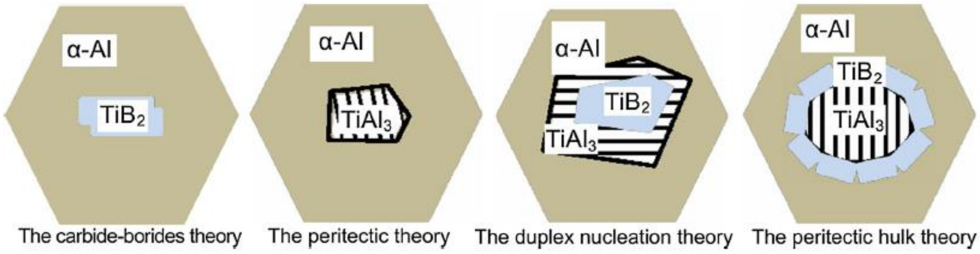

Figure 1.21 : Schematic of different nucleation theories [10].

Table 1.11 : Positive and negative viewpoints of different grain refinement mechanisms using grain refiner [10].

Theory	Positive viewpoints	Negative viewpoints
The carbide-borides theory	TiB_2 is observed in Al grain The Al–Ti–B master alloy shows a better grain refinement effectiveness than Al–Ti alloy	Al–TiB_2 master alloy has no grain refinement to high pure Al. But Al–Ti alloy has grain refinement effectiveness to high pure Al The carbide (or borides) has no grain refinement in the absence of solute Ti
The peritectic theory	The refinement behaviors by Al–Ti series alloys are explained This theory is reasonable in Al alloy melt contain $TiAl_3$ $TiAl_3$ is observed at the center of the Al grain	This theory cannot explain the invigorating effect of B element on grain refinement The amount of free Ti is much lower than the Ti level required for peritectic reaction The $TiAl_3$ phase is not thermodynamically stable for the peritectic reaction
The peritectic hulk theory	$TiAl_3$ phase is stable even at lower concentration in case of B addition The refinement behavior by Al–Ti–B (Ti/B > 2.22) is explained by the duplex nucleation theory	The boron has no effect on the Al–Ti phase diagram and stability of $TiAl_3$ The grain refinement by Al–Ti–B refiner fades with the prolongation of holding time, but this fading disappears after stirring
The duplex nucleation theory (the hypernucleation theory)	The existence of a Ti-rich layer on the surface of TiB_2	The thin phase between TiB_2 and amorphous Al is difficult to identify In theory, pure Al, the mixture of Al and Al_3Ti, or an intermediate Al–Ti structure all can nucleate on the surface of TiB_2 particle
The solute theory	Solute element has an effect on the growth restriction of grain The increased solute contents induce increased nucleation	The restrictive effect of solute element has a negligible influence on nucleation behavior and final grain size

1.10.2 Modification

Al-Si alloys are widely used for many different applications. Figure 1.22 illustrates Al-Si phase diagram with microstructures and Si morphology with different Si content (hypoeutectic <12.5%, eutectic, hypereutectic >12.5%).

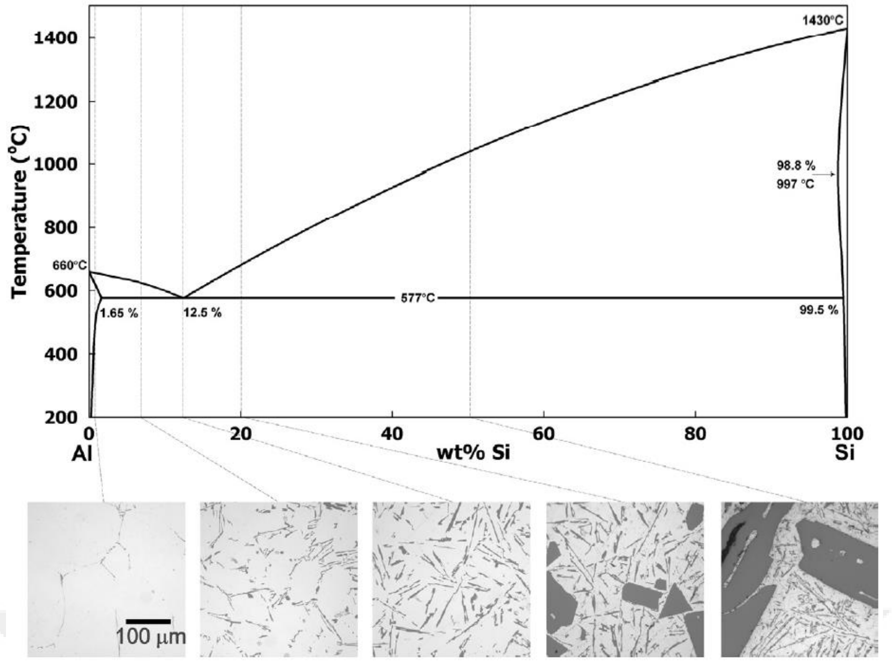

Figure 1.22 : Microstructure change with different Si contents in Al-Si phase diagram [2].

Si particles are located in grain boundaries, particularly in between dendrites because, according to phase diagram, a-grains nucleate first, and then, when the temperature drops below 577ºC (the eutectic temperature), the remaining liquid solidifies as the eutectic structure. The shape of Si phase is sharped-edged plate and it acts as crack initiators. Therefore, the mechanical properties are negatively affected. The addition of sodium or strontium modifies the Si phase from acicular needle shape to fibrous finer particles. Addition of these modifiers converts coarse eutectic Si flakes into fine eutectic (Figure 1.23). Effects of the precipitate shape on dislocation movement shows in Figure 1.24.

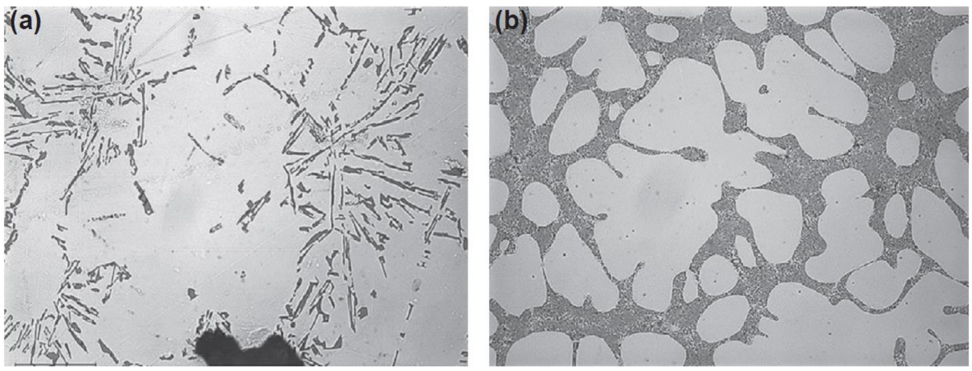

Figure 1.23 : Eutectic Si in Al-7Si (a) unmodified, (b)modified by Sr addition [1].

The modification of Si by Sr reduces the eutectic temperature to 571ºCs. Thus, feedability and fluidity increases.

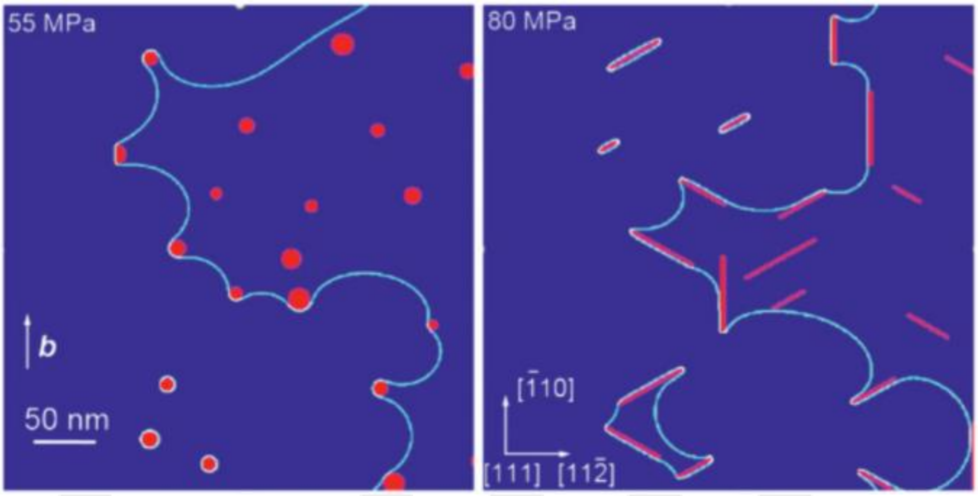

Figure 1.24 : The effect of different precipitate shape on the dislocation motion [2].

The eutectic Si modification with Na addition was patented in1921 by A.Paczk*. Although The eutectic Si modification has been used more than 100 years, a modification mechanism accepted by everyone has not been found yet [21]. Various theories, such as restricted growth theory and restricted nucleation theory, have been proposed to elucidate the mechanism of chemical modification in eutectic Si in hypoeutectic Al-Si alloy. The twin-plane re-entrant edge (TPRE) mechanism and the impurity induced twinning (IIT) mechanism explain the restricted growth theory. The TPRE mechanism proposes that a modifier retards or suppresses the subsequent attachment of silicon atoms during eutectic silicon growth. The IIT mechanism postulates that the modifier's atoms are absorbed in the growth steps of the silicon solid-liquid interface, which causes an increase in the twinning density of the silicon. Furthermore, the mechanism of chemical modification is explained by other important factors such as intermetallic clusters and altered surface tension [21-24].

1.10.3 Rare earth elements

Over the past few years, the effect of adding trace amount of rare earth elements have been examined on primary α-Al grain refinement. Rare earth elements can refine primary α-Al and/or modified the eutectic Si from acicular or coarse plate-like to fibrous or globular morphology. Even though scandium (Sc) addition provides the most effective refining and strength effect. Sc addition cannot widely used due to its high price [10] .

The low cost and better efficiency rare earth elements have been searching for simultaneous grain refinement and modification effect. Phase diagrams of rare earth elements Er and Eu with Al are shown in Figure 1.25 – 1.26.

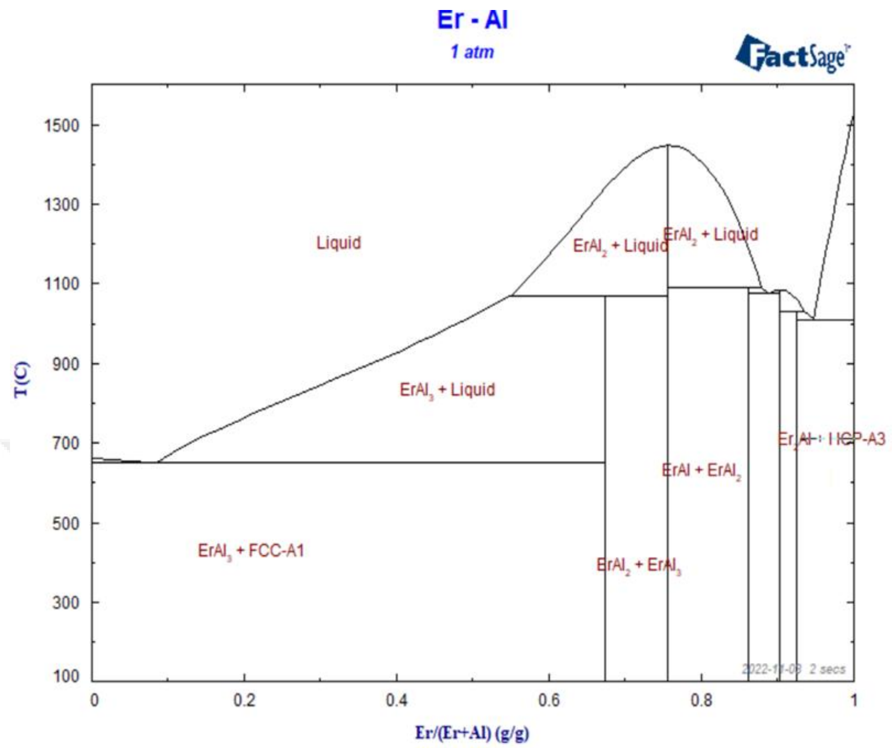

Figure 1.25 : Al-Er phase diagram

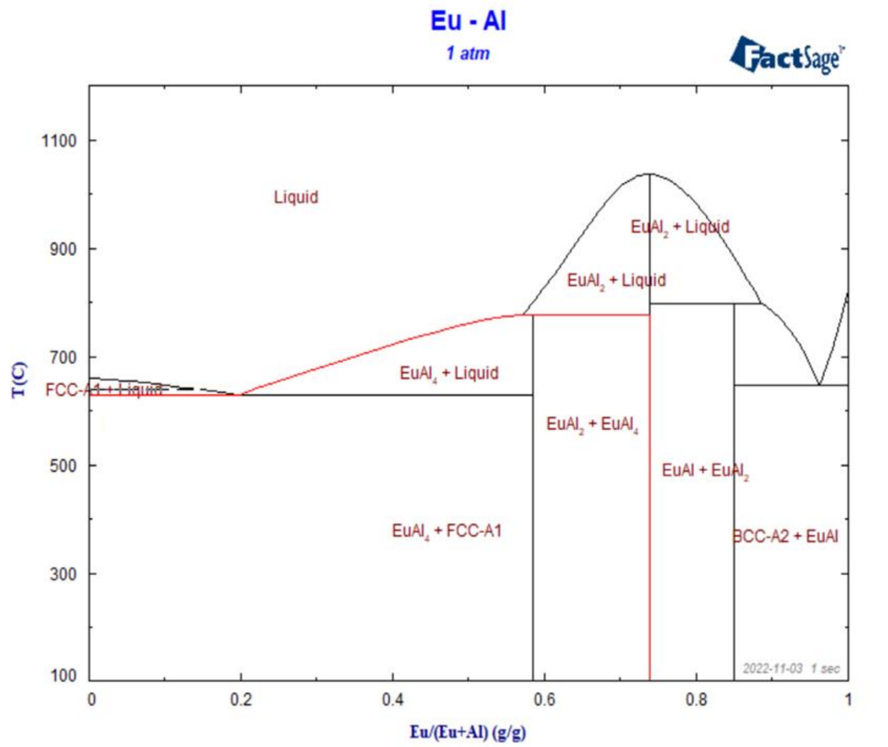

Figure 1.26 : Al-Eu phase diagram

1.11 Heat Treatment

The traditional heat treatment of a precipitation-hardened aluminum alloy includes 3 steps, a solution treatment, water quench and age (natural aging or artificial aging) as shown in Figure 1.27. The main purpose of heat treatment is to distribute the secondary phase homogenously and finer shape within the microstructure. As a result, mechanical properties are improved by modification-like mechanism.

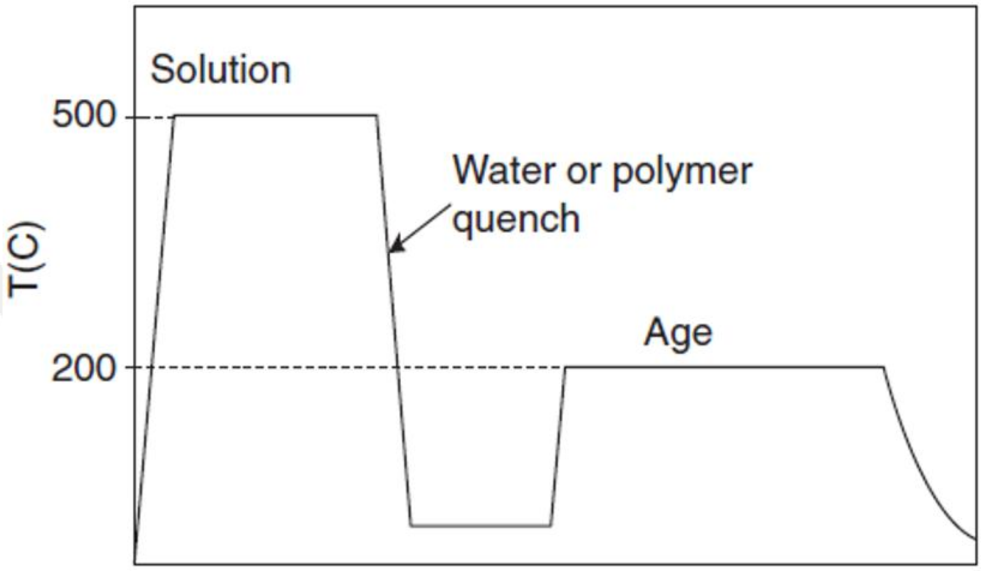

Figure 1.27 : The precipitation-hardened aluminum alloy heat treatment steps [1].

According to the phase diagram, the alloy must represent a curved solvus line. In this way, when the alloy is heated to temperatures between solvus and eutectic temperature, the composition consists of only α-phase. Since the cast microstructure at room temperature consists of a- and b- (two) phases, when the alloy is heated above solvus temperature, the secondary phase dissolves; thus, this stage is called "solutionizing". Then, the alloy is quenched in water. During this stage, the temperature of the alloy drops from above 500ºC's down to room temperature. Since the thermal contraction cannot occur regularly, the rapidly cooled structure contains point defects. This is important because at the following step; i.e. aging; the secondary phases start to nucleates on these point defects (due to high energy regions), and thus, the secondary phases become smaller and homogeneously distributed in the microstructure as seen in Figure 1.28. Temper designation was shown in Table 1.12 in detail.

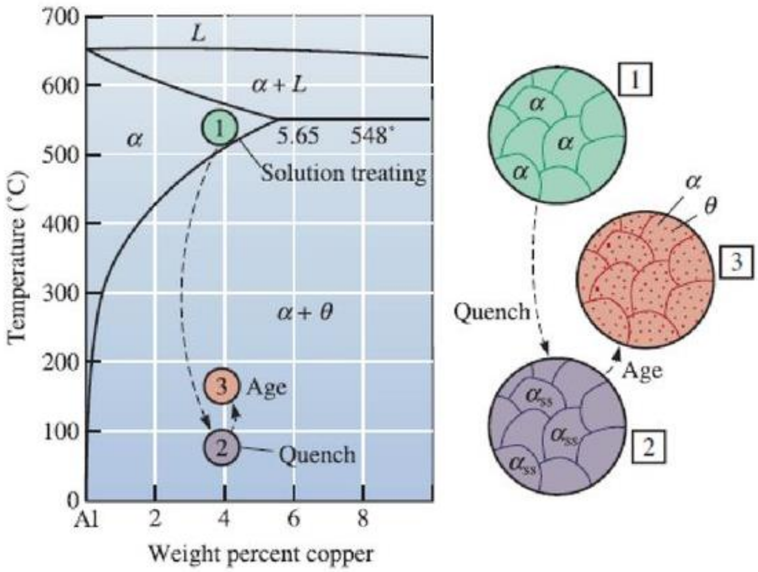

Figure 1.28 : The phase diagram and microstructure schematic representation of heat treatment stages [2].

Table 1.12 : Temper designation of casting alloys [1].

Temper designation	Temper
As cast	F
Annealed	O
Controlled cooling from casting and naturally aged	T1
Solution heat treated and naturally aged where application	T4
Controlled cooling from casting and artificially aged or over-aged	T5
Solution heat treated and fully artificially aged	T6
Solution heat treated and artificially under-aged	T64
Solution heat treated and artificially over-aged (stabilized)	T7

2. EXPERIMENTAL

2.1 Tensile Test Mold design and optimization

Dimension of tensile test bar mold for aluminum alloy according to ASTM B108/B 108M [25] is shown in Figure 2.1 The data was drawn using SolidWorks and it was subjected to filing and solidification analysis in Anycast software. ASTM B108/B 108M tensile test mold design is drawn in 3D in SolidWorks. The drawing was saved as STL format to prepare for analysis in Anycast program. A356 (Al-7Si-0.3Mg) alloy was selected and simulated in sand mold with a casting temperature of 750ºC for all design. Liquid metal enters the mold with a radius of 14 mm and completely filled in 2.8 seconds in ASTM B108/B 108M tensile test mold.

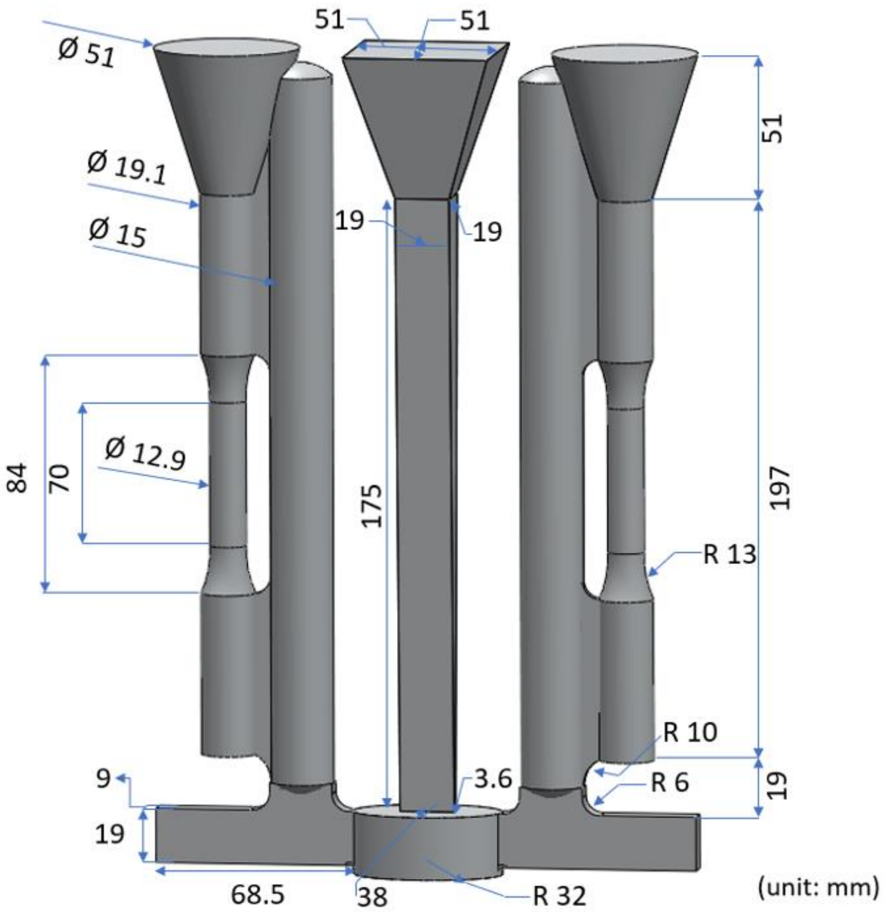

Figure 2.1 : The sketch image and dimensions of ASTM mold design.

V1 tensile test mold was designed (Figure 2.2), which can produce 10 samples in one casting. The liquid metal entered the mold with a radius of 10 mm in the V1 design and was completely filled in 4.8 seconds.

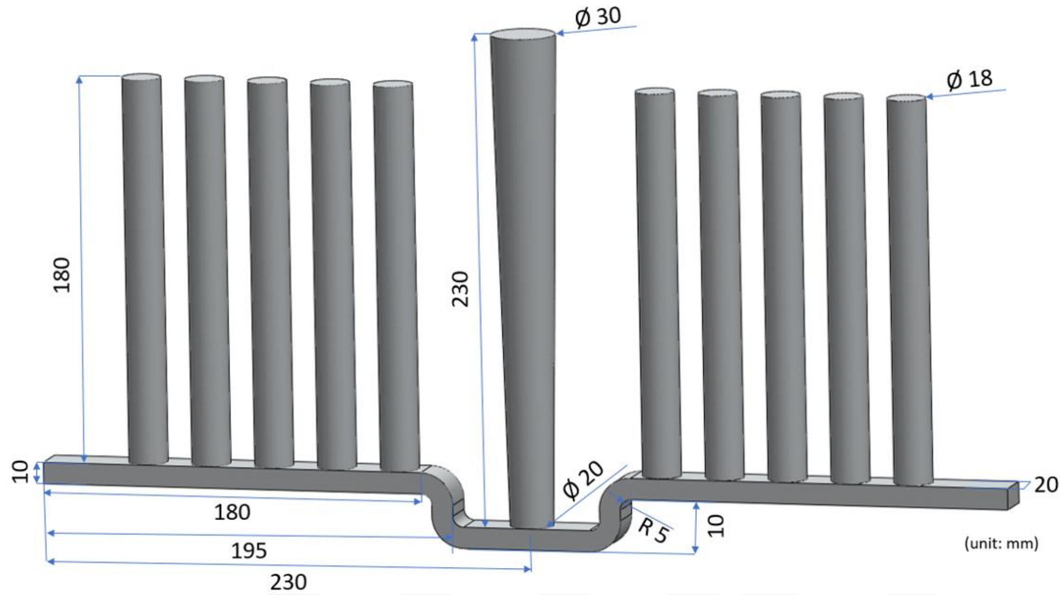

Figure 2.2 : The sketch image and dimensions of V1 mold design.

Figure 2.3 showed the V2 design with smaller height and diameter of bars with narrowing runner. The liquid metal entered the mold with a radius of 6 mm in the V2 design and was completely filled in 4 seconds.

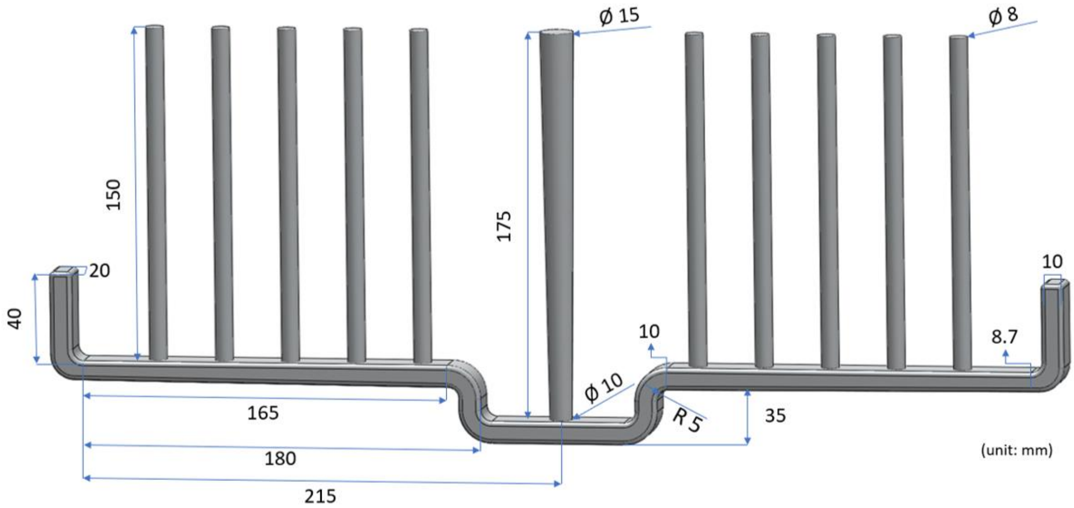

Figure 2.3 : The sketch image and dimensions of V1 mold design.

In the V3 design (Figure 2.4), the sprue was enlarged, making it suitable for tilt casting. The mold was tilted at a 30° angle and after the casting begins it was slowly lifted upright. Casting ended when the mold reaches the vertical position at an angle of 90° i.e. tilt casting. The liquid metal entered the mold with a radius of 10 mm in the V3 design and is completely filled in 4.8 seconds.

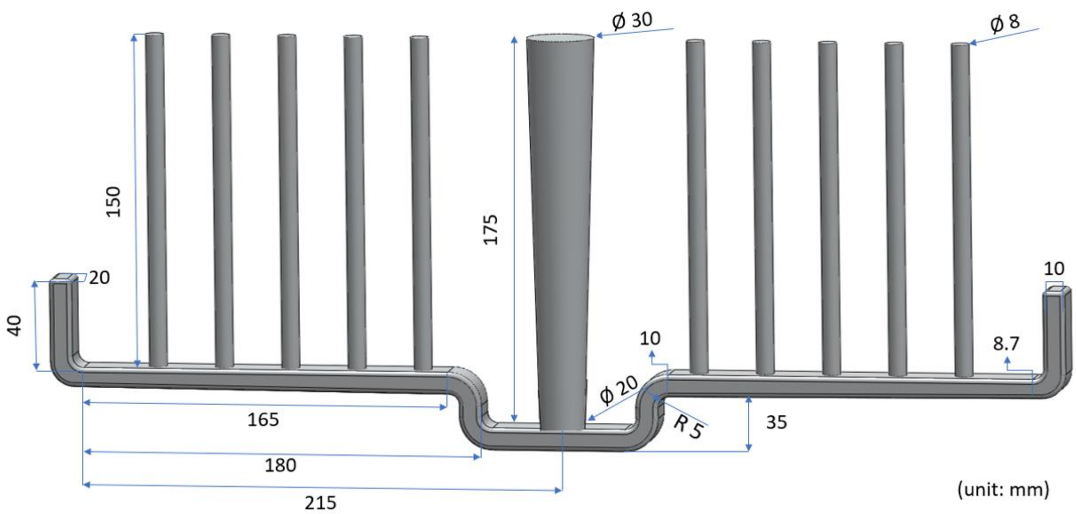

Figure 2.4 : The sketch image and dimensions of V3 mold design.

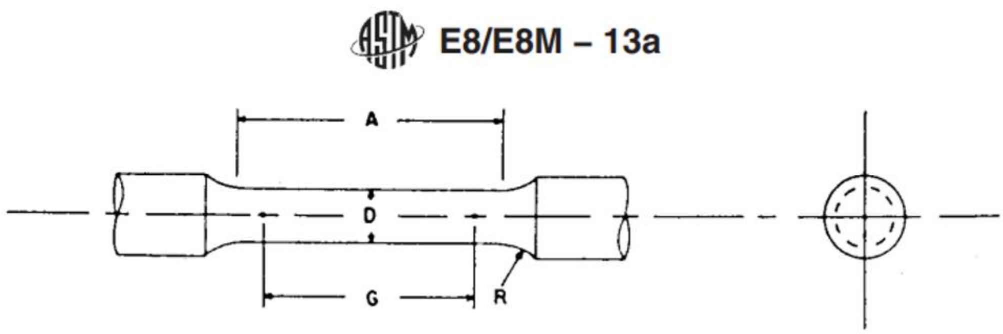

	Specimen 3
G—Gauge length	30.0 ± 0.1 [1.250 ± 0.005]
D—Diameter (Note 1)	6.0 ± 0.1 [0.250 ± 0.005]
R—Radius of fillet, min	6 [0.188]
A—Length of reduced section, min (Note 2)	36 [1.4]

Figure 2.5 : The dimensions of E8/E8M tensile test bar [26].

It was cast with A356 alloy at 750ºC in mold designs V1, V2 and V3. According to T6 state, A356 bars were solution treated for 6 hours at 540ºC at resistance furnace. Following by the hot water quenched at 75ºC, the alloys were aged at 160ºC for 4 hours, and cooled in the air. The heat-treated bars were machined in accordance with ASTM E8/E8M standard [26]. Figure 2.5 showed schematic representation of machined tensile test bar. The tensile test was performed on the Zeiss device at 1mm/min. Yield strength (YS), ultimate tensile strength (UTS) and % elongation (e%) were obtained as a result of tensile test.

2.2 Materials and Methods

In this study, A356(Al-7Si-0.3Mg) alloy was used. Its chemical composition was shown in Table 2.1. Al-3%Er and Al-10%Eu master alloys were used for alloying in appropriate proportions. The desired alloying amounts were shown in Table 2.2.

Table 2.1 : The chemical composition ranges of A356 alloy.

	Si	Mg	Fe	Cu	Ti	Al
A356	6.5-7.5	0.25-0.45	<0.10	<0.20	<0.20	91.1-93.3

Table 2.2 : Alloying ratios of Er and Eu.

	Er	Eu
0.0	-	-
0.1 Er	0.1	-
0.1 Er + 0.1 Eu	0.1	0.1
0.3 Er	0.3	-
0.3 Er + 0.1 Eu	0.3	0.1

To prepare a sand mold, 60-65 AFS sand was mixed with 2 wt% resin and 0.5 wt% hardener. The mixture is put into the wooden model and compressed. After one hour the mold is set to be ready to be removed from the pattern (Figure 2.6). The molds were prepared one day before casting, allowing the moisture inside to be completely removed.

Figure 2.6 : The sand mold prepared for casting.

15 kg base alloys were melted in A50 Mammut SiC crucibles at 750ºC in ICS MELT induction furnace (Figure 2.7).

Figure 2.7 : Induction metal melting furnace.

Before degassing, solidification test under vacuum was applied to determine the liquid metal quality. When the liquid metal in the crucible is at 750ºC, approximately 250 grams of alloy is poured into preheated and coated metal mold with ladle in the fastest way and vacuum (80-100 mbar) is applied. Reduced Pressure Test (RPT) sample is taken from vacuum chamber after 5 minutes. RPT samples were taken for each alloy before degassing and after degassing. Optic Emission Spectrometer (OES) sample was taken to determine the chemical composition.

Half of the liquid metal was cast as ingot to have the same chemical composition in different alloying. Degassing was applied to the remaining liquid metal in the crucible. The remaining liquid metal in the crucible was degassed with N_2 for 10 minutes with Pyrotek ceramic diffusor. Nitrogen flow was adjusted to have small bubbles on the surface (f 2,2,5,1). After removing the dross from the liquid metal surface, it was poured into the prepared V3 design tensile test mold by tilt casting method. The first casting is the base alloy without any alloying with the rare earth elements. Considering the remaining liquid metal amount, the required master amount was calculated for 0.1 wt% Er by weight. 5 minutes was waited at 750ºC for alloying then 5 minutes of degassing was done. The dross from the liquid metal surface was skimmed before casting. The remaining metal has 0.1 wt% Er. Considering the remaining liquid metal amount, the required master amount was calculated for 0.1 wt % Eu by weight. As a result, an alloy containing 0.1 wt% Er and 0.1 wt% Eu was obtained. The alloy casted into sand mold, after 5 minutes of degassing and skimming of the dross. The rest of alloy was poured as an ingot. Half of the previously separated base metal was charged into the crucible and melted. The required master amount was calculated for 0.3 wt% Er. 5 minutes was waited at 750ºC for alloying then 10 minutes of degassing and removing slag were done. It was casted. Considering the remaining liquid metal amount, the required master amount was calculated for 0.1 wt% Eu by weight. The last alloying metal which included 0.3 wt% Er and 0.1 wt% Eu, was casted after 5 minutes degassing and skimming of the dross. Consequently, 1 base and 4 alloying metal was obtained:

1. 0.0 wt% (Base alloy without master alloy)
2. 0.1 Er wt%
3. 0.1 Er + 0.1 Eu wt%
4. 0.3 Er wt%
5. 0.3 Er + 0.1 Eu wt%

Liquid metal was casted at 770ºC.

2.2.1 Optic emission spectrometer analysis

Optic Emission Spectrometer (OES) sample was taken during the casting was grinded with 120 grit sandpaper. Optic Emission Spectrometer Analysis was employed on the prepared samples with QUANTOLUX QLX3 Optic Emission Spectrometer Analysis. Same samples were employed X-ray fluorescence (XRF) analysis in Bruker brand XRF Spectrometers device.

2.2.2 Reduced Pressure Test

RPT samples were taken before and after degassing. RPT samples were cut in cross-section, were grinded with 120, 220, 400 and 800 grit sandpapers, respectively. The prepared samples were scanned at 800 dpi. Bifilm dimensions from scanned images measured in Kameram software.

2.2.3 Microstructure analysis

10-bar were cut from taper runner. 10 mm thick sample was cut from the bottom of the bar before heat treatment. After heat treatment, 10 mm thick sample was cut from the bottom of the bar (Figure 2.8). In this way, microstructure changes before and after heat treatment were examined from similar regions. The cut pieces after taking warm bakallite, the bakallites were grinded with 120, 220, 400, 800, 1000, 1500 and 2000 grit sandpapers, respectively. The grinded specimens were polished with felt and diamond fluid. Microstructure images were taking with Zeiss electron microscope.. Polished sample were electrolytic etched in 2.5% HBF_4 solution at 24 V and 0.04 A for 120 seconds for grain size analysis. 50 grains were measured for the grain size measurement. 50X for determination of secondary phase formation without etching.

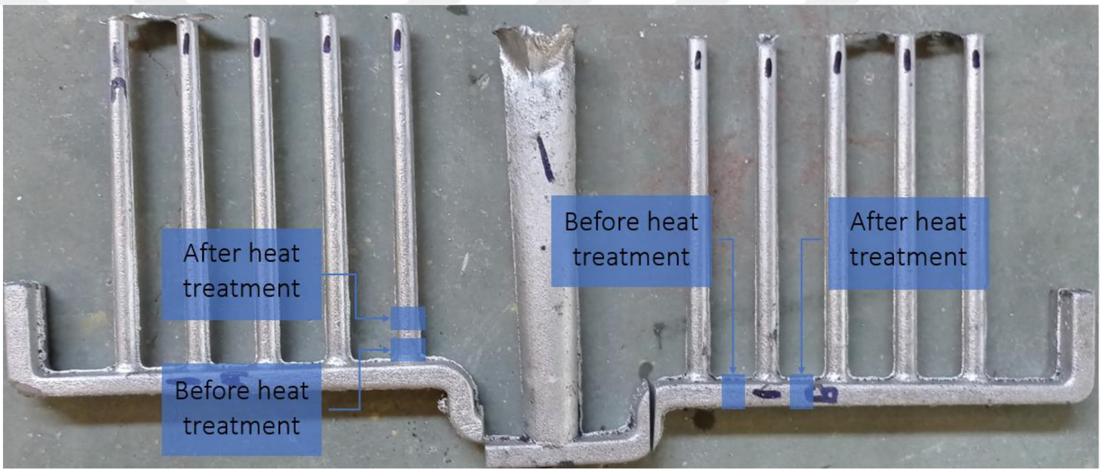

Figure 2.8 : Sampling for microstructure analysis.

2.2.4 Heat treatment

3 of 10 bar were processed without heat treatment, 7 of them were processed after heat treatment. Termnevo resistance furnace was used for heat treatment (Figure 2.9).

Regarding T6 state, A356 base and alloyed bars were solution treated for 6 hours at 540ºC at resistance furnace. Following by the hot water quenched at 75ºC, the alloys were aged at 160ºC for 4 hours, and cooled in the air (Figure 2.10).

Figure 2.9 : Resistance furnace for heat treatment.

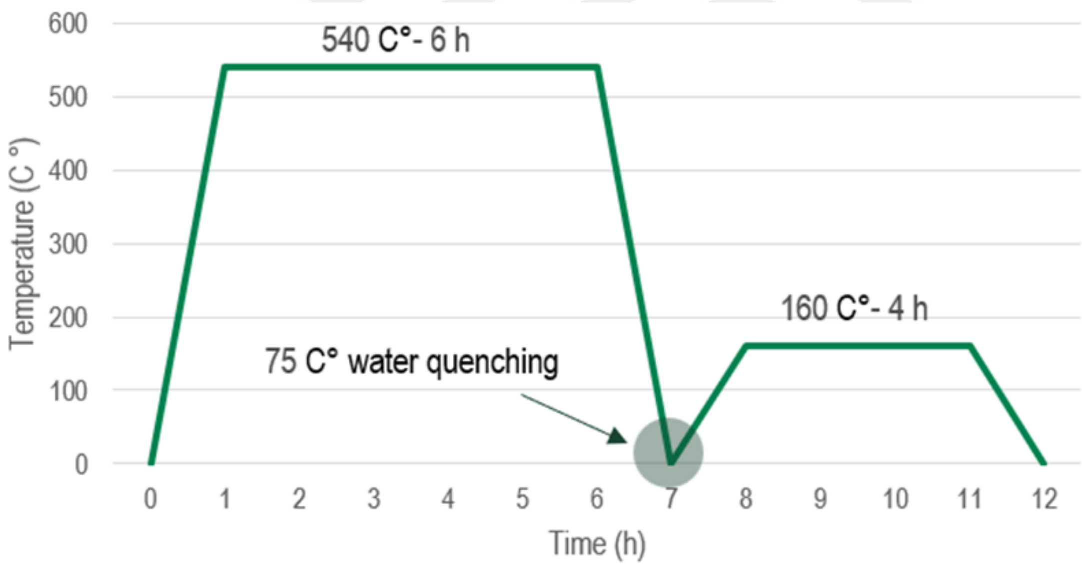

Figure 2.10 : T6 heat treatment steps.

2.2.5 Tensile test

As-cast and heat-treated bars were machined in accordance with ASTM E8/E8M standard. The tensile test was performed on the Zeiss device at 1 mm/min. Yield strength (YS), ultimate tensile strength (UTS) and % elongation (e%) were obtained as a result of tensile test (Figure 2.11).

Figure 2.11 : Tenstile test machine

2.2.6 Hardness Test

10 mm thick section from the taper runner was obtained from casting before and after heat-treatment. These samples were taken warm bakallite. The bakallites were grinded with 120, 220, 400, 800, 1000, 1500 and 2000 grit sandpapers, respectively. The sanded specimens were polished with felt and diamond fluid. Samples were prepared before hardness test.

2.2.7 SEM and EDS analysis

Scanning electron microscope (SEM) images and energy dispersive X-ray spectroscopy (EDS) analyzes were performed on the samples prepared for microstructure in Zeiss brand SEM device.

3. RESULT AND DISCUSSION

3.1 Tensile Test Mold Design and Optimization

The velocity and temperature filling of the ASTM B108/B 108M tensile test mold were shown in Figure 3.1 and Figure 3.2. New designs were tired due to turbulence during filling the mold, only 2 samples taken in one casting, increased operator effect, loss of time and excessive metal loss in feeders and runners.

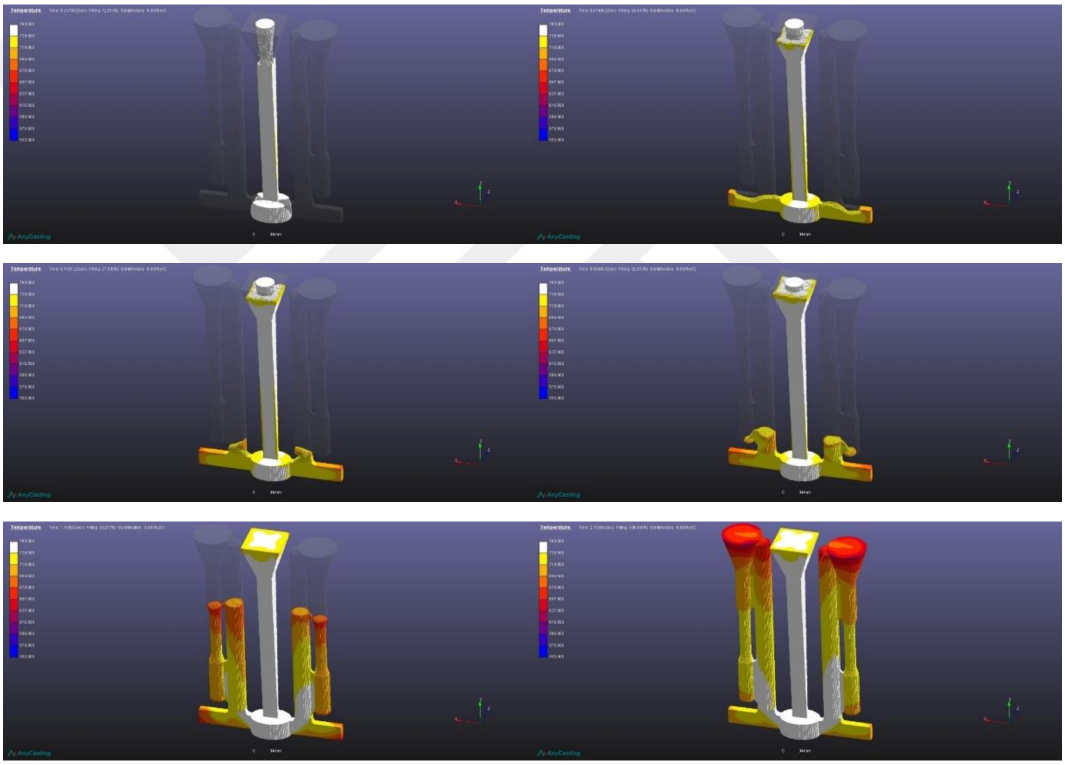

Figure 3.1 : The filling of ASTM B108/B 108M tensile test mold with temperature unit.

The idea of statistical work is fundamental to science. Therefore, the more test samples, the higher the reliability of the results. Instead of taking two samples from one mold, it would be possible to obtain ten samples from a single casting with the new design. Since there are no difference in molds, it will be ensured that there is no effect of any other parameter on the properties of the casting due to the filling and casting temperature. In consideration of these, the V1 mold design was made.

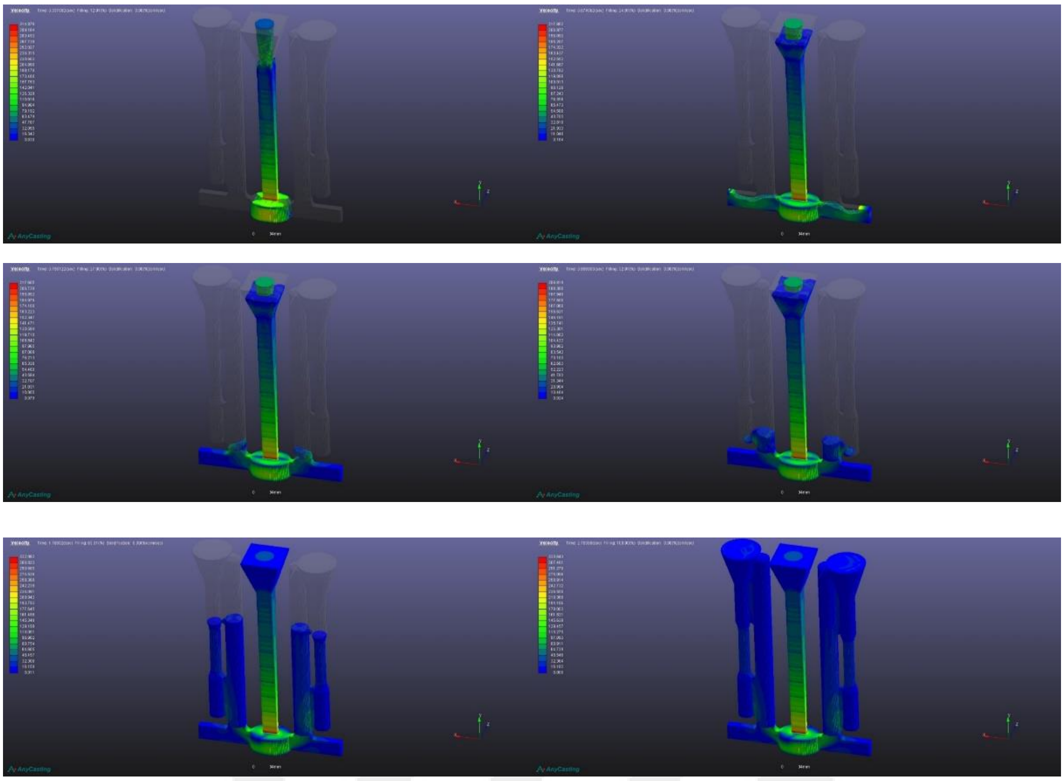

Figure 3.2 : The filling of ASTM B108/B 108M tensile test mold with velocity unit.

V1 mold design has pros and cons. Falling molten metal tapers. Thanks to taper sprue design liquid metal does not have enough space to provide turbulence. Provides a 50% reduction in speed for each turn in the runner. When the turn does not have radius, flow is unstable and providing turbulence. There are two turns with angle decreases velocity without providing turbulence. Figure 3.3 and Figure 3.4 illustrated filling of the V1 design. There are so many turbulences as the velocity of the liquid increases. The main reason for the speed increase is due to the metallostatic pressure caused by the mold height. The turns have not enough radius to decrease the velocity of the molted metal. By reducing the mold size, the speed is reduced, but narrowing in diameter is required to produce parts in accordance with the ASTM E8/E8M Standard Test Methods for Tensile Testing of Metallic Materials.

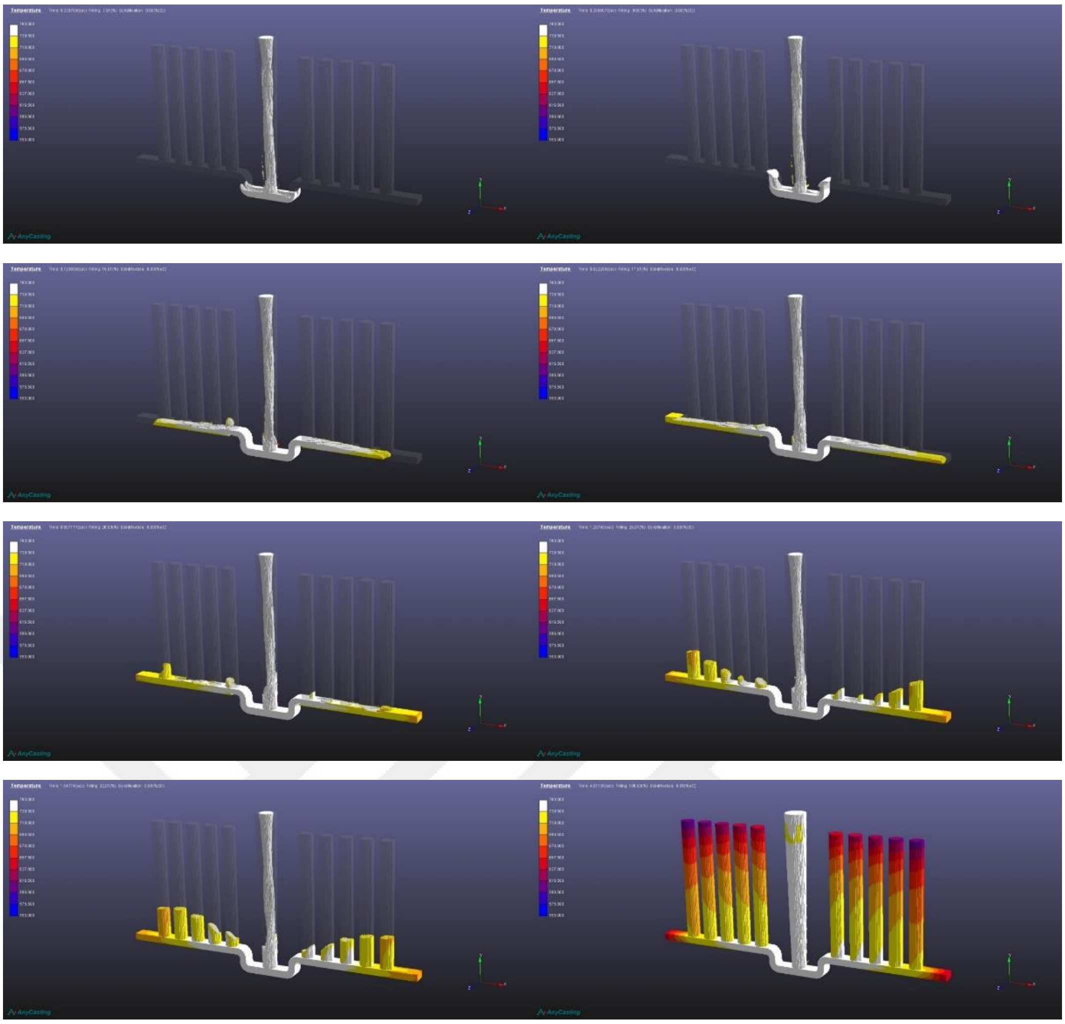

Figure 3.3 : The filling of V1 tensile test mold with temperature unit.

V2 mold was designed with smaller height and diameter of bars with narrowing runner. Diameter of taper sprue is decreased because of smaller volume requirement. Runner formation change to taper runner and trapper was added end of the tapper runner. Trapper provides to catch the first entrained oxides or inclusions rather than carrying them to the bars. Taper runner also provides the bars to be filled at the same time due to pressure generated from both sides together with the pressure coming from the runner. Figure 3.5 and Figure 3.6 showed some filling images. The tensile samples were filled simultaneously without turbulence due to taper runner design. On the other hand, the velocity of the liquid metal when it contacted with the runner could not be controlled and it caused more turbulence in the 90 degree turn that should decrease the speed of liquid metal [8].

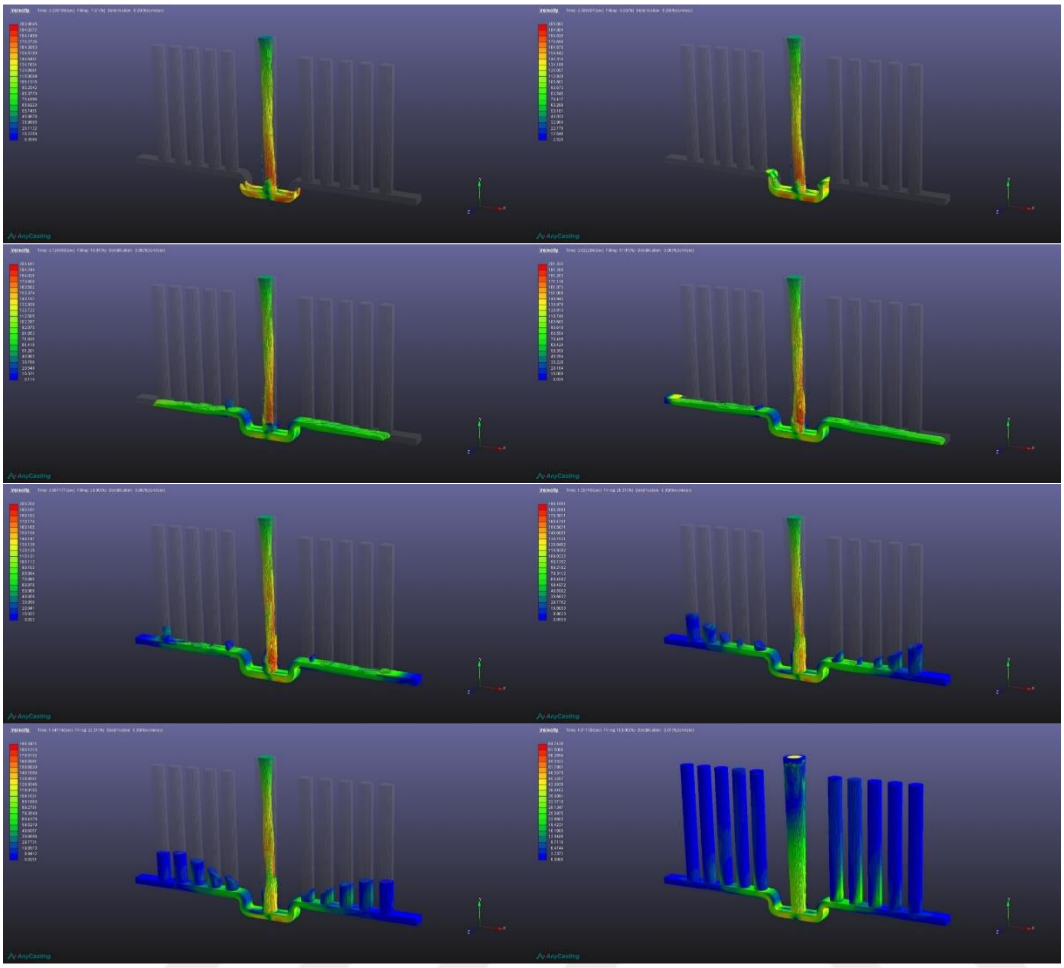

Figure 3.4 : The filling of V1 tensile test mold with velocity unit.

Even though using pouring basin and stopper, the turbulence at the entrance of the liquid metal to the bars is reduced, it is not completely prevented. Instead of changing the mold design, the casting method was changed to provide more controlled filling. Tilt casting reduces the acceleration of the liquid metal velocity by reducing the effect of gravity. Taper sprue volume is extended so that it does not to solidify before filling the mold. Filling analysis of the V3 mold design with tilt casting result in shown in Figure 3.7 and Figure 3.8. With the V3 design and tilt casting method, the velocity of the liquid metal when it contacted with the runner was controlled, so that the mold was filled free-turbulence [8].

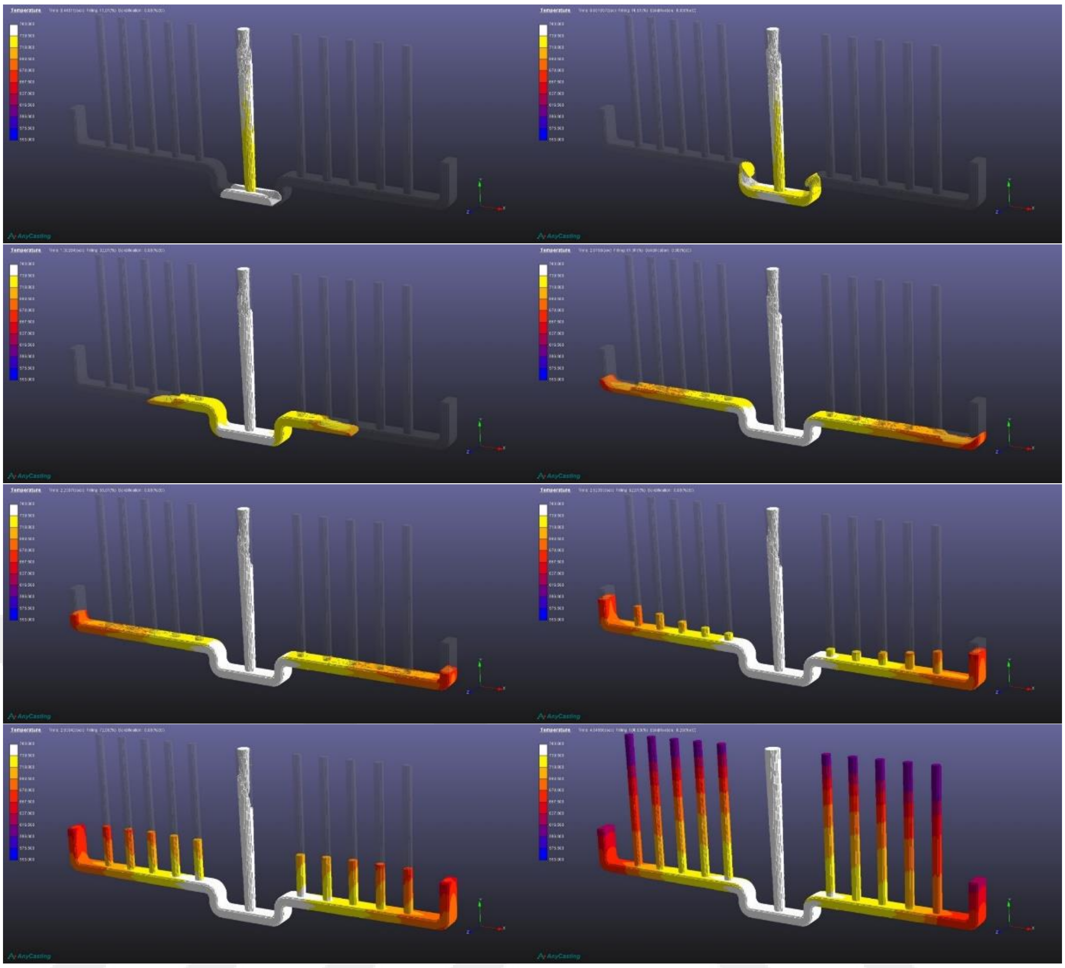

Figure 3.5 : The filling of V2 tensile test mold with temperature unit.

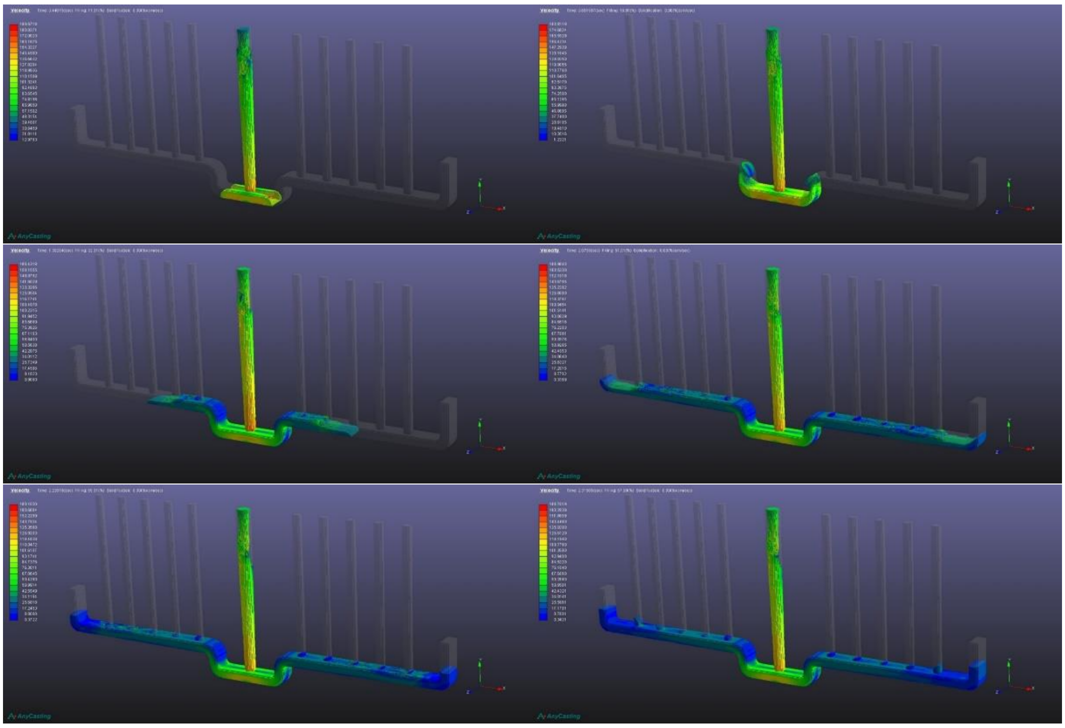

Figure 3.6 : The filling of V2 tensile test mold with velocity unit.

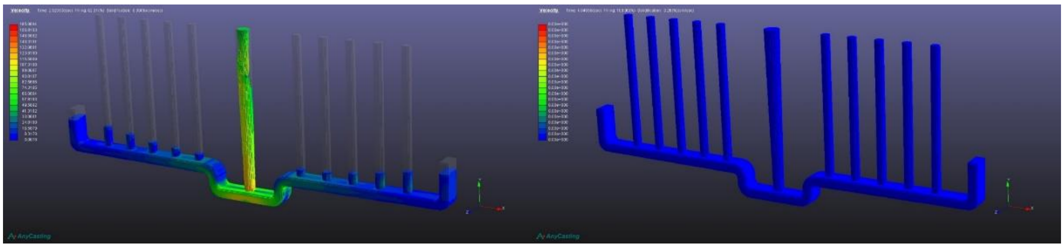

Figure 3.6 : The filling of V2 tensile test mold with velocity unit.

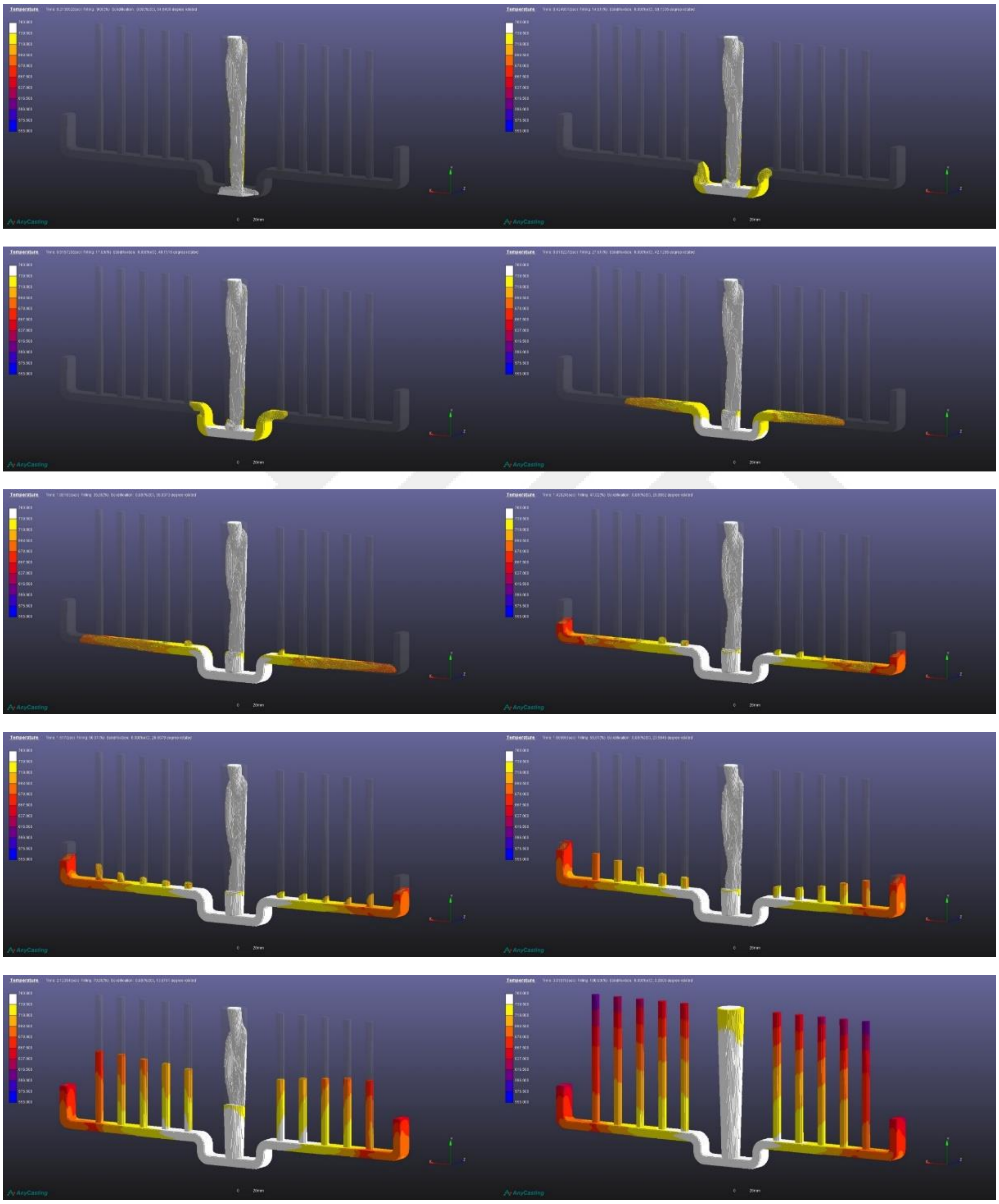

Figure 3.7 : The filling of V3 tensile test mold with temperature unit by tilt casting method.

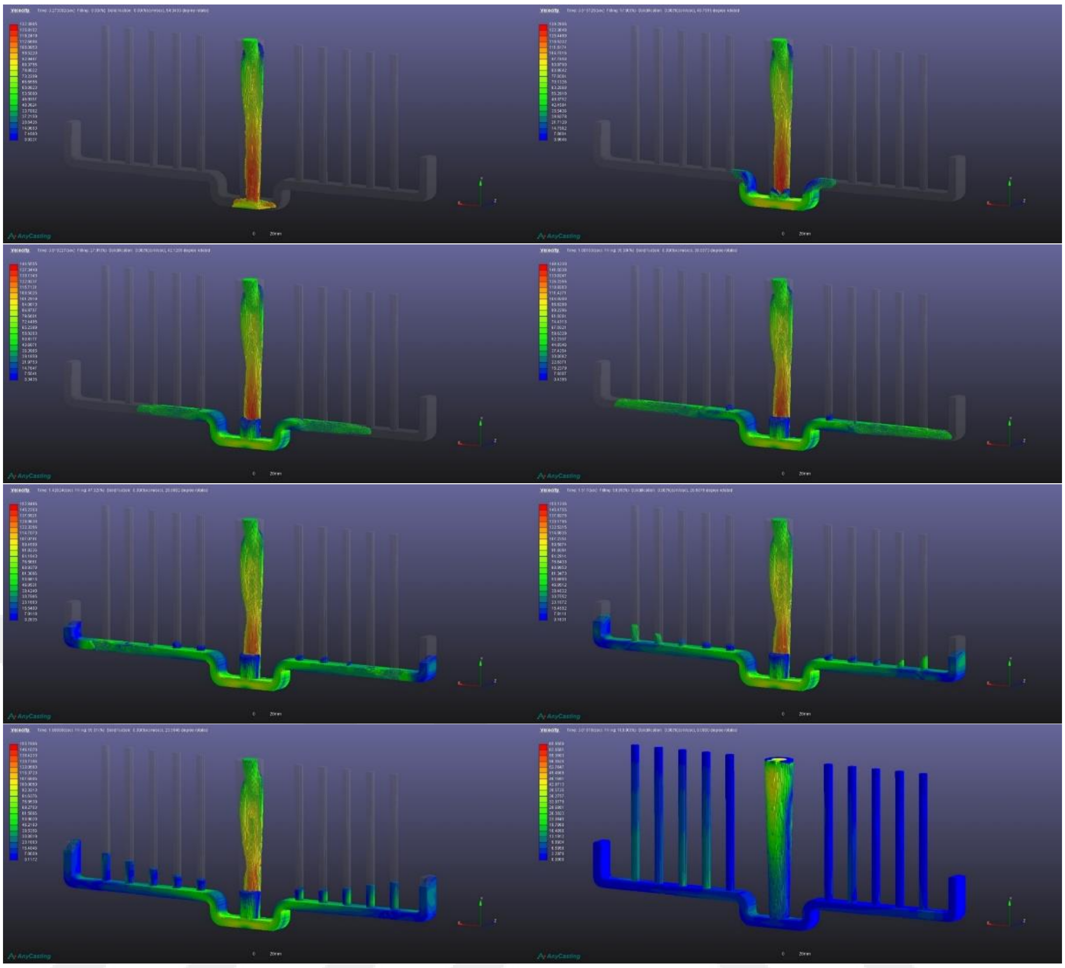

Figure 3.8 : The filling of V3 tensile test mold with velocity unit by tilt casting method.

The tensile test was employed to the new mold designs that were treated with T6 heat treatment after casting. Quality index values (equation 3.1), which include a relationship between, ultimate tensile strength (UTS) and % elongation (%e) obtained from tensile test results, are calculated with Equation 1. The K value is a constant value for each alloy and heat treatment state, this value is 150 for heat treated Al-7Si-0.3Mg commercial purity alloy.

$$Q = UTS + K\log(\%e) \tag{3.2}$$

In the evaluation of the data obtained, survivability plot curves were drawn in order to make an easier interpretation. In survival charts, the steeper the curve, the more reproducible the results. In Figure 3.9, when the quality indexes obtained from the tensile test results for V1, V2 and V3 patterns are compared, it is seen that the steepest curve is V3, V2 and V1 respectively.

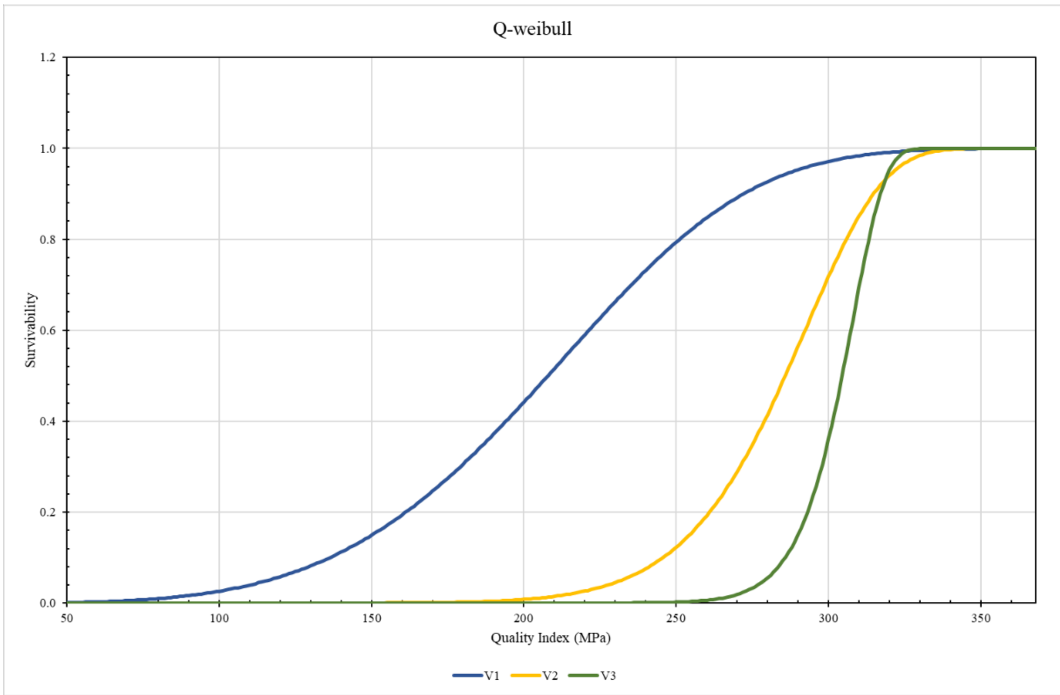

Figure 3.9 : Survivability plots of quality index of tensile test results

Considering these results, V3 mold was casted by tilt casting method in subsequent alloying castings.

3.2 Casting and Characterization

3.2.1 OES-XRF

The chemical composition of the A356 alloy obtained from the analysis with the OES device was as in Table 3.1 and XRF was in Table 3.2.

Table 3.1 : Composition of Al-7Si-0.3Mg alloy with OES.

Si	Fe	Cu	Mn	Mg	Ti	Al
7.1	0.24	0.07	0.1	0.33	0.09	Bal.

Table 3.2 : Composition of Al-7Si-0.3Mg alloy with XRF.

	Si	Fe	Cu	Mn	Mg	Ti	Er	Eu	Al
0.0	6.99	0.30	0.09	0.03	0.71	0.09	-	-	Bal.
0.1 Er	6.96	0.30	0.11	0.03	0.71	0.08	0.14	-	Bal.
0.1 Er + 0.1 Eu	5.23	0.35	0.09	0.07	0.65	0.07	0.13	0.31	Bal.
0.3 Er	6.25	0.30	0.12	0.03	0.68	0.08	0.52	-	Bal.
0.3 Er + 0.1 Eu	5.51	0.32	0.12	0.06	0.63	0.07	0.49	0.02-0.30	Bal.

3.2.2 RPT

The cross-section images of the RPT samples taken to determine the liquid metal quality were shown in Figure 3.10. The bifilm index of the A356 alloy before degassing was 71 mm, after degassing it decreased to 4 mm. In order not to increase the amount of oxide with alloying, degassing was applied again after each alloying. In this way, the casting process was carried out below 5 mm (Figure 3.11) which represents good melt quality for casting.

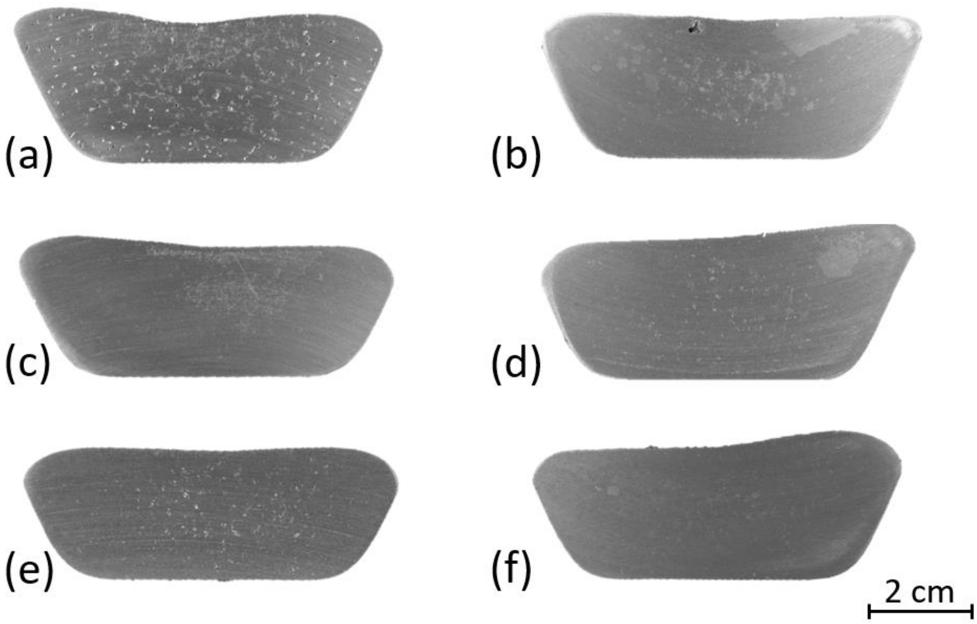

Figure 3.10 : RPT cross sections (a) before degassing, (b) after degassing (0.0), (c) 0.1 Er, (d) 0.1 Er + 0.1 Eu, (e) 0.3 Er, (f) 0.3 Er + 0.1 Eu.

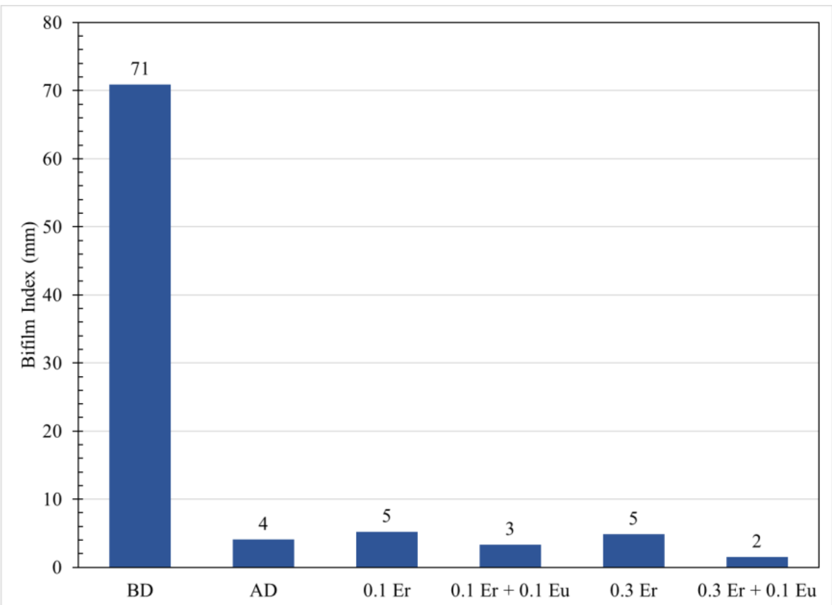

Figure 3.11 : Bifilm index values of different addition.

Colombo, M., et al. determined that the pore size and number increased with the addition of Er [27]. On the other hand, Li, J. H., et al. showed the eutectic Si modification with the addition of Eu was shown by CT investigation to reduce the size and size distribution of casting defects [28].

3.2.3 Grain size

The different alloying images created by combining photographs taken under polarized light after etching were shown in Figure 3.12 to reflect the overall grain size. Images at 50x magnification at different alloying ratios are illustrated at Figure 3.13.

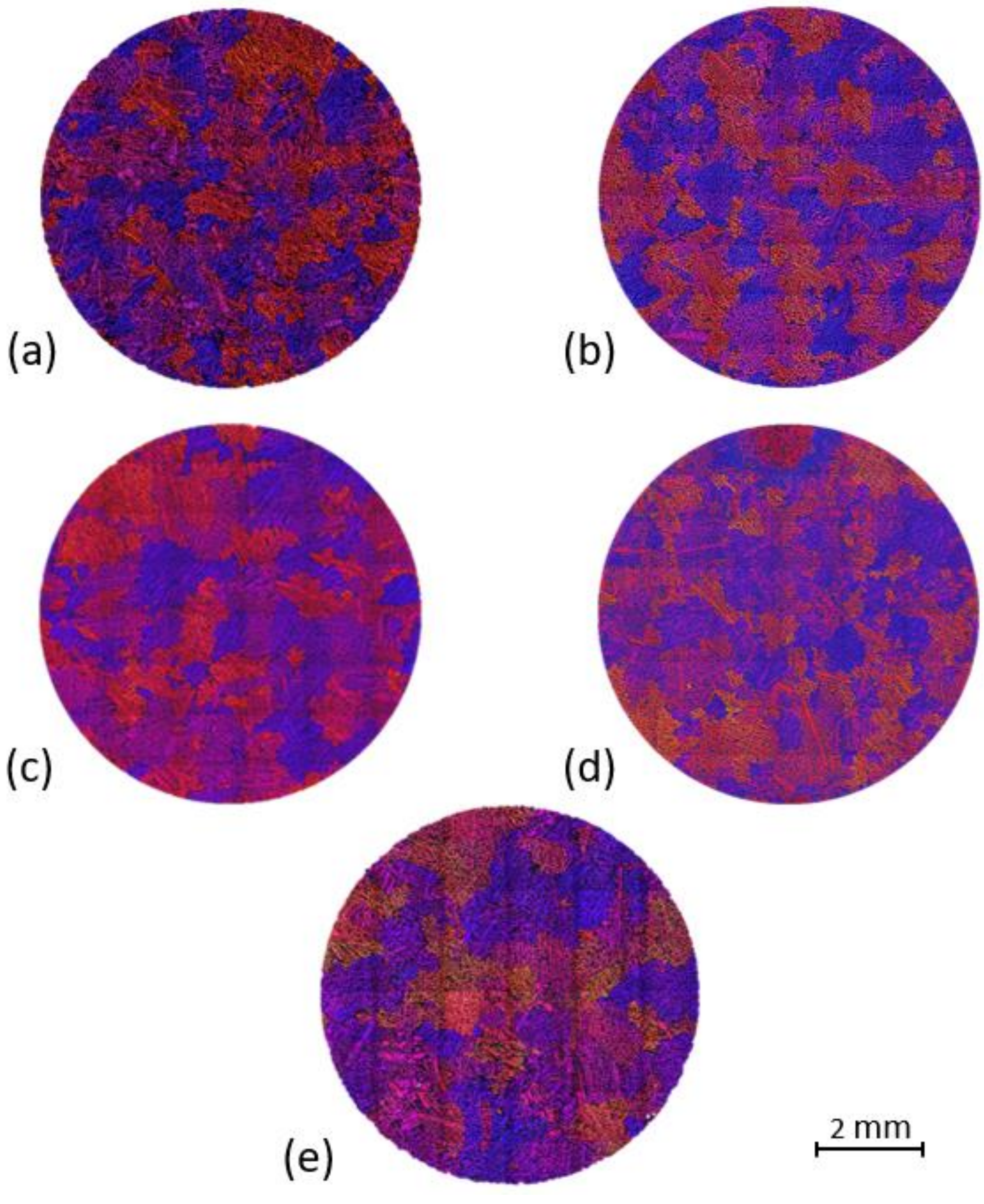

Figure 3.12 : Overall grain size (a) 0.0, (b) 0.1 Er, (c) 0.1 Er + 0.1 Eu, (d) 0.3 Er, (e) 0.3 Er + 0.1 Eu.

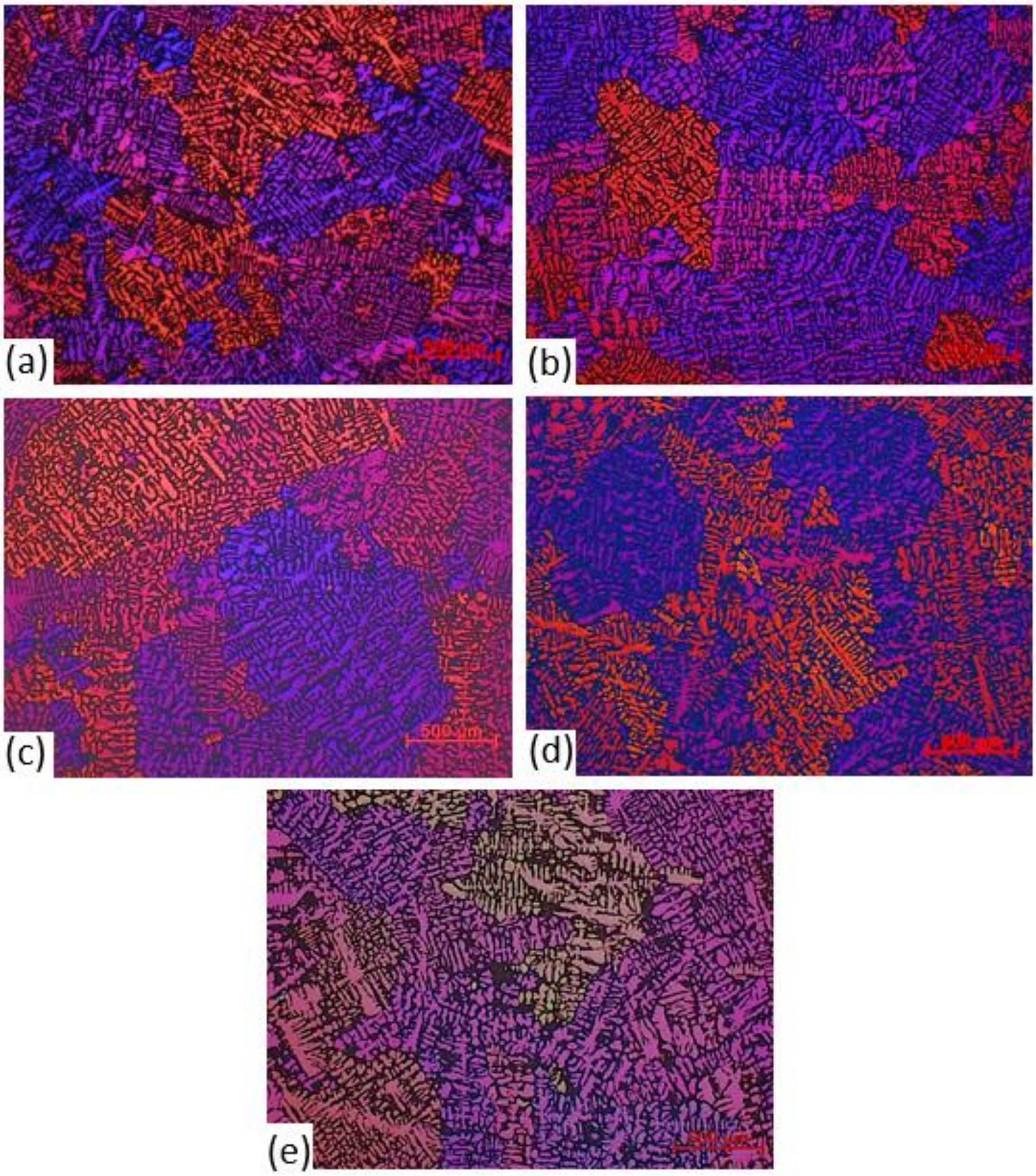

Figure 3.13 : Microstructure images with different alloying additions (a) 0.0, (b) 0.1 Er, (c) 0.1 Er + 0.1 Eu, (d) 0.3 Er, (e) 0.3 Er + 0.1 Eu.

The grain size of the sample that was not heat treated with the addition of 0.0 alloy was 789 µm. While there was not much change with the addition of 0.1 wt% Er, the grain size increased slightly to 795 µm, with the addition of 0.3 wt% Er and became 852 µm (Figure 3.14). On the other hand, grain coarsening was clearly seen with the addition of Eu on Er. There was 25% grain coarsening with 0.3 Er + 0.1 Eu addition wt%. The highest grain coarsening of 31% was obtained at 0.1 Er + 0.1 Eu addition wt% (Figure 3.15).

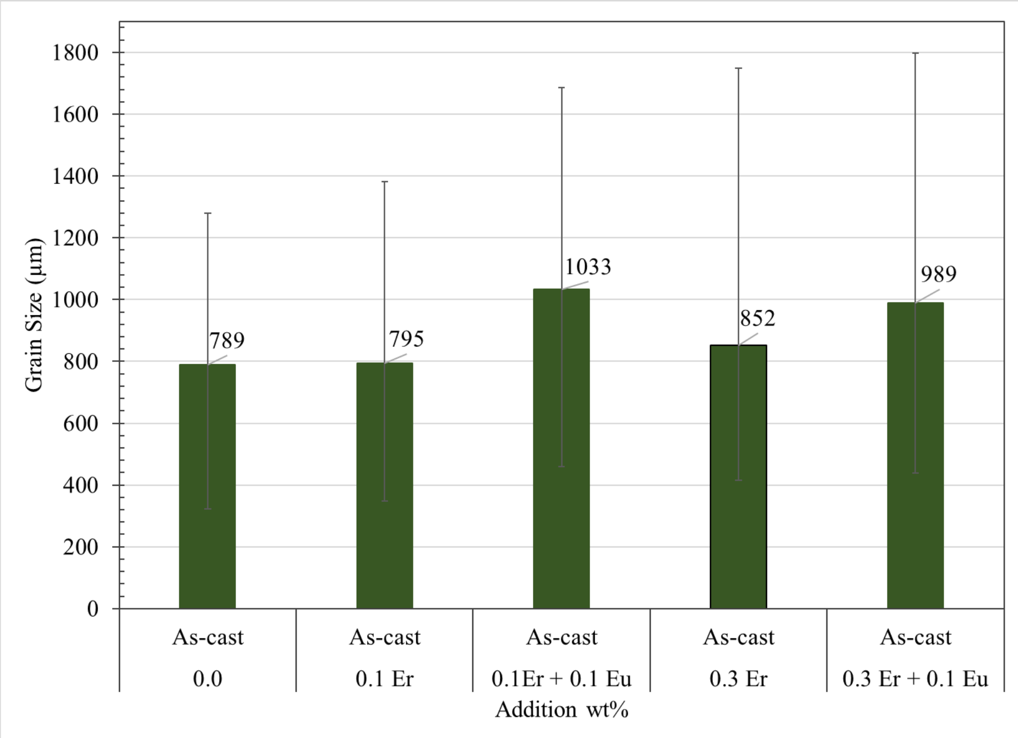

Figure 3.14 : Average grain size measurement in untreated alloy with different alloy addition.

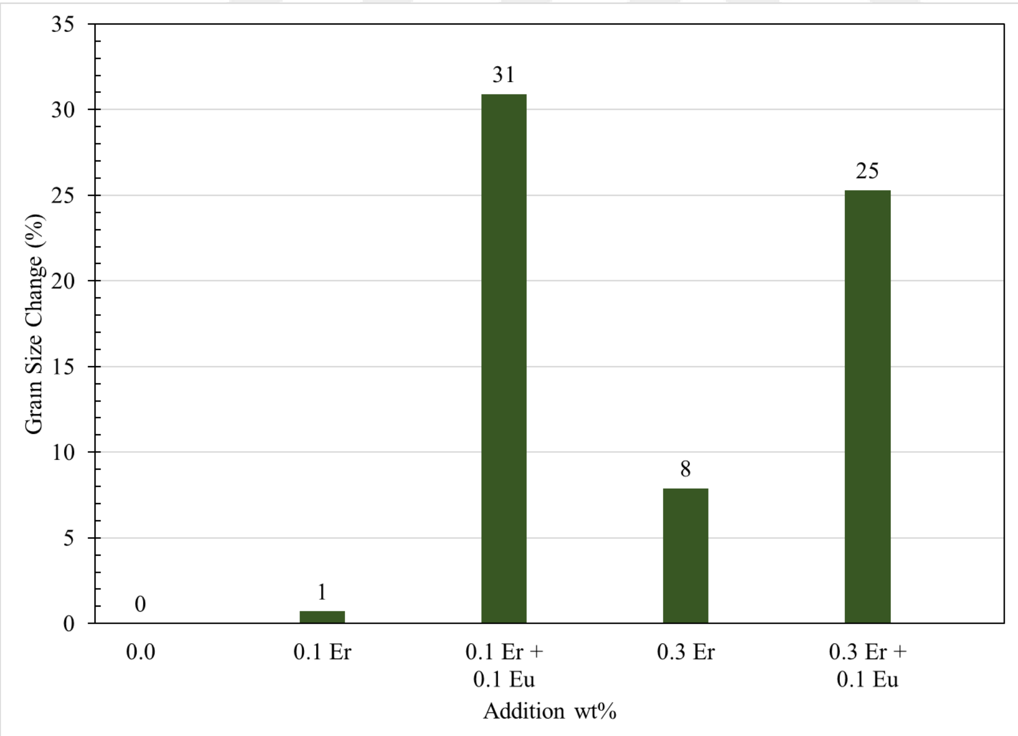

Figure 3.15 : Grain size change in untreated alloy with different alloy addition.

In t6 heat treated samples, the grain size of the 0.0 addition wt% was 950 µm (Figure 3.16). Grain refinement was achieved by adding 0.1 Er and 0.3 Er wt% to the heat-treated A356 alloy (811 and 873 µm respectively), different from the non-heat-treated samples. However, grain coarsening with the addition of Eu was observed in heat-treated and non-heat-treated A356 alloys. The best grain refinement effect with 32% was gained at 0.3 wt% Er addition. On the other hand, %8 grain coarsening was obtained with the addition wt% of 0.1 Er + 0.1 Eu (Figure 3.17).

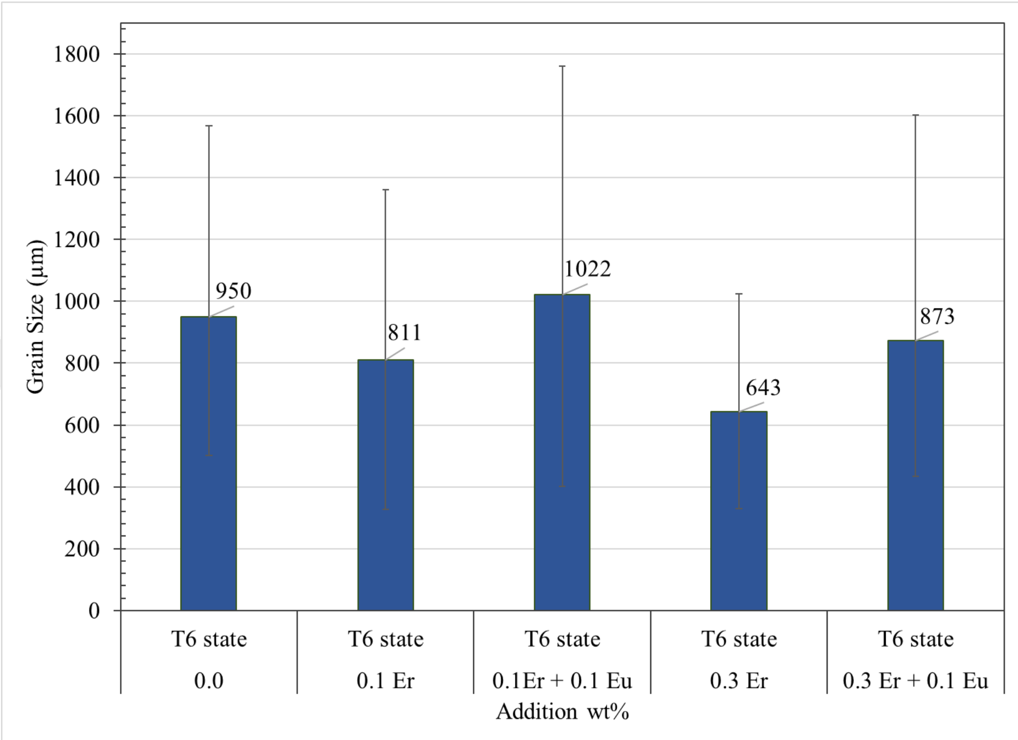

Figure 3.16 : Average grain size measurement in heat treated alloy with different alloy addition.

In the Al-Er phase diagram (Figure 1.25), in additions of 0.1 Er and 0.3 Er wt%, the Al3Er particle formed first during solidification creates a heterogeneous nucleation point and causes grain refinement. When the Al-Eu phase diagram is examined, since the α-Al and then the Al4Eu phase is formed in the 0.1 Eu wt% addition during solidification, it cannot have a positive effect on grain refinement.

Niazi et al. worked on the effects of different Er addition rate (0, 0.2, 0.4 and 0.6 wt%) on permanent mold. The best grain refinement effect was obtained at the addition of 0.2 Er wt%. With the increase of Er addition amount, grain coarsening was obtained [29].

Qi, Peng, et al. investigated the effect of 0, 0.1, 0.3, 0.5 and 0.8 Er wt% addition with electromagnetic stirring in semi solid A356 alloy. With 0.4 Er wt% addition, α-Al grain refined well. [30].

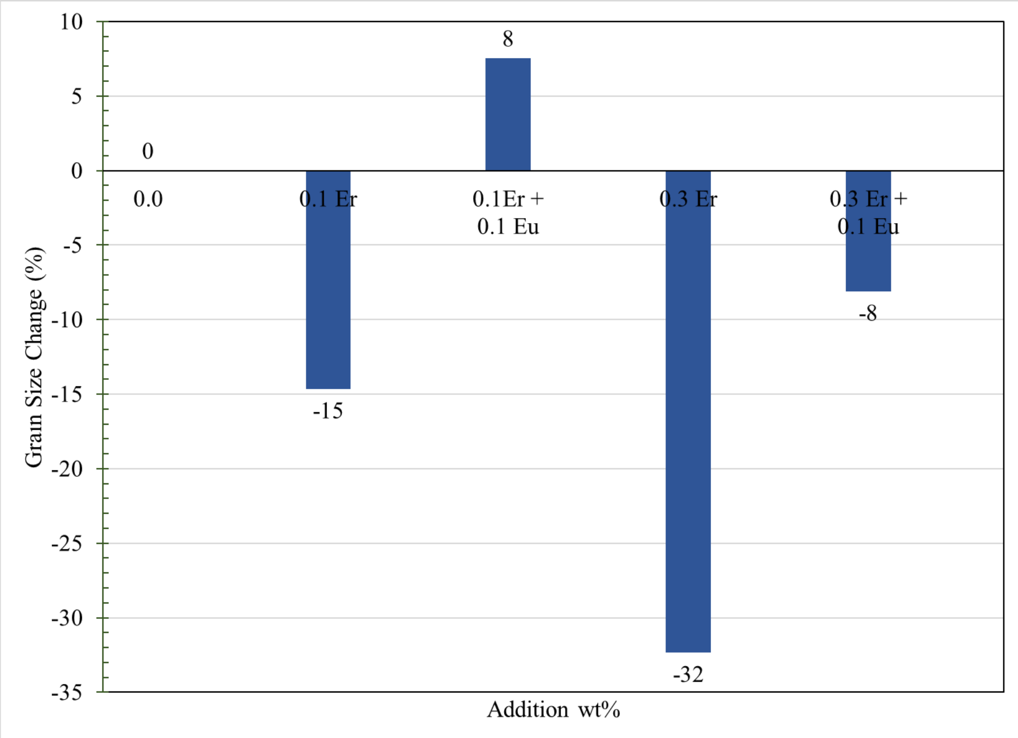

Figure 3.17 : Grain size change in heat treated alloy with different alloy addition.

Er and Zr different amount of combination were added to the A356 alloy at rates of 0, 0.15, 0.3, 0.5, 0.6 and 0.8 wt% by Ji, Liantao, et al. T6 heat treatment was carried out to examine the heat treatment effect in these additions. The best result was obtained with the addition of 0.3 Er-Zr wt% addition in heat treated and non-heat treated samples. The best grain refinement was observed in that addition [31].

The effect of addition of Er up to 0.6 at 0 with an increase of 0.2 wt% in A356 was investigated at two different cooling rates and as-cast, T6 heat-treatment conditions by Pandee, P., et al. While the grain size dramatically decreased with the addition of Er at the 1ºC /s cooling rate. The grain refinement effect was also observed at the 3ºC/s cooling rate. The maximum α-Al refinement effect was observed in the addition of 0.4 Er wt%.There was no fading effect in grain size and eutectic morphology at the addition of 0.4 Er wt%. [32].

The effect of 0.0, 0.3, 0.6 wt% Er addition on A356 alloy was investigated by Colombo, M., et al. SDAS size decreased with the increase of Er addition [27].

The effect of addition of Er to A356 alloy with an increase of 0.1 from 0.0 to 0.4 wt%, before and after heat treatment was investigated by Shi, Z. M., et al. α-Al grains and eutectic Si morphology were refined with an increase of Er addition up to 0.3 wt%. When the amount of Er increased to 0.4 wt%, it had negative effect[33].

3.2.4 Si Morphology

3.2.4.1 As-cast

Si morphologies with different alloy addition as as-cast conditions are shown in Figure 3.18.

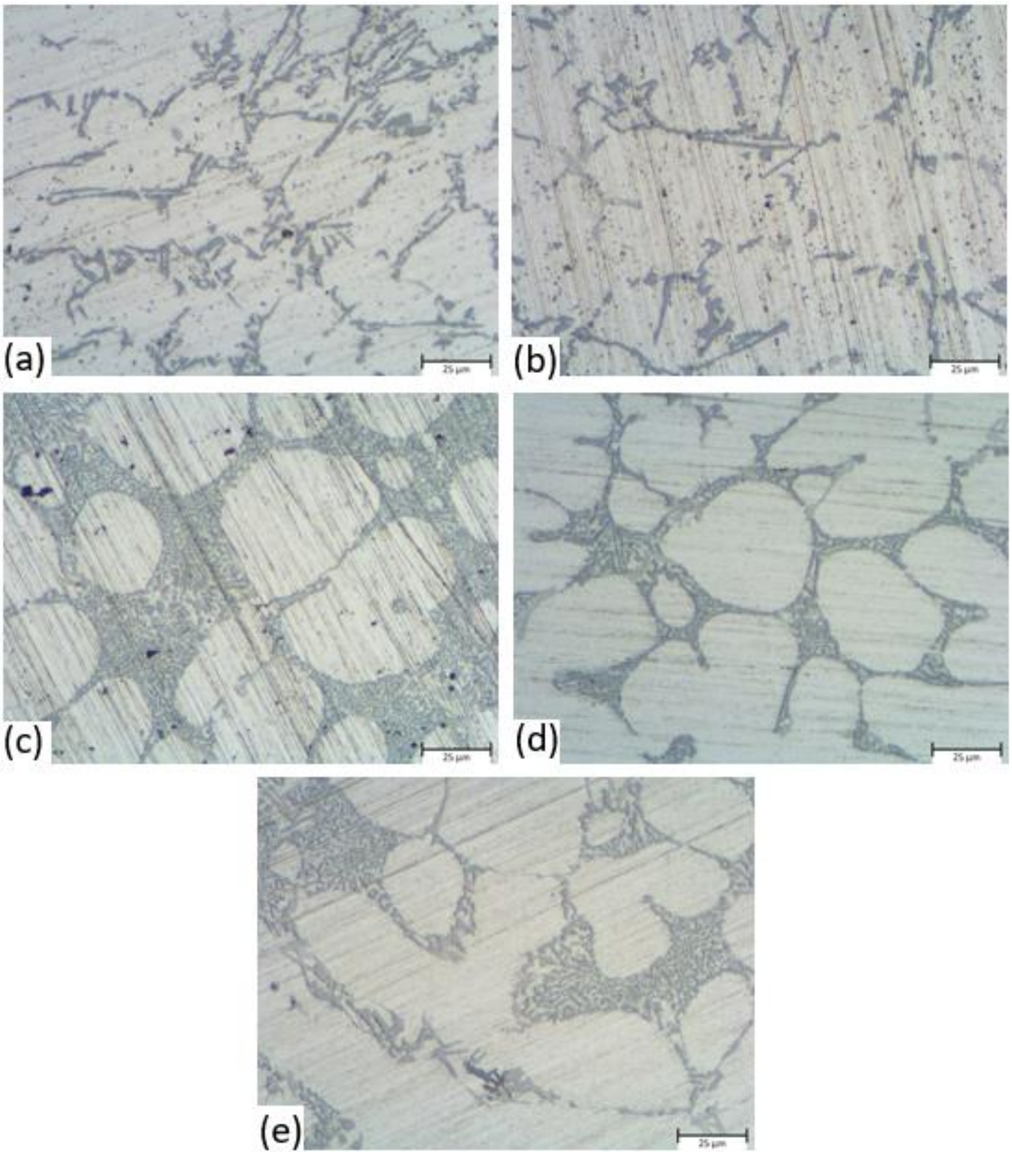

Figure 3.18 : Eutectic Si morphology in untreated with different alloying additions (a) 0.0, (b) 0.1 Er, (c) 0.1 Er + 0.1 Eu, (d) 0.3 Er, (e) 0.3 Er + 0.1 Eu.

With additions other than the addition of 0.1 wt% Er, Si was very well modified and decreased in length. With the addition of 0.1 Er + 0.1 Eu wt%, the Si length with the shortest average length was obtained 2.4 µm. Si length was reduced by 80% with this addition. When the amount of Er increased to 0.3 Er wt%, the modification effect on the Si size also increased. It decreased by 71.6% and reached an average of 3.4 µm(Figure 3.19).

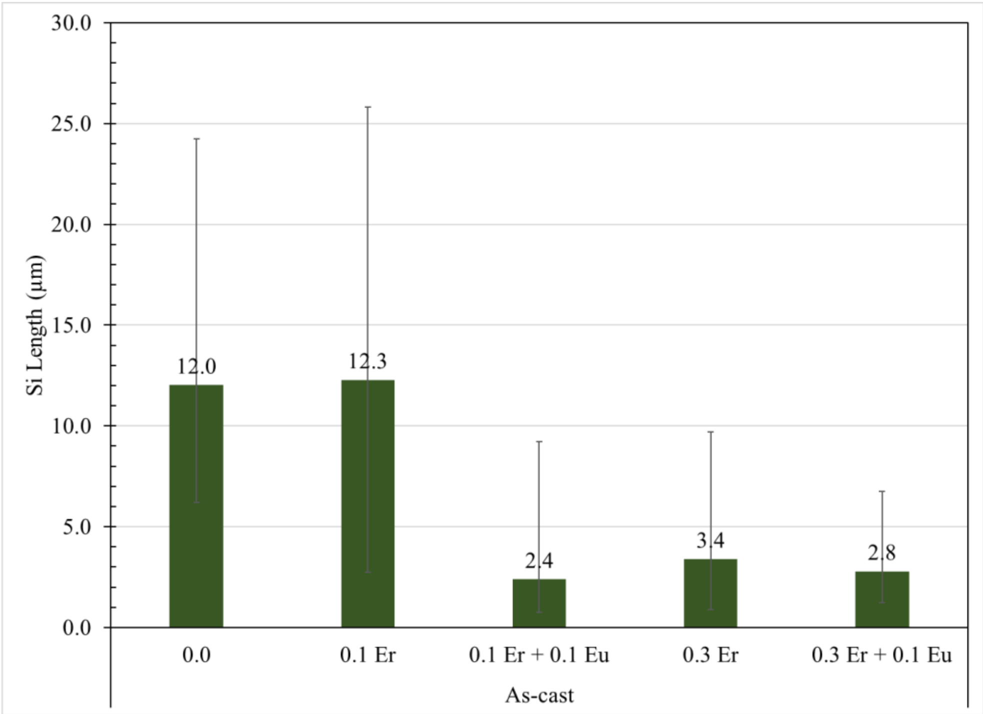

Figure 3.19 : Average eutectic Si measurement in untreated alloy with different alloy addition.

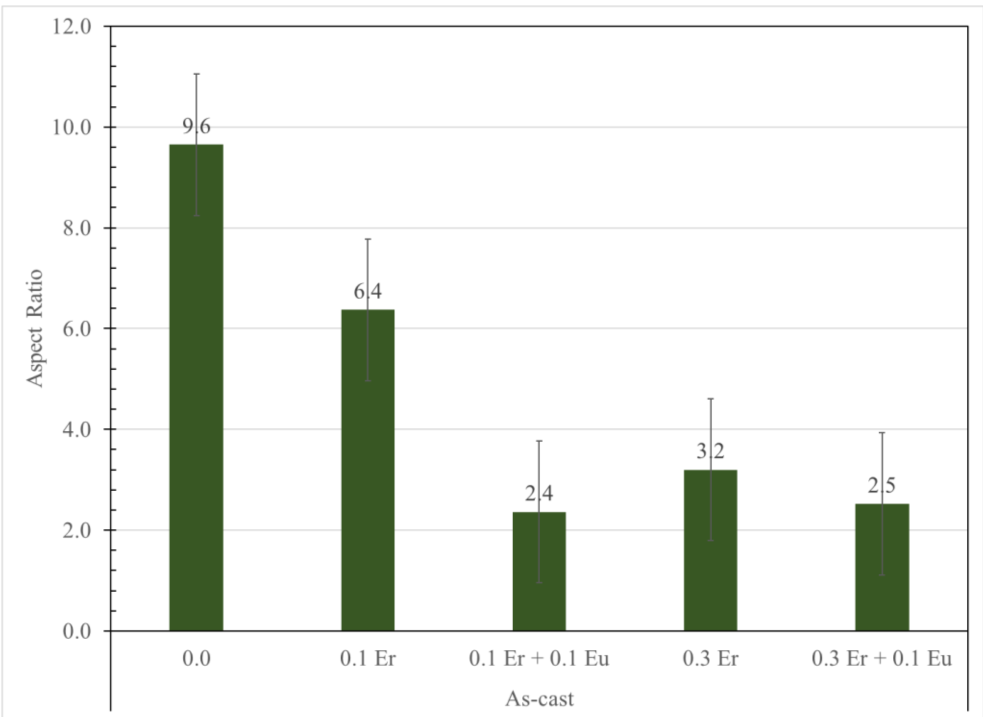

Figure 3.20 : Average eutectic Si aspect ratio measurement in untreated alloy with different alloy addition.

Si aspect ratio of unalloyed A356 alloy was 9.6 µm. Si was modified with the addition of alloying elements and the Si aspect ratio was decreased. As in Si aspect ratio and Si length, the best modification results were obtained when Er and Eu additions were together. With the addition of 0.1 Er + 0.1 Eu wt%, the aspect ratio was reduced by 64.6% and an average of 2.4 was reached (Figure 3.20).

3.2.4.2 T6 heat treated

The change in Si morphology with heat treatment is clearly seen in Figure 3.21. Si flake like morphology was spheroidized.

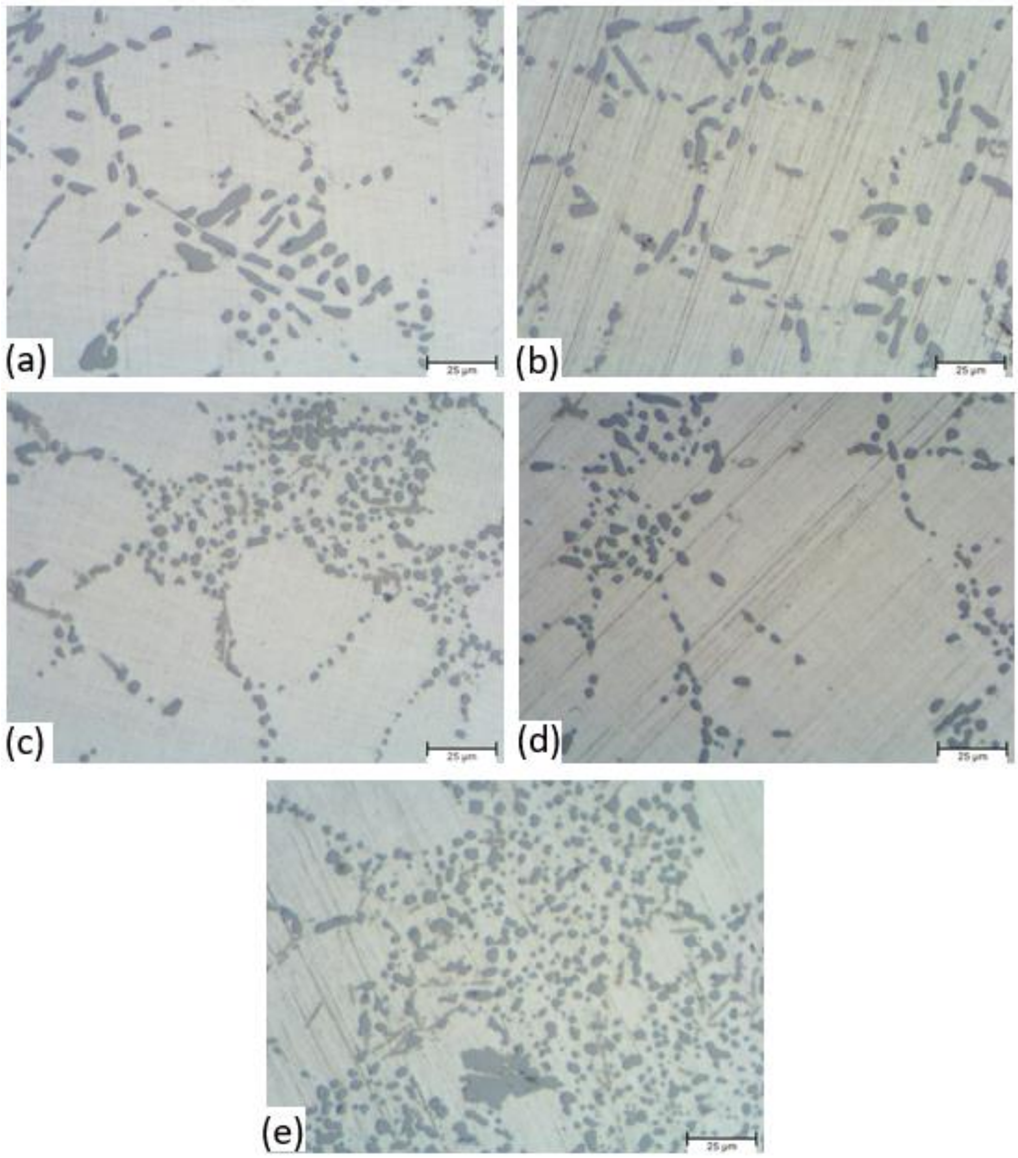

Figure 3.21 : Eutectic Si morphology in heat treated with different alloying additions (a) 0.0, (b) 0.1 Er, (c) 0.1 Er + 0.1 Eu, (d) 0.3 Er, (e) 0.3 Er + 0.1 Eu.

Although the scatter in Si length was high in the heat treated and non-alloyed A356 alloy, its average decreased by 51.7% from 12 to 5.8 µm. The lowest Si size was obtained with the addition of 0.1 Er + 0.1 Eu wt% and it was declined 51.7% to 2.8 µm (Figure 3.22).

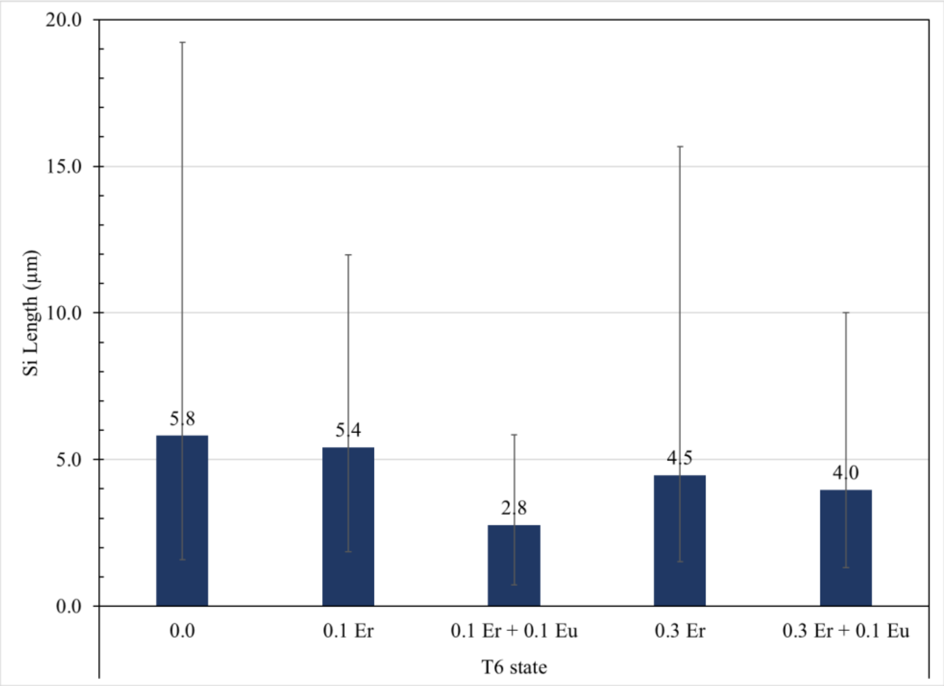

Figure 3.22 : Average eutectic Si measurement in heat treated alloy with different alloy addition.

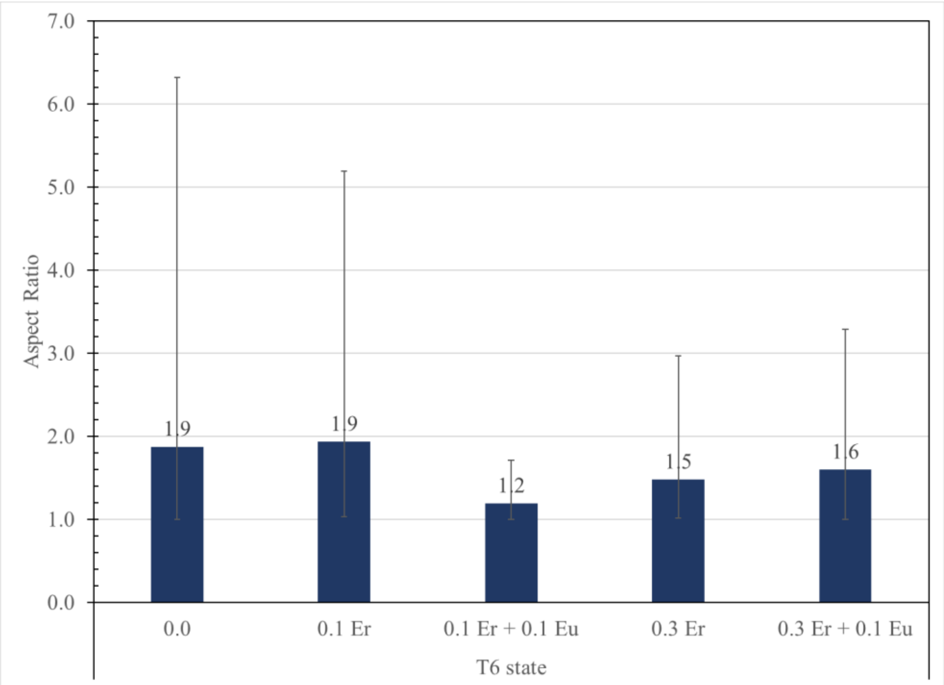

Figure 3.23 : Average eutectic Si aspect ratio measurement in heat treated alloy with different alloy addition.

Even though, the Si distribution was also high in the aspect ratio, the aspect ratio was reduced by 80.2% to 1.9 without alloying with T6 heat treatment state. The addition of 0.1 Er + 0.1 Eu wt% again had the best Si aspect ratio. It was 1.2 and decreased by 80%. It was seen that the scattering of values was very low (Figure 3.23).

Although the main purpose of the Er addition is to refine the α-Al grain, it is also seen the literature that Er addition also modifies the eutectic Si phases from need-like, flake to fine, spherical shape. [30-32].

Mao, Feng, et al. Added Eu to the Al-7Si alloy in an increment of 0.05 from 0 to 0.3 wt%. No modification was not observed up to the addition of 0.1 Eu wt%. The eutectic Si was completely modified at the addition of 0.1 Eu wt%. When the amount of Eu increased, there was no over modification [22].

Different ratios of Eu (0-0.05-0.1-0.2 wt%) were added to high purity Al-16Si, commercial purity and commercial purity Al-16Si-0.06P alloy by Mao, Feng, et al. The eutectic Si modification increased with increase of Eu addition in Al-16Si alloy. While the eutectic Si phases were coarsened by the addition of Eu, the eutectic Si phases were modified with the addition of P until the addition of 0.15 Eu wt% in the commercial purity Al-16Si alloy. It showed the importance of the purity of the master alloy in Figure 3.24 [34].

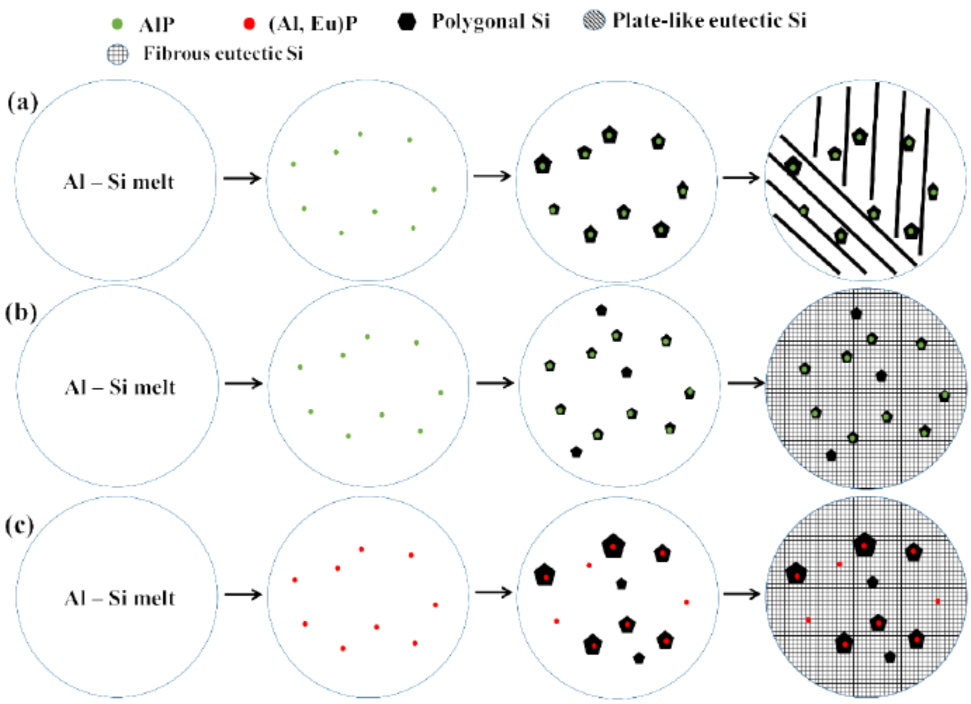

Figure 3.24 : The effect of the amount of Eu on the refinement mechanism (a) unchanged (b) 0.15% Eu (c) 0.2% Eu [34].

Li, J. H., et al. investigated the effect of combination of Eu (0-50-100-200 ppm) and P (0-3-10 ppm) addition in the Al-5Si, Al-7Si-0.7Mg-0.2Mn and Al-10Si-0.7Mg-0.2Mn alloys. When Eu and P were added together, the eutectic Si was better modified [28].

The addition of Eu with an increase of 0.02 from 0 to 0.1 wt% in A356 alloy with and without heat treated was investigated by Mao, Feng, et al. The decrease was observed in Si area, Si aspect ratio, SDAS value and primary α-Al with T6 state and as-cast condition. [36].

0.05 Eu was added to the Al-5Si alloy by Li, J. H., et al. It modified eutectic Si [24].

3.2.5 Tensile test

3.2.5.1 As-cast

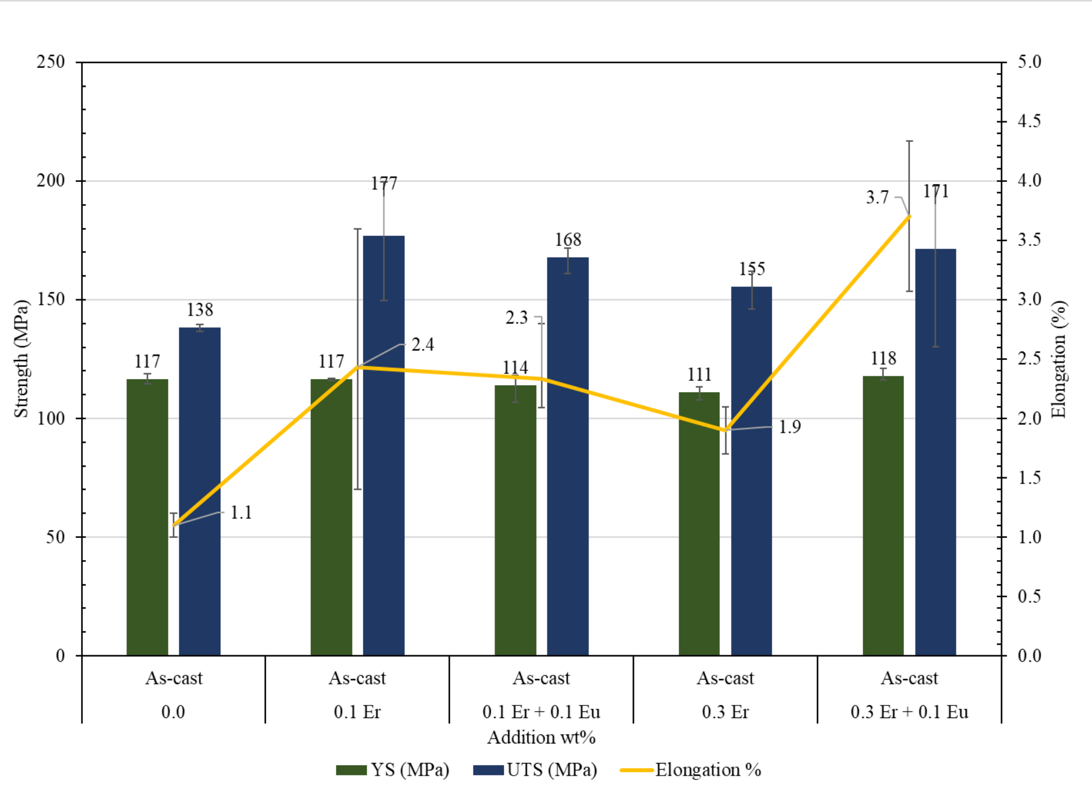

Figure 3.25 : Untreated tensile test result in different alloy additions.

Yield strength (YS), ultimate tensile strength (UTS) and % elongation (%e) obtained from the tensile test results without heat treatment samples were given in Figure 3.25. There was not change in YS, which was 117 MPa before the alloying element addition. On the other hand, with the addition of alloying element, UTS and %e values were improved. The best UTS and %e values were obtained at 0.1 Er wt% and 0.3 Er + 0.1 Eu wt% (177 MPa, 171 MPa UTS and 2.4%, 3.7% %e repectively)

3.2.5.2 T6 heat treated

The tensile test results of T6 treated samples are given in Figure 3.26. While there was a slight improvement in YS with the addition of alloying element. There was a clear improvement in UTS and %e. The highest YS and UTS values were achieved with the addition of 0.1 Er wt% (250 MPa and 302 MPa, respectively). The best %e value was 2.4% and it was obtained with the addition of 0.3 Er + 0.1 Eu wt%.

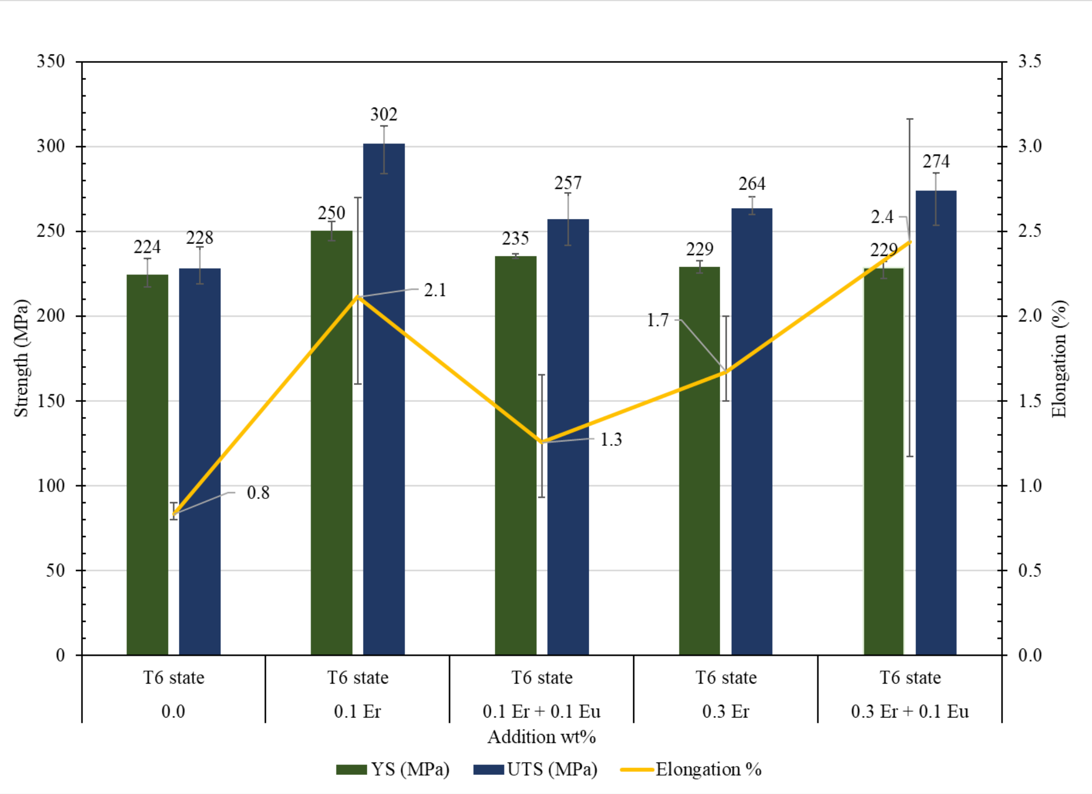

Figure 3.26 : Heat treated tensile test result in different alloy additions.

3.2.6 Hardness test

The hardness values increased more than 4 times with the heat treatment. The hardness value in the unalloyed A356 alloy was 11.5 HRB 10 in as-cast condition and 58.5 HRB10 in T6 state (Figure 3.27).

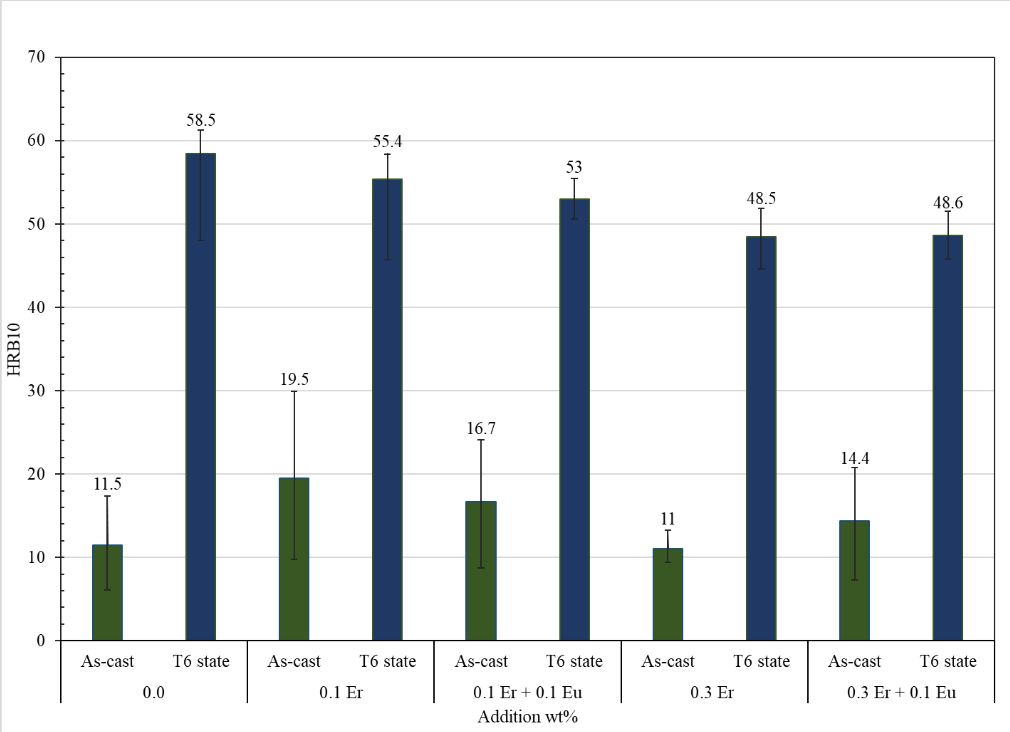

Figure 3.27 : Hardness test result in different alloy additions with and without heat treatment.

The hardness increased to 19.5 HRB 10 with the addition of Er in untreated condition. It was observed that the hardness value decreased at different addition rates (Figure 3.28).

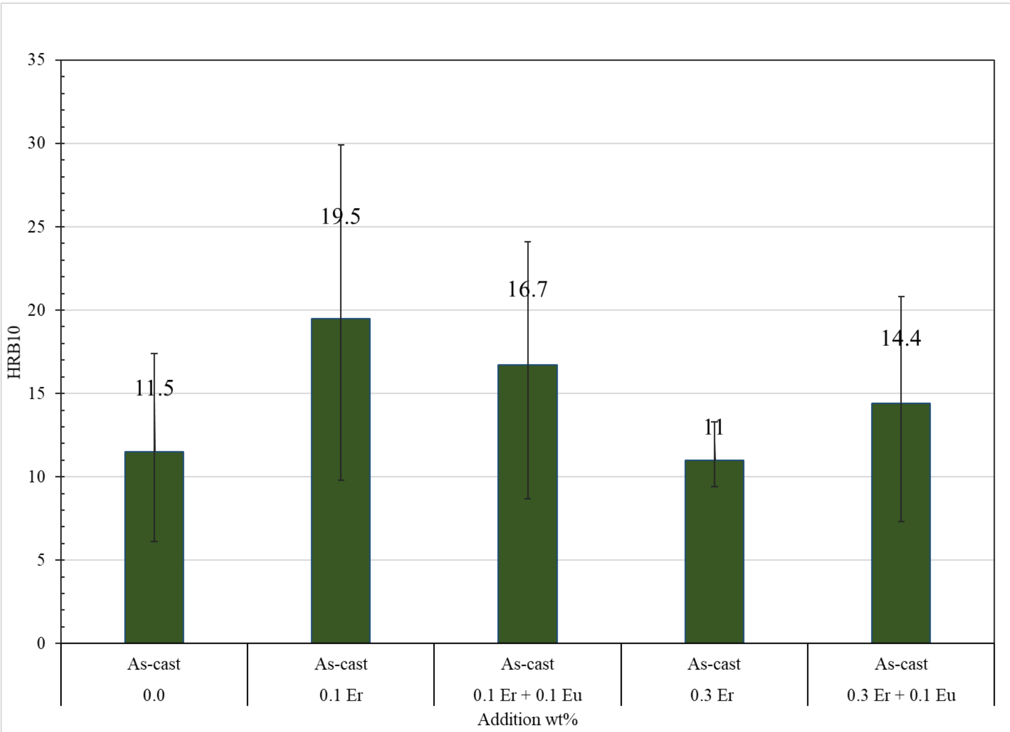

Figure 3.28 : Untreated hardness test result in different alloy additions.

The hardness of the heat-treated samples decreased slightly with the increase of alloy addition. The highest hardness was 58.5 HRB 10 without alloy addition (Figure 3.29).

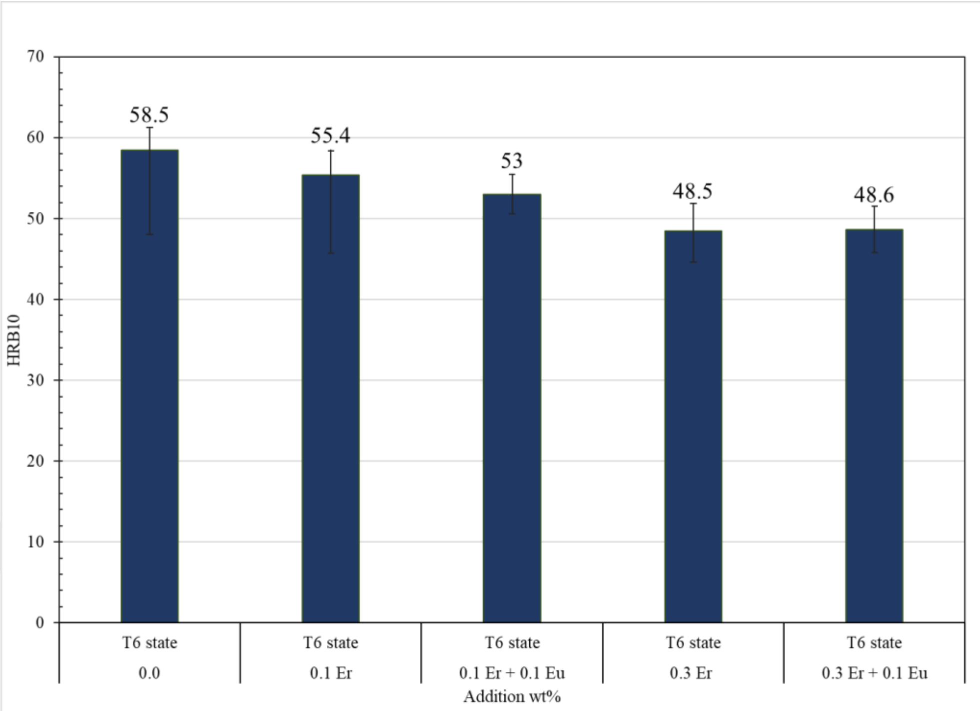

Figure 3.29 : Heat treated tensile test result in different alloy additions.

In many studies in the literature, it has been observed that the addition of Er to the A356 alloy improved the mechanical properties up to approximately 0.3 wt% Er addition, then adversely affects it both in as-cast and T6 heat treated [27,29,30,32,33].

Moreover, it has been shown in the literature that the addition of 0.1 Eu% improved the mechanical properties of Al-Si alloys [34,35].

3.2.7 Microstructure SEM Analysis

SEM images, EDX analysis and mapping analysis results containing different ratios of alloying elements with and without heat treatment were shown in Figure 3.30-3.48.

3.2.7.1 As-cast

It was seen that the intermetallic phases formed in the mapping analysis of the sample, which non-heat treated and without alloying addition, contained Mg and Fe. Dark colored intermetallic contained Mg, while the whiter colored ones contained high level of Fe (Figure 3.30). Mapping also showed these intermetallic phases include Mg and Fe (Figure 3.31).

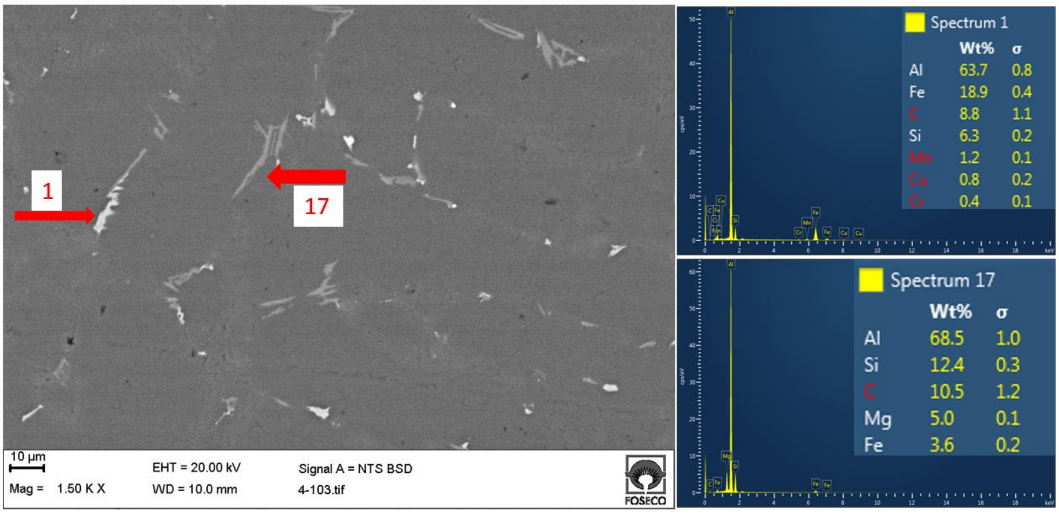

Figure 3.30 : SEM and point EDS analysis on unalloyed specimen without heat treatment.

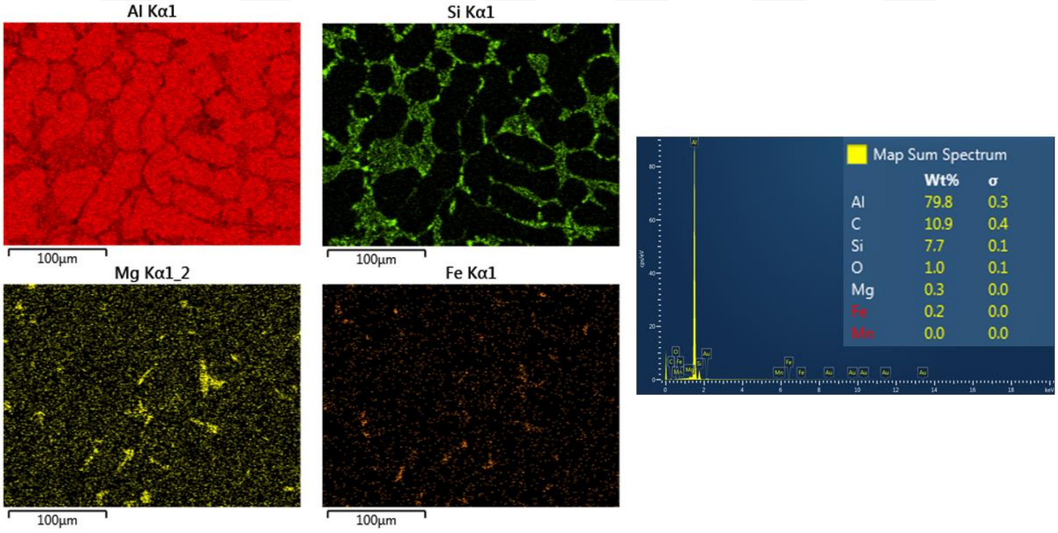

Figure 3.31 : Mapping analysis on unalloyed specimen without heat treatment.

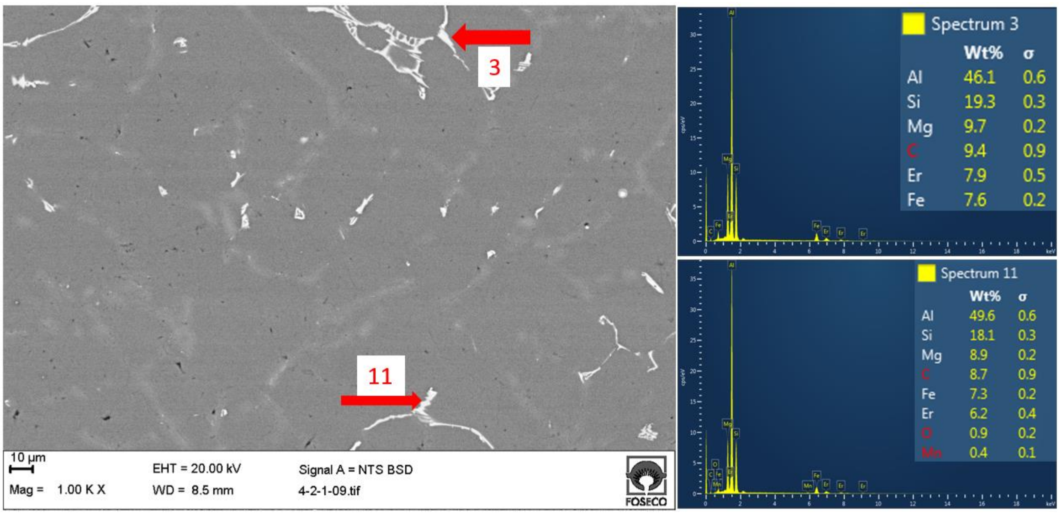

Figure 3.32 : SEM and EDS analysis in 0.1 Er alloy addition without heat treatment.

With the addition of 0.1 wt% Er, the size and number of white colored intermetallic containing Er, Mg and Fe increased (Figure 3.32). Mapping also show these intermetallic phases obtain Mg, Fe and Er (Figure 3.33).

Discontinues acicular intermetallic phases were observed in the addition of 0.1 Er + 0.1 Eu wt%. ın Figure x. Even tough, EDX results show there are around 5 % Er and Eu (Figure 3.34). Mapping did not show these phases (Figure 3.35).

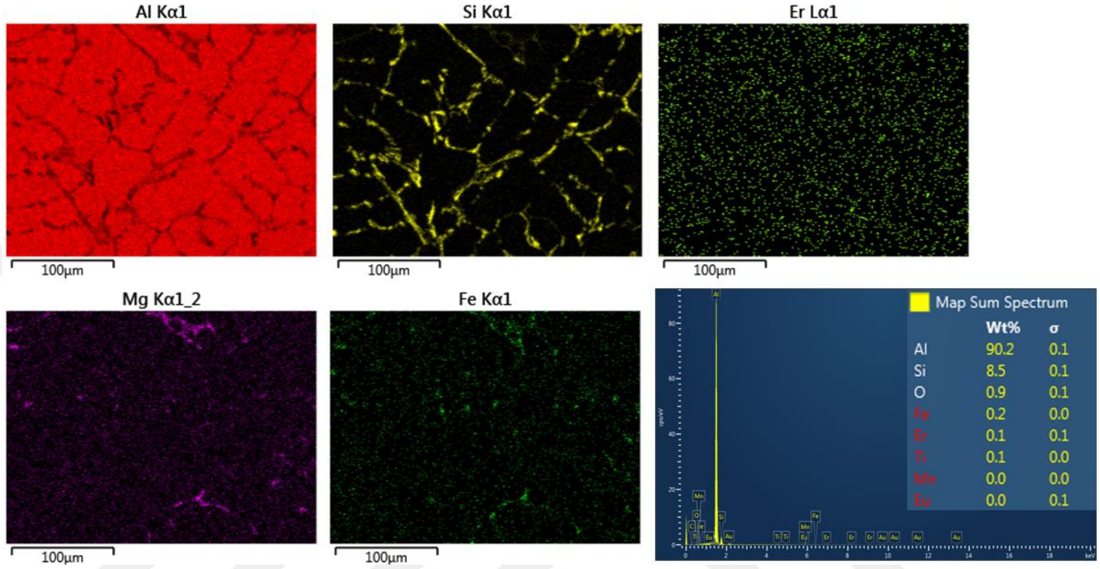

Figure 3.33 : Mapping analysis in 0.1 Er alloy addition without heat treatment.

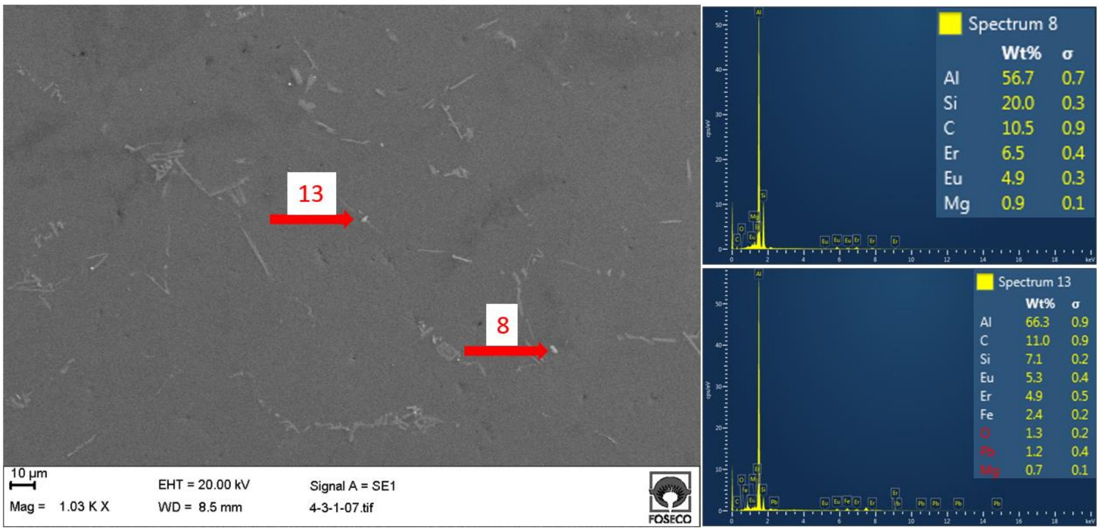

Figure 3.34 : SEM and EDS analysis in 0.1 Er + 0.1 Eu alloy addition without heat treatment.

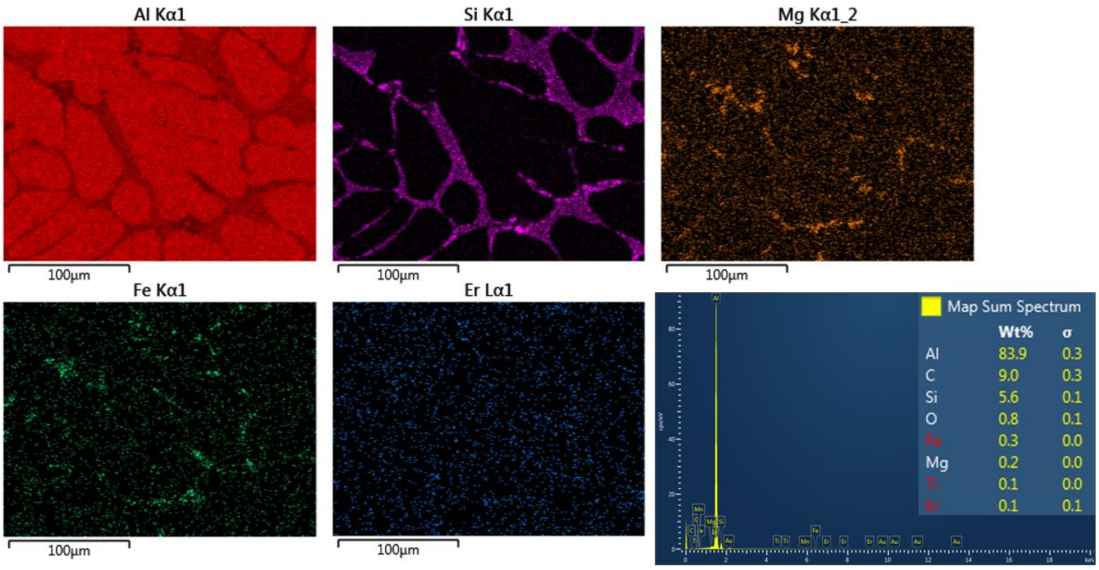

Figure 3.35 : Mapping analysis in 0.1 Er + 0.1 Eu alloy addition without heat treatment.

As the alloy addition increased to 0.3 Er wt%, coarsening was observed in the intermetallic dimensions, while the amount of Er contained in the intermetallic also increased (Figure 3.36). As the amount of Er increased, Er is getting more obvious in mapping (Figure 3.37).

It was observed that the intermetallic shrunk and turned into acicular phases with the addition of 0.3 Er + 0.1 Eu wt%. A chucky intermetallic of 35% Eu was observed (Figure 3.38). Mapping showed that many intermetallic phases contain Mg and Fe (Figure 3.39).

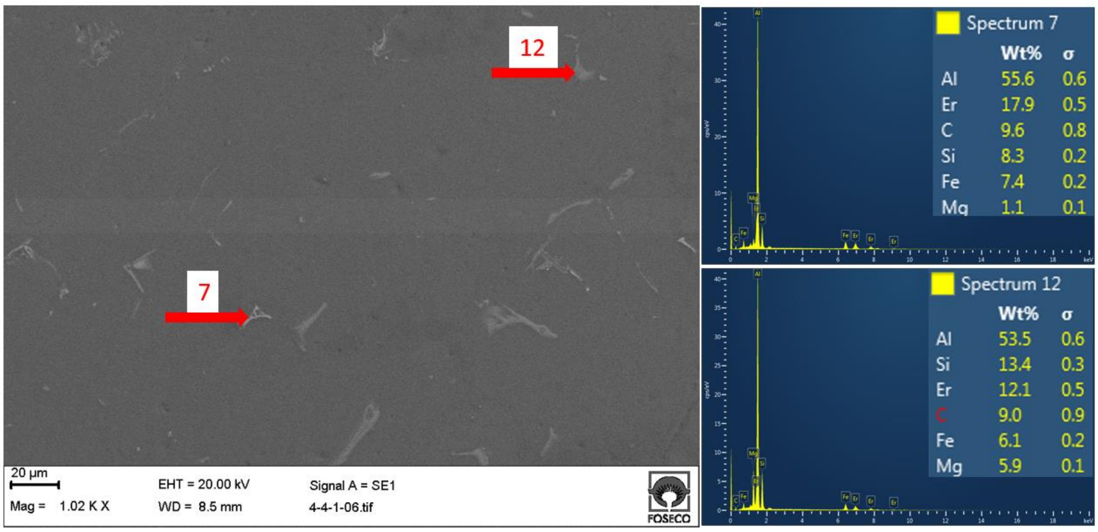

Figure 3.36 : SEM and EDS analysis in 0.3 Er alloy addition without heat treatment.

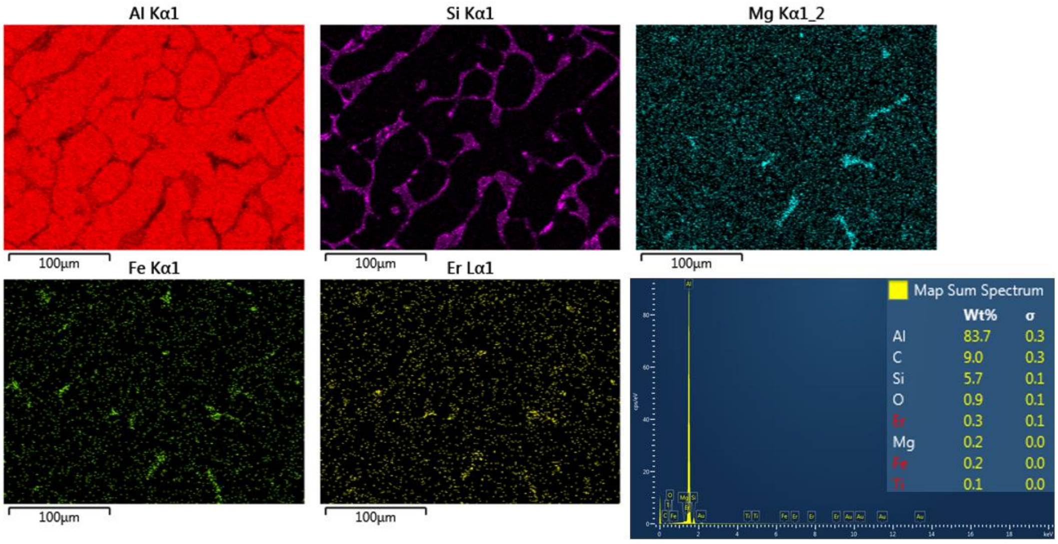

Figure 3.37 : Mapping analysis in 0.3 Er alloy addition without heat treatment.

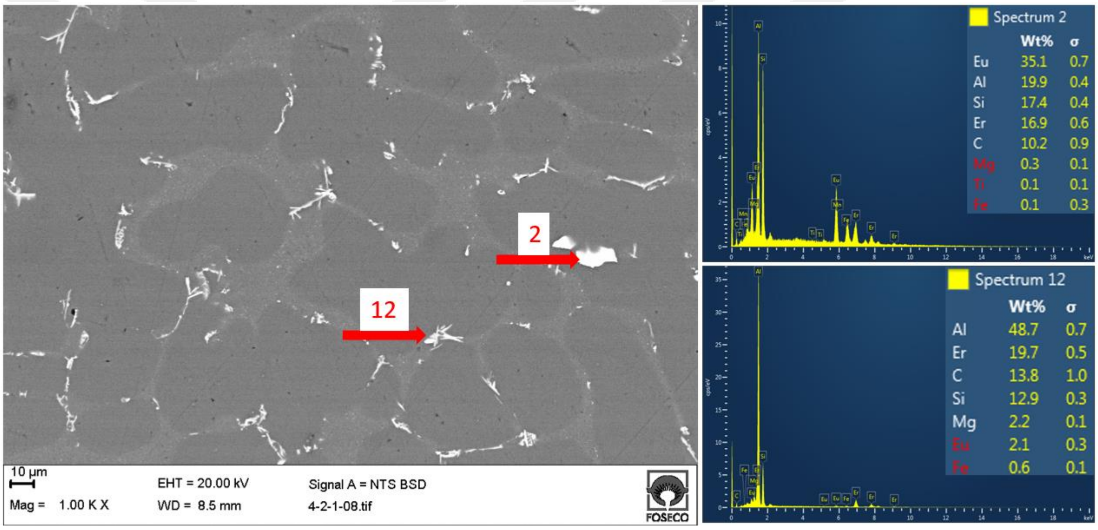

Figure 3.38 : SEM and EDS analysis in 0.3 Er + 0.1 Eu alloy addition without heat treatment.

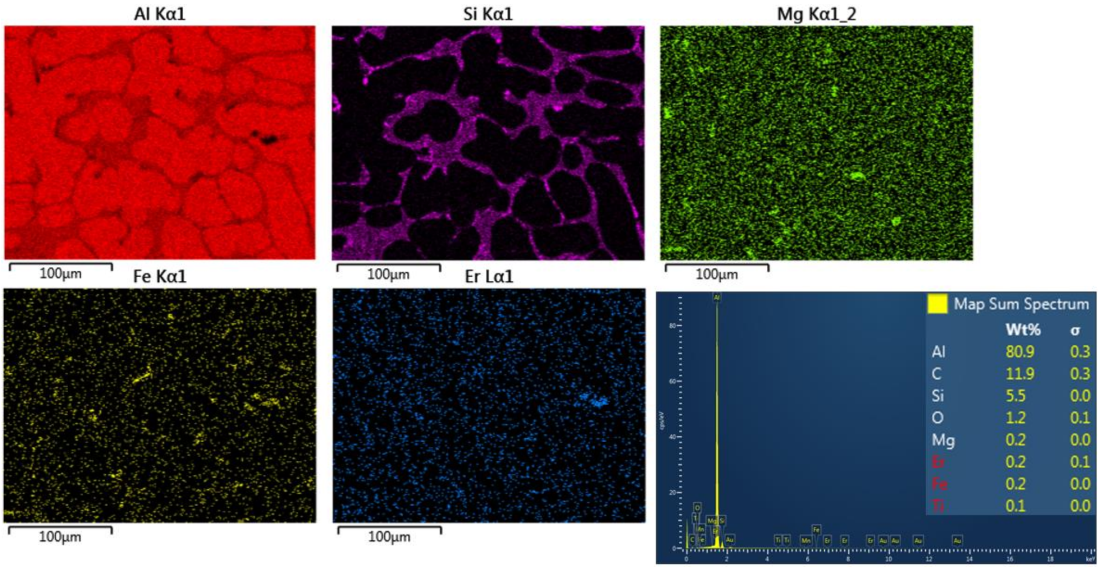

Figure 3.39 : Mapping analysis in 0.3 Er + 0.1 Eu alloy addition without heat treatment.

3.2.7.2 T6 heat treated

The intermetallic containing Fe shrank a little due to the heat treatment effect and the sharp corners of the some of the intermetallic were more rounded in non-alloyed t6 heat treated A356 alloy (Figure 3.40). In the mapping, the specificity of Mg decreased after heat treatment (Figure 3.41).

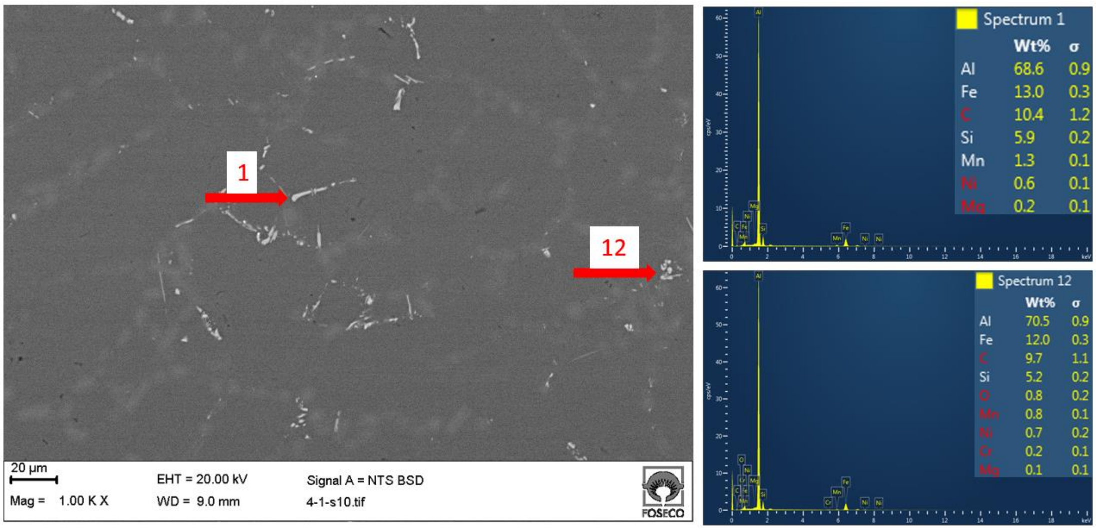

Figure 3.40 : SEM and point EDS analysis on unalloyed specimen with heat treatment.

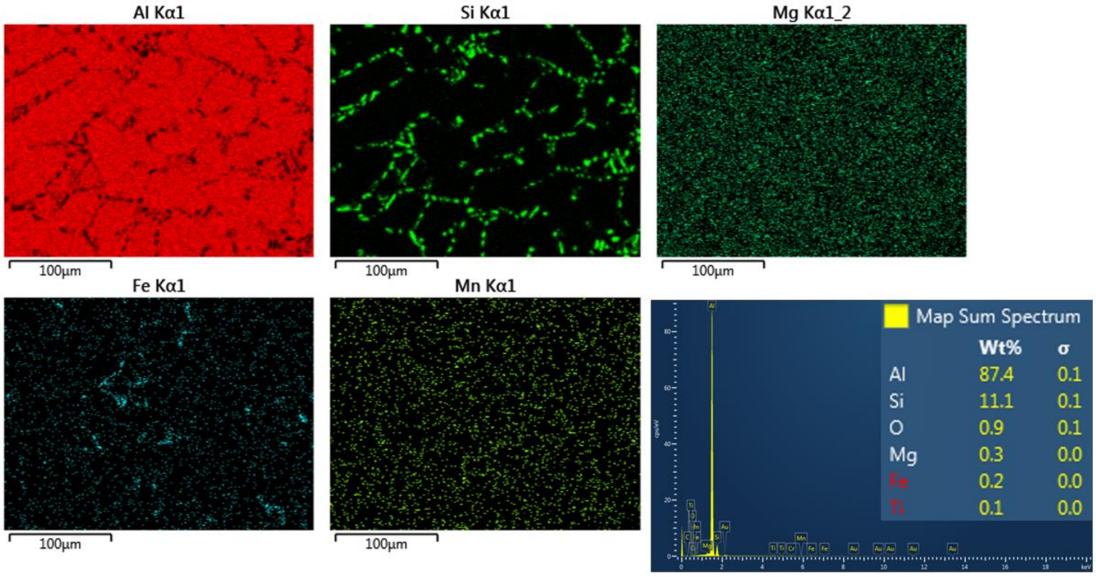

Figure 3.41 : Mapping analysis on unalloyed specimen with heat treatment.

With the addition of 0.1 Er wt%, small acicular intermetallic phases containing Er appeared whiter in the structure (Figure 3.42).

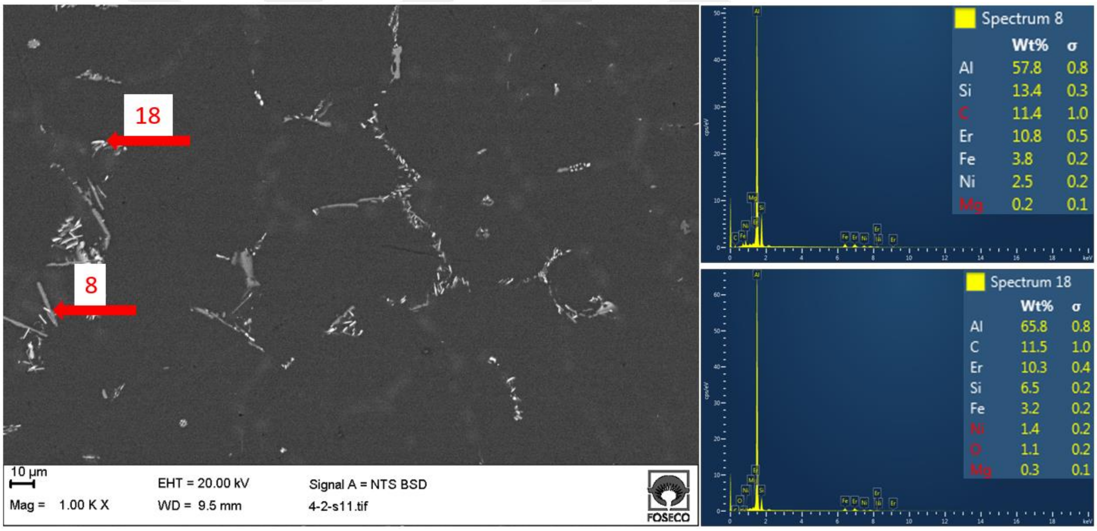

Figure 3.42 : SEM and EDS analysis in 0.1 Er alloy addition with heat treatment.

The waiter acicular intermetallics contained Er and Eu with addition of 0.1 Er + 0.1 Eu wt%. There was a chucky intermetallic containing 40% Er (Figure 3.42). In mapping and ED, Mg phases lost their prominence after heat treatment (Figure 3.43).

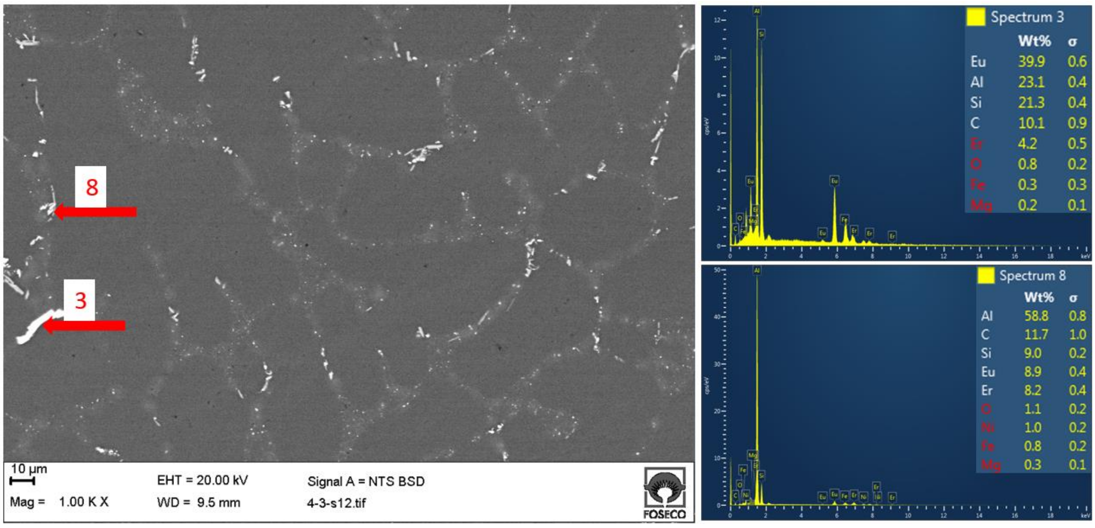

Figure 3.43 : SEM and EDS analysis in 0.1 Er + 0.1 Eu alloy addition with heat treatment.

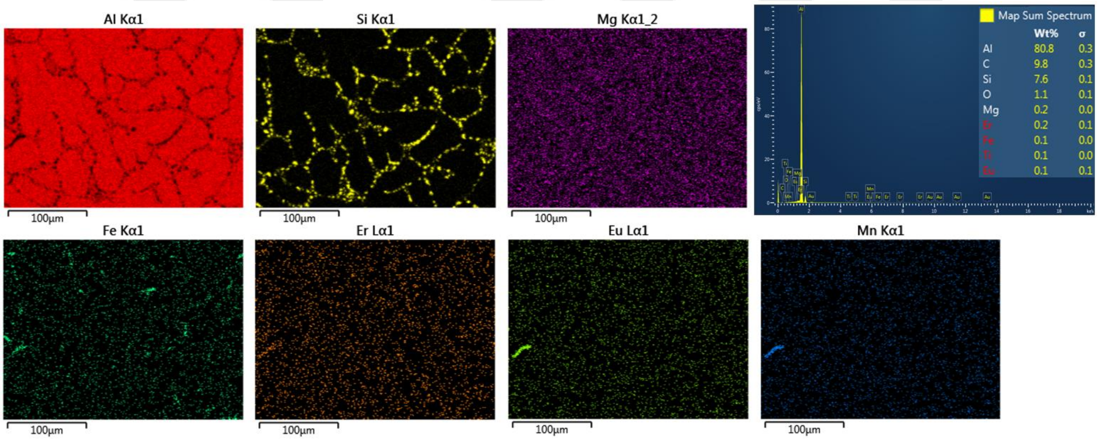

Figure 3.44 : Mapping analysis in 0.1 Er + 0.1 Eu alloy addition with heat treatment.

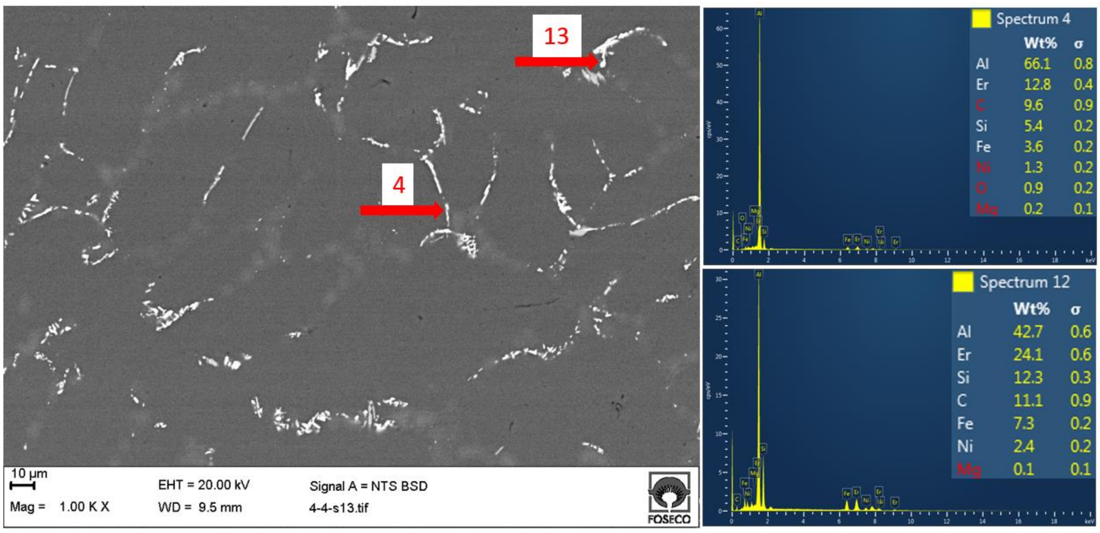

Figure 3.45 : SEM and EDS analysis in 0.3 Er alloy addition with heat treatment.

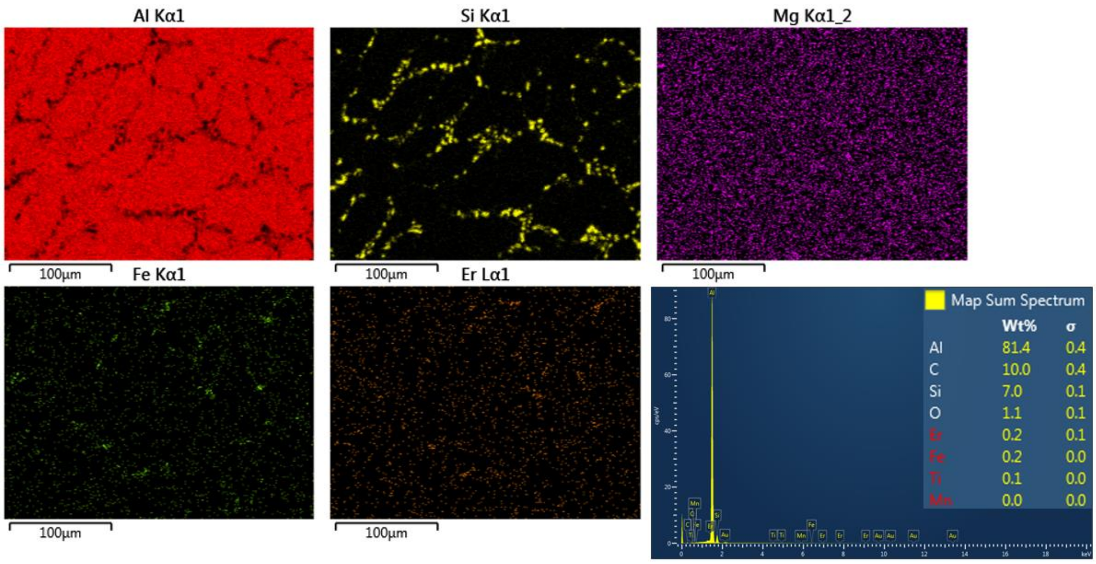

Figure 3.46 : Mapping analysis in 0.3 Er alloy addition with heat treatment.

As the amount of Er increased to 0.3 wt%, the amount of Er of the formed intermetallic phases increased and the number of white phases containing Er also increased (Figure 3.45). In addition, the Er phases became more distinct in mapping (Figure 3.46).

It contained white acicular intermetallic phases Er and Eu with the addition of 0.3 Er + 0.1 Eu wt% (Figure 3.47). In the mapping, Fe phases appeared very clearly, Er phases appeared vaguely, Mg and Eu phases were not seen (Figure 3.48).

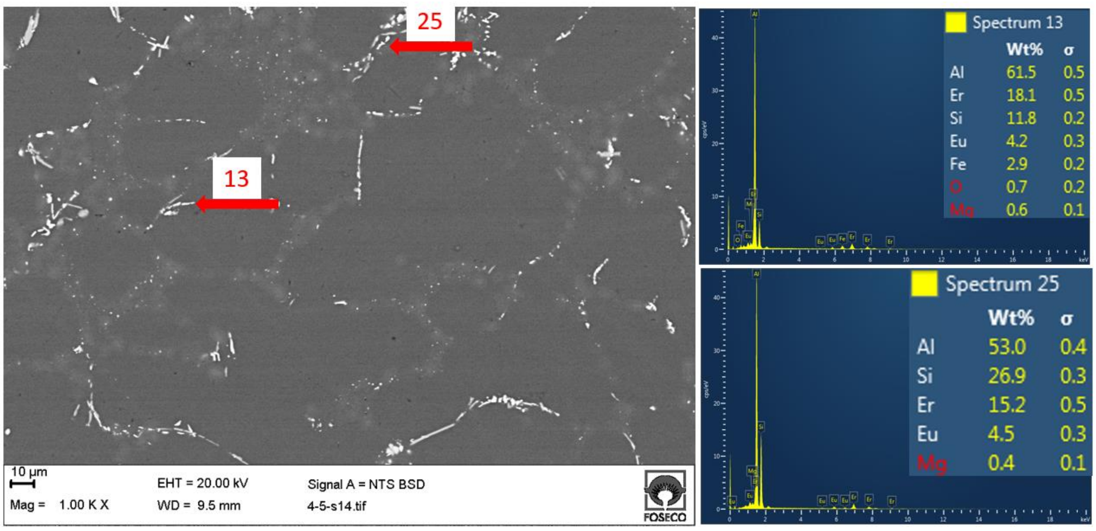

Figure 3.47 : SEM and EDS analysis in 0.3 + 0.1 Er alloy addition with heat treatment.

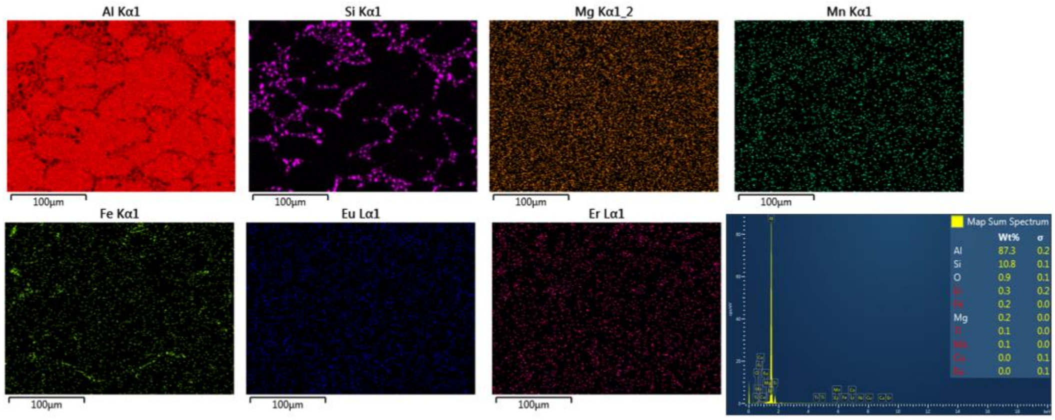

Figure 3.48 : Mapping analysis in 0.3 Er + 0.1 Eu alloy addition with heat treatment.

3.2.8 Fracture Surface SEM Analysis

3.2.8.1 As-cast

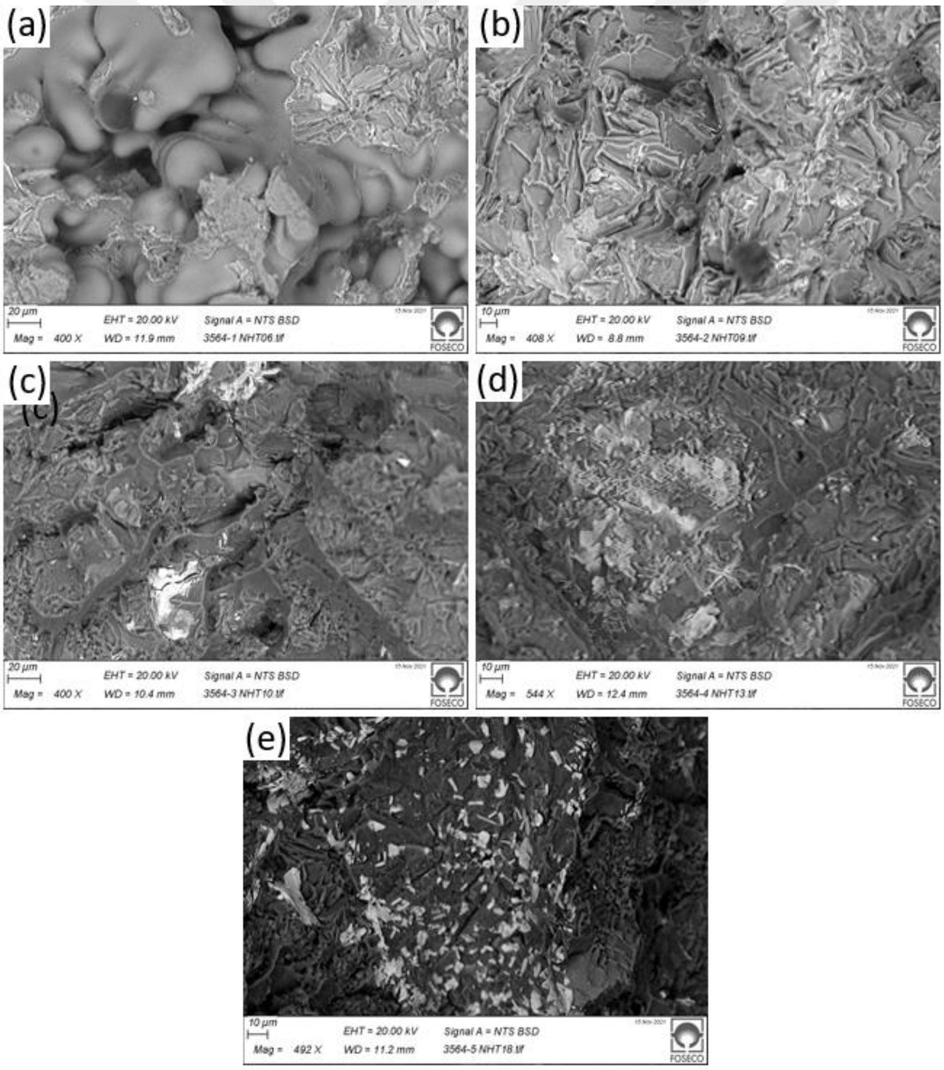

Figure 3.49 : SEM images of the as-cast condition fracture surfaces with additions (a) 0.0, (b) 0.1 Er, (c) 0.1 Er + 0.1 Eu, (d) 0.3 Er, (e) 0.3 Er + 0.1 Eu.

Figure 3.49 showed the SEM overview images of the as-cast condition tensile test sample fracture surface with different alloy addition rates.

It was seen that lighter colored structures on the fracture surface area are intermetallic containing Fe (Figure 3.50).

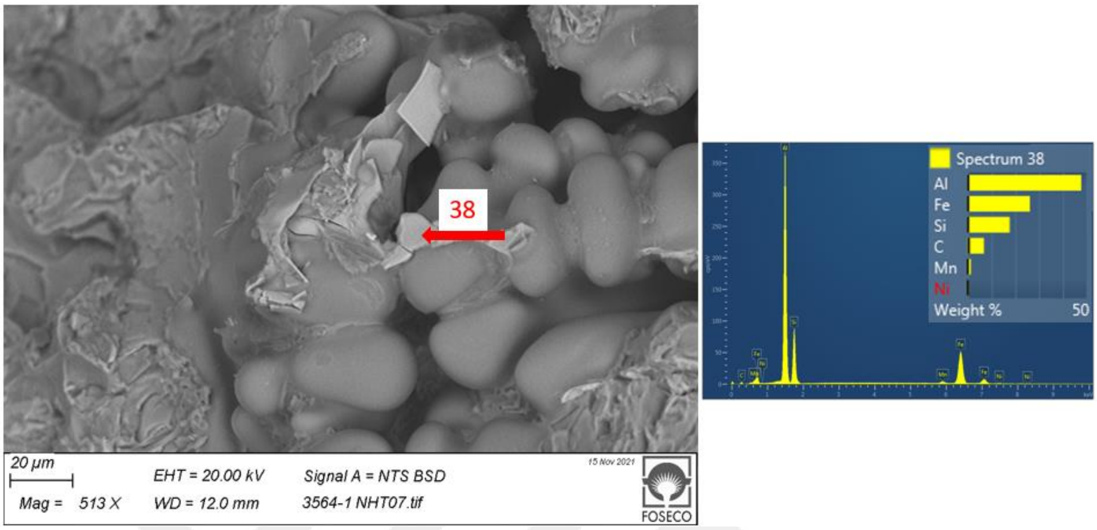

Figure 3.50 : SEM and EDS analysis of the as-cast condition tensile test sample fracture surfaces with 0.0 alloying addition.

It was shown in fig x that with the addition of 0.1 Er wt%, the fracture surface was covered by intermetallic phases and these phases containing Er and Fe (Figure 3.51).

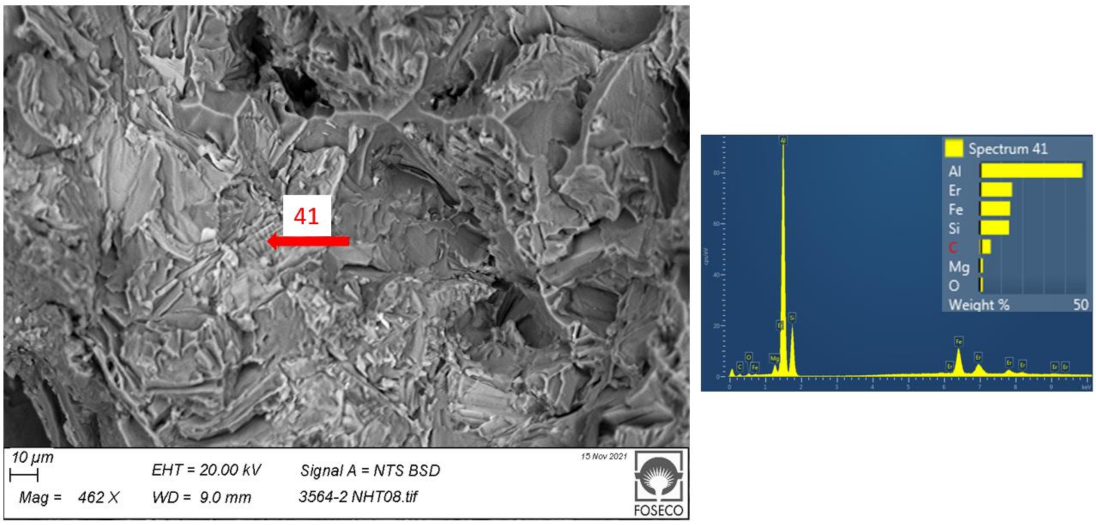

Figure 3.51 : SEM and EDS analysis of the as-cast condition tensile test sample fracture surfaces with 0.1 Er alloying addition.

The white phases clustered with the addition of 0.1 Er + 0.1 Eu wt% contained a high amount of Eu (Figure 3.52).

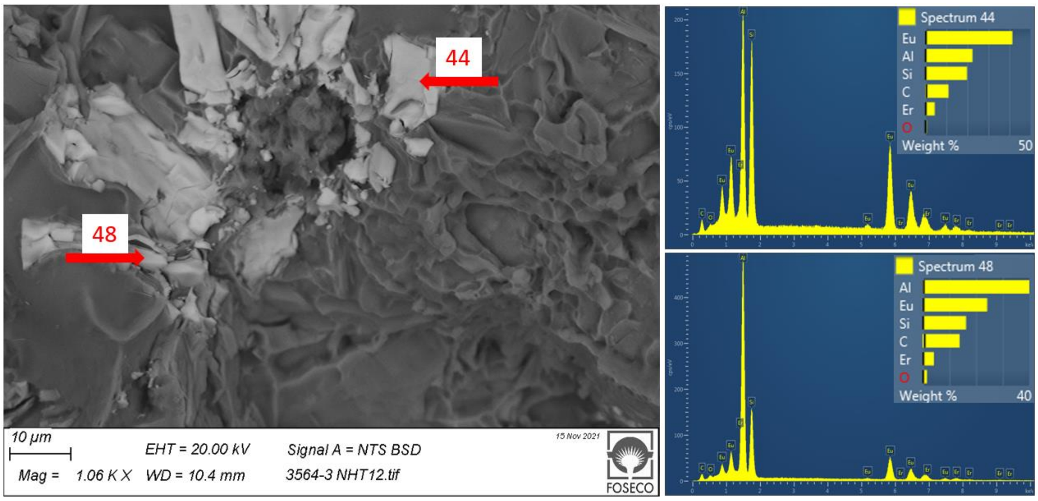

Figure 3.52 : SEM and EDS analysis of the as-cast condition tensile test sample fracture surfaces with 0.1 Er + 0.1 Eu alloying addition.

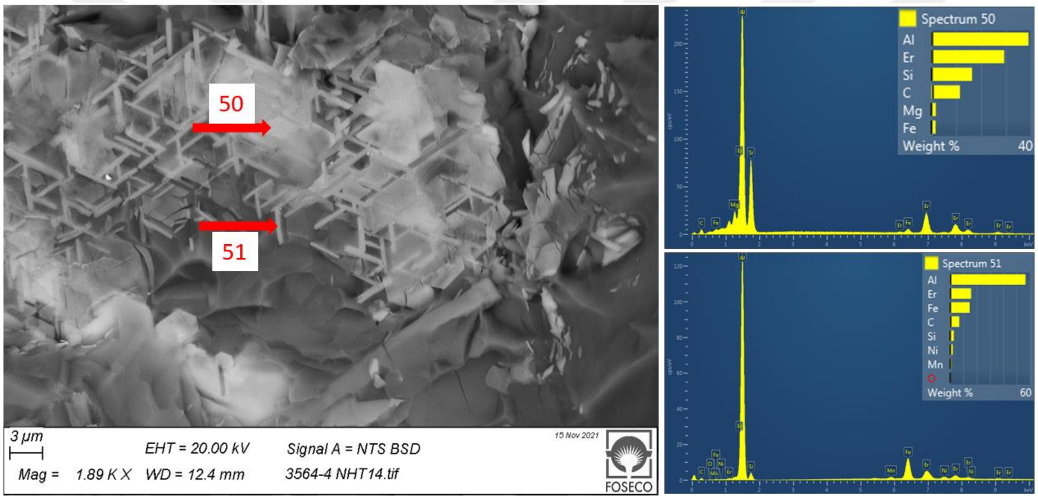

Figure 3.53 : SEM and EDS analysis of the as-cast condition tensile test sample fracture surfaces with 0.3 Er alloying addition.

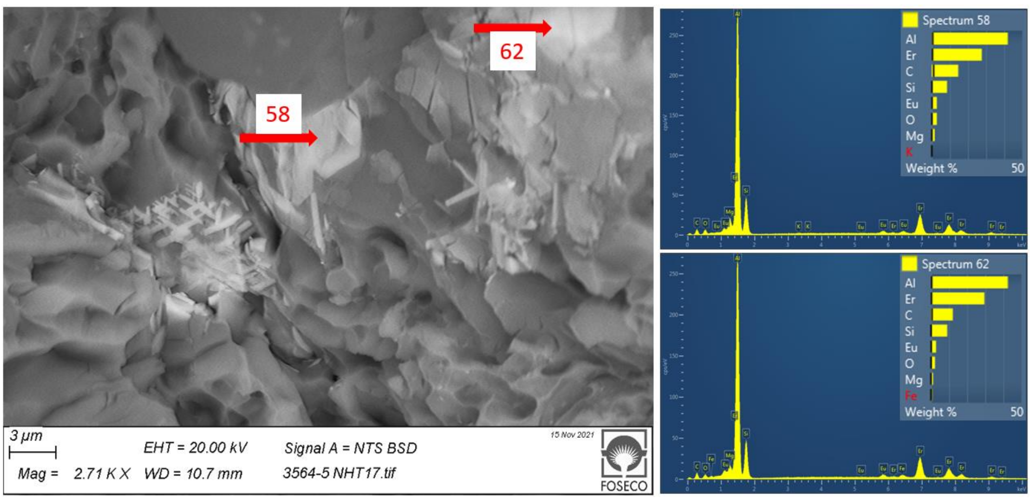

Figure 3.54 : SEM and EDS analysis of the as-cast condition tensile test sample fracture surfaces with 0.3 Er + 0.1 Eu alloying addition.

Intermetallic phases containing Er were observed on the fracture surface with the addition of 0.3 Er wt% (Figure 3.53).

The white intermetallic phases containing high Er and less Eu and without Fe were observed on the fracture surface with the addition of 0.3 Er + 0.1 Eu wt% (Figure 3.54).

3.2.8.2 T6 heat treated

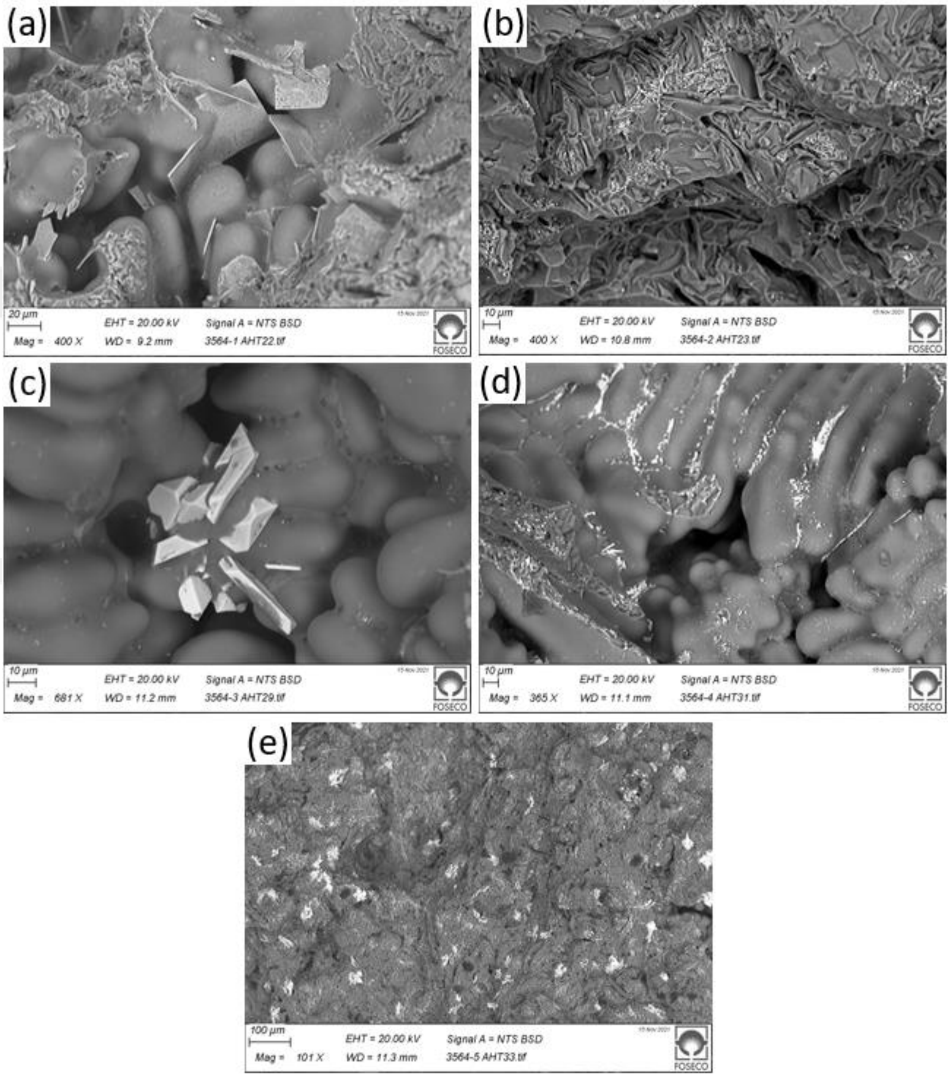

Figure 3.55 : SEM images of the t6 condition fracture surfaces with additions (a) 0.0, (b) 0.1 Er, (c) 0.1 Er + 0.1 Eu, (d) 0.3 Er, (e) 0.3 Er + 0.1 Eu.

Figure 3.55 showed the SEM overview images of the T6 heat treated condition tensile test sample fracture surface with different alloy addition rates.

Fe-containing intermetallic phases such as flake-like and intermetallic phases surrounding the Si surface were observed on the fracture surface of the t6 state heat treated A356 alloy without addition (Figure 3.56).

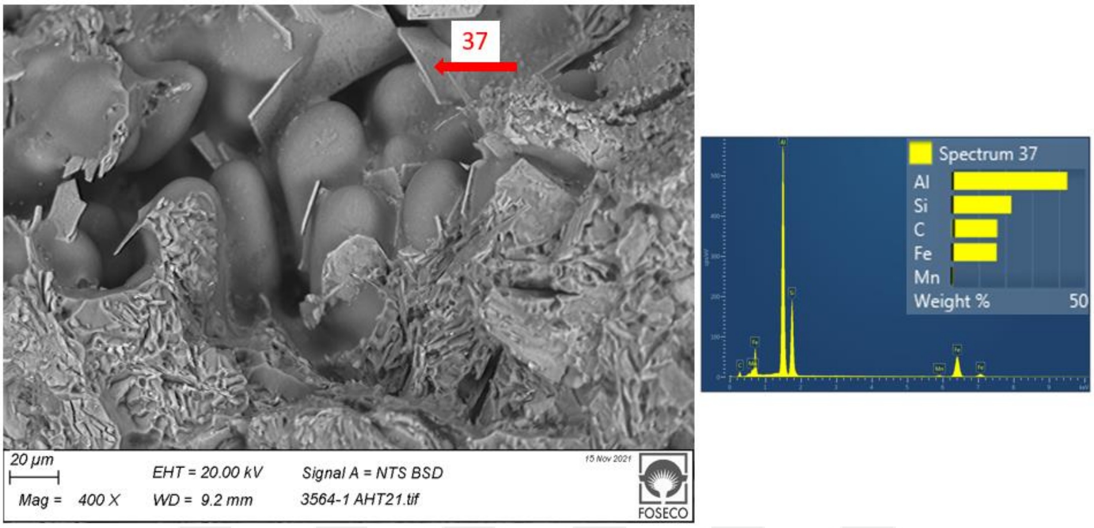

Figure 3.56 : SEM and EDS analysis of the heat treated condition tensile test sample fracture surfaces with 0.0 alloying addition.

Fine acicular structures containing Er and Fe were observed with the addition of 0.1 Er wt% (Figure 3.57).

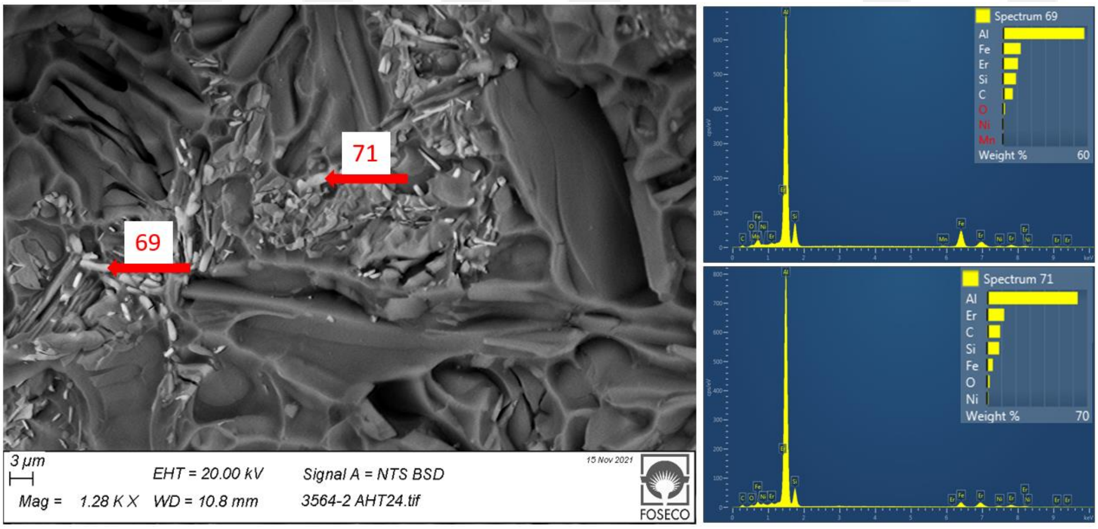

Figure 3.57 : SEM and EDS analysis of heat treated condition tensile test sample fracture surfaces with 0.1 Er alloying addition.

The white chunky intermetallic phases with high Eu and less Er and without Fe content were observed on the fracture surface with 0.1 Er + 0.1 Eu wt% addition (Figure 3.58).

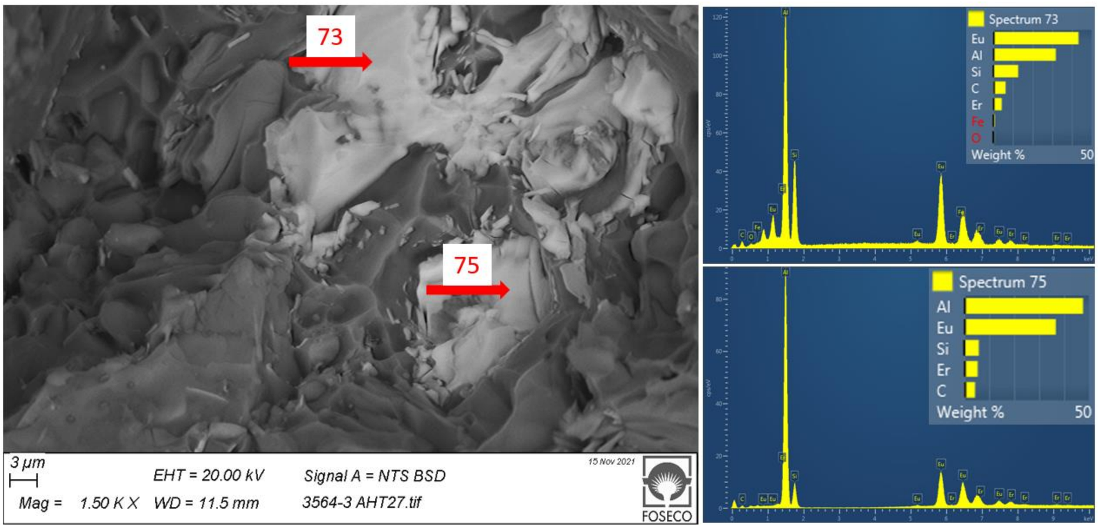

Figure 3.58 : SEM and EDS analysis of heat treated condition tensile test sample fracture surfaces with 0.1 Er + 0.1 Eu alloying addition.

The white continuous intermetallic phases containing high Er and negligible Fe and discontinuous intermetallic phases containing higher Er and Fe were observed with 0.3 wt% Er (Figure 3.59).

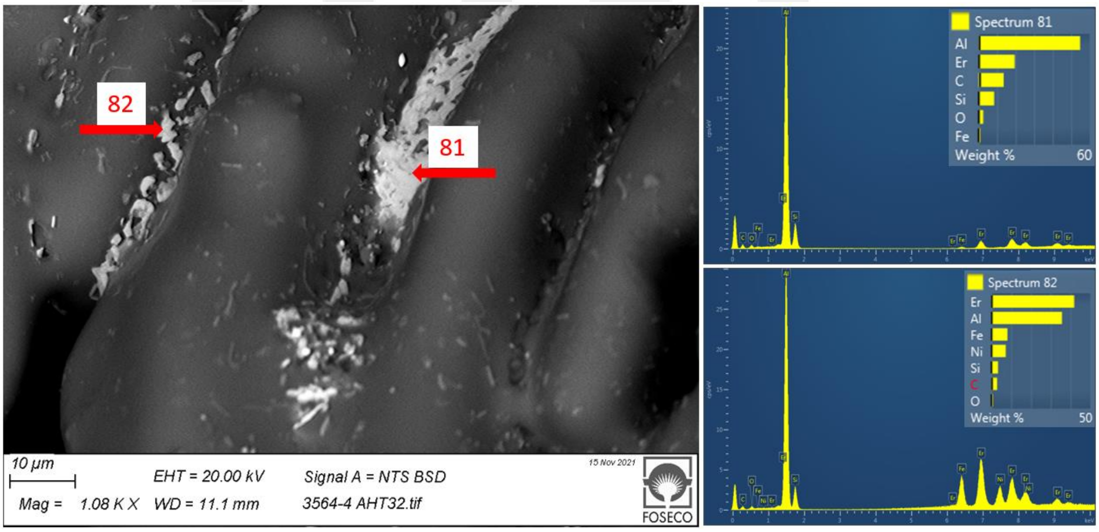

Figure 3.59 : SEM and EDS analysis of heat treated condition tensile test sample fracture surfaces with 0.3 Er alloying addition.

The white chunky intermetallic phases with high Eu and high Er and without Fe content were observed on the fracture surface with 0.3 Er + 0.1 Eu wt% addition. The amount of Er of intermetallic also increased with the increase of Er addition (Figure 3.60).

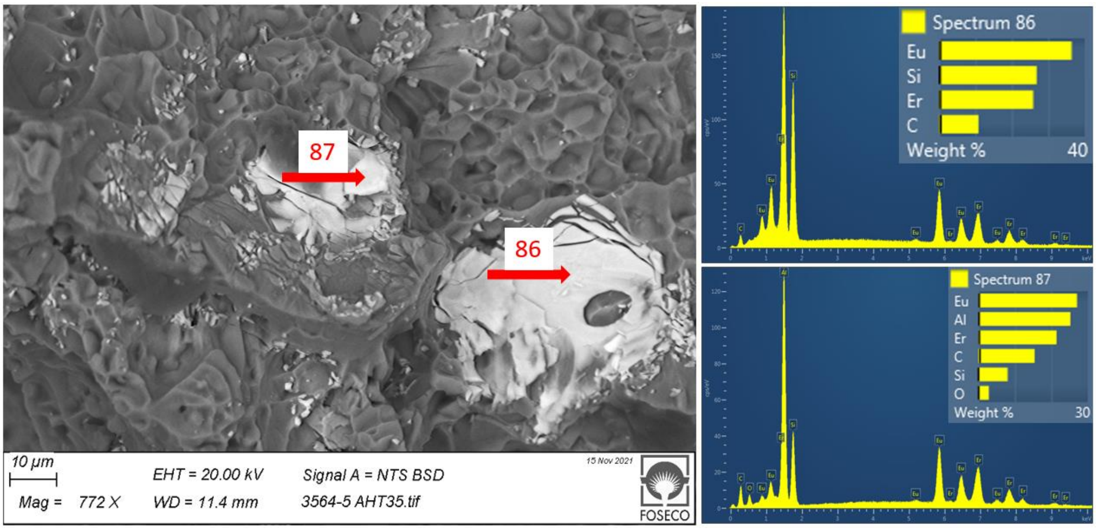

Figure 3.60 : SEM and EDS analysis of heat treated condition tensile test sample fracture surfaces with 0.3 Er + 0.1 Eu alloying addition.

In the studies in the literature, it has been observed that the intermetallic phases morphology and chemical composition changed with Er and Eu addition [22,24,28,30,33,35-37].

Qi, Peng, et al. investigated that n-Fe phase (AlSiFeMg) modified to fine and globular Er-poor n phase (AlSiFeMgEr) with Er addition [30]. In addition, Shi, Z. M., et al. studied that the bulk, needle-like and rods of Al_3Er phases were modified into fine particles and short rods and dispersed in the structure with T6 heat treatment. The harmful acicular β-Al5FeSi was eliminated by the T6 heat treatment and the addition of Er [33].

Addition of 0.0, 0.1, 0.3, 0.5 wt% Er to Al-2wt%Fe alloy was investigated by Liang, Y. H., et al. With the addition of Er, first Al_3Er particles then eutectic α-Al and Al_3Fe were nucleated in the molten aluminum (Figure 3.61). In this way, α-Al grain refinement and modification of Al_3Fe intermetallic phases were achieved. The smallest Al_3Fe intermetallic phases was observed at the addition of 0.3 Er wt%. $Al_{10}Fe_2Er$ intermetallic was found in the structure with the addition of Er [36].

The Al2Si2Eu intermetallic phases were observed in the matrix by adding Eu to the Al-Si alloy [22,24,35].

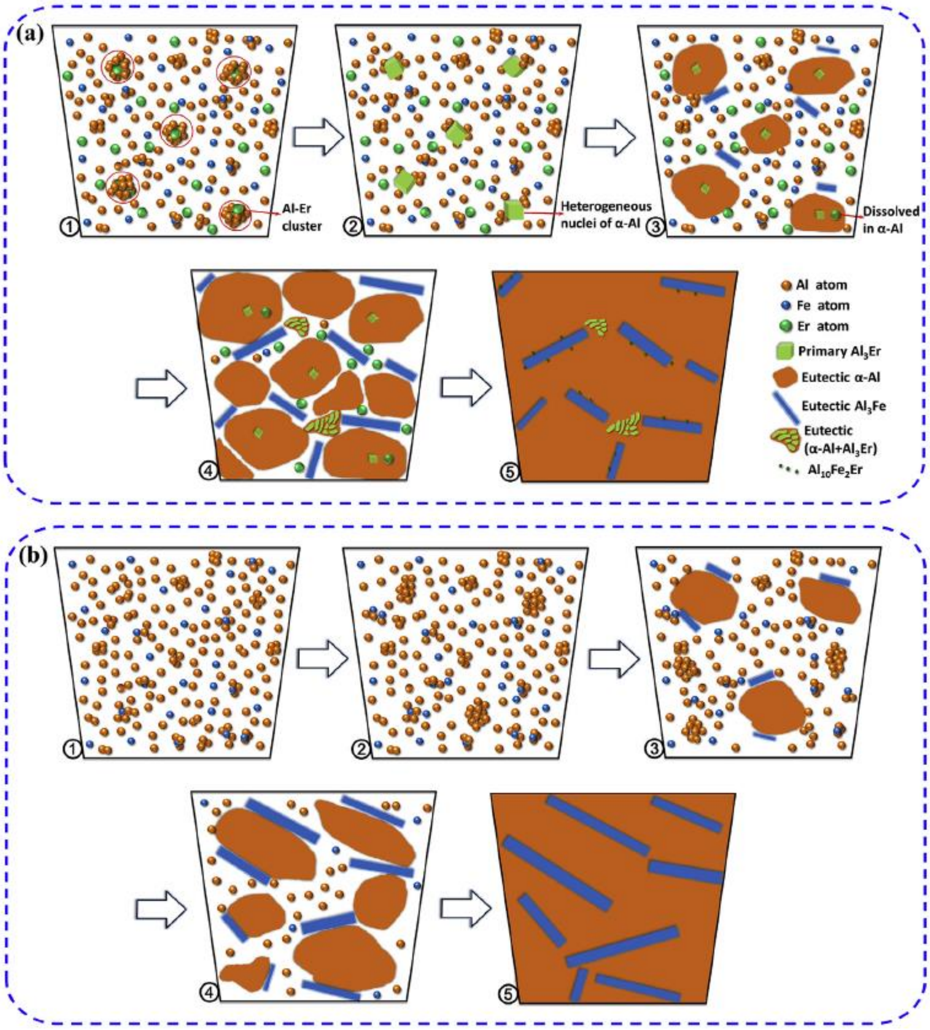

Figure 3.61 : Solidification and its mechanism (a) with Er addition and (b) unalloyed [36].

4. CONCLUSIONS AND RECOMMENDATIONS

It is possible to get stable and reliable castings with initial liquid metal cleaning with laminar flow and appropriate mold design. With the changes made in the mold design and changing the casting method, better results were obtained in each design in the quality index values. Among the mold design and casting methods, it has been shown in the survivability plots that tilt casting and V3 mold design give the most reproducible quality index results. In this way, a statistically sufficient amount of sample (10) was produced in a single casting to give a reliable mechanical property result, eliminating the extrinsic effects.

While the grain refinement effect was achieved with the addition of Er, it did not have much effect on the eutectic Si modification. In t6 heat treated samples, the grain size of the 0.0 addition wt% was 950 µm. The best grain refinement effect with 32% was gained at 0.3 wt% Er addition (643 µm). On the other hand, grain coarsening occurred with the addition of Eu, but its effect on the eutectic Si modification was clearly observed. The eutectic Si length was 12.0 µm and the Si aspect ratio was 9.6 in the unheat-treated 0.0-alloyed addition. With the addition of 0.1 Er + 0.1 Eu wt%, the Si length with the shortest average length was obtained 2.4 µm. Si length was reduced by 80%. With the effect of heat treatment, acicular long eutectic Si phases have been modified and started to form spherical. Moreover, it has reached the most spherical form with the addition of Eu. The eutectic Si length was 5.8 µm and aspect ratio was 1.9 at T6 state. With the addition of 0.1 Er + 0.1 Eu wt%, the Si length with the shortest average length was obtained 2.8 µm. Si length was reduced by 51.7% with this addition. The addition of 0.1 Er + 0.1 Eu wt% again had the best Si aspect ratio. It was 1.2 µm and decreased by 80%.

As a reflection of these changes in the microstructure, the mechanical properties improved with the addition of heat treatment and alloying elements. In as-cast condition UTS was 138MPa and %e was 1.1%. The best UTS was 177 MPa with 0.1 Er addition. The best %e value was 3.7% with 0.3 Er + 0.1 Eu addition. The UTS was 228 MPa and %e was 0.8 with unalloyed t6 heat treatment. The highest UTS was achieved with the addition of 0.1 Er wt%(302 MPa) and the highest %e value was

2.4% and it was obtained with the addition of 0.3 Er + 0.1 Eu wt%. However, the hardness value decreased with the addition of alloying elements in the heat treated samples. The best hardness value, which was 11.5 HRB10 before heat treatment, became 58.5 HRB10 with heat treatment.

In microstructure and fracture surface SEM analysis results, the number and size of intermetallics increased with the addition of alloying element. Although these acicular intermetallic phases are reduced in size by heat treatment, they were not spherical.

REFERENCES

[1] **Campbell, J.** (2015). Complete casting handbook: metal casting processes, metallurgy, techniques and design. Butterworth-Heinemann.

[2] **Polmear, I., StJohn, D., Nie, J. F., & Qian, M.** (2017). Light alloys: metallurgy of the light metals. Butterworth-Heinemann.

[3] **Rowe, J. (Ed.).** (2012). Advanced materials in automotive engineering. Elsevier.

[4] **Vargel, C.** (2020). Corrosion of aluminium. Elsevier.

[5] **Url-1** <http://www.talsad.org.tr/>, date retrieved 12.05.2022.

[6] **Menzie, W. D., Barry, J. J., Bleiwas, D. I., Bray, E. L., Goonan, T. G., & Matos, G.** (2010). The global flow of aluminum from 2006 through 2025. Reston: US Department of the Interior, US Geological Survey.

[7] **Prasad, N. E., & Wanhill, R. J. (Eds.).** (2017). Aerospace materials and material technologies (Vol. 3). Singapore: Springer.

[8] **Assoc. Prof. Dr. Dispinar, D.** Personal discussions.

[9] **Dispinar, D., & Campbell, J.** (2004). Critical assessment of reduced pressure test. Part 1: Porosity phenomena. International Journal of Cast Metals Research, 17(5), 280-286.

[10] **Guan, R. G., & Tie, D.** (2017). A review on grain refinement of aluminum alloys: progresses, challenges and prospects. Acta Metallurgica Sinica (English Letters), 30(5), 409-432.

[11] **Fan, Z., Wang, Y., Zhang, Y., Qin, T., Zhou, X. R., Thompson, G. E., ... & Hashimoto, T.** (2015). Grain refining mechanism in the Al/Al–Ti–B system. Acta Materialia, 84, 292-304.

[12] **Mohanty, P. S., & Gruzleski, J. E.** (1995). Mechanism of grain refinement in aluminium. Acta Metallurgica et Materialia, 43(5), 2001-2012.

[13] **Zhou, L., Gao, F., Peng, G. S., & Alba-Baena, N.** (2016). Effect of potent TiB2 addition levels and impurities on the grain refinement of Al. Journal of Alloys and Compounds, 689, 401-407.

[14] **Guzowski, M. M., Sigworth, G. K., & Sentner, D. A.** (1987). The role of boron in the grain. Metallurgical and Materials Transactions A, 18(4), 603-619.

[15] **Murty, B. S., Kori, S. A., & Chakraborty, M.** (2002). Grain refinement of aluminium and its alloys by heterogeneous nucleation and alloying. International Materials Reviews, 47(1), 3-29.

[16] **Seminar on Refining and Alloying of Liquid Aluminium and Ferro-Alloys Engh T. A. Lyng S. Øye H. A. & Norges tekniske høgskole.** (1985). Refining and alloying of liquid aluminium and ferro-alloys : proceedings of the international seminar on refining and alloying of liquid aluminium

and ferro-alloys the norwegian institute of technology trondheim august 1985. Aluminium-Verlag.

[17] **Wearing, D., Horsfield, A. P., Xu, W., & Lee, P. D.** (2016). Which wets TiB2 inoculant particles: Al or Al3Ti?. Journal of Alloys and Compounds, 664, 460-468.

[18] **Schumacher, P., Greer, A. L., Worth, J., Evans, P. V., Kearns, M. A., Fisher, P., & Green, A. H.** (1998). New studies of nucleation mechanisms in aluminium alloys: implications for grain refinement practice. Materials science and technology, 14(5), 394-404.

[19] **Wang, F., Liu, Z., Qiu, D., Taylor, J. A., Easton, M. A., & Zhang, M. X.** (2013). Revisiting the role of peritectics in grain refinement of Al alloys. Acta materialia, 61(1), 360-370.

[20] **Zhang, H. R., Liu, Z. B., Li, Z. Z., Li, G. W., & Zhang, H.** (2016). Cooling Rate Sensitivity of RE-Containing Grain Refiner and Its Impact on the Microstructure and Mechanical Properties of A356 Alloy. Acta Metallurgica Sinica (English Letters), 29(5), 414-421.

[21] **Li, J., Hage, F., Wiessner, M., Romaner, L., Scheiber, D., Sartory, B., ... & Schumacher, P.** (2015). The roles of Eu during the growth of eutectic Si in Al-Si alloys. Scientific reports, 5(1), 1-10.

[22] **Mao, F., Qiao, Y., Zhang, P., Ou, L., Chen, C., Zhang, C., & Wang, Y.** (2022). Modification Mechanism of Rare Earth Eu on Eutectic Si in Hypoeutectic Al-Si Alloy. International Journal of Metalcasting, 16(2), 634-645.

[23] **Mazahery, A., & Shabani, M. O.** (2014). Modification mechanism and microstructural characteristics of eutectic Si in casting Al-Si alloys: A review on experimental and numerical studies. Jom, 66(5), 726-738.

[24] **Li, J. H., Wang, X. D., Ludwig, T. H., Tsunekawa, Y., Arnberg, L., Jiang, J. Z., & Schumacher, P.** (2015). Modification of eutectic Si in Al–Si alloys with Eu addition. Acta Materialia, 84, 153-163.

[25] **Astm, I.** (2009). ASTM B108/B 108M : Standard Specification for Aluminum-Alloy Permanent Mold Castings. West Conshohocken, PA, USA: ASTM International.

[26] **Astm, I.** (2016). ASTM E8/E8M-16a: Standard Test Methods for Tension Testing of Metallic Materials. West Conshohocken, PA, USA: ASTM International.

[27] **Colombo, M., Gariboldi, E., & Morri, A.** (2017). Er addition to Al-Si-Mg-based casting alloy: Effects on microstructure, room and high temperature mechanical properties. Journal of Alloys and Compounds, 708, 1234-1244.

[28] **Li, J. H., Ludwig, T. H., Oberdorfer, B., & Schumacher, P.** (2018). Solidification behaviour of Al–Si based alloys with controlled additions of Eu and P. International Journal of Cast Metals Research, 31(6), 319-331.

[29] **Niazi, R., Tohidlou, E., & Khosravi, H.** (2020). Microstructure-property relationships in an erbium-modified Al-Si-Mg alloy. Iranian Journal of Materials Science and Engineering, 17(3), 40-48.

[30] **Qi, P., Li, B., Wang, T., Zhou, L., & Nie, Z.** (2019). Effect of Erbium on the Microstructure and Mechanical Properties of Semi-Solid Al–7Si–0.4 Mg Alloy. Advanced Engineering Materials, 21(3), 1801037.

[31] **Ji, L., Wang, W., Huang, H., Wen, S., Gao, K., & Wu, X.** (2017, July). Effect of Erbium–Zirconium Composite Modifications on the Microstructure and Mechanical Properties of A356 Aluminum Alloy. In Chinese Materials Conference (pp. 87-94). Springer, Singapore.

[32] **Pandee, P., Patakham, U., & Limmaneevichitr, C.** (2017). Microstructural evolution and mechanical properties of Al-7Si-0.3 Mg alloys with erbium additions. Journal of Alloys and Compounds, 728, 844-853.

[33] **Shi, Z. M., Wang, Q., Zhao, G., & Zhang, R. Y.** (2015). Effects of erbium modification on the microstructure and mechanical properties of A356 aluminum alloys. Materials Science and Engineering: A, 626, 102-107.

[34] **Mazahery, A., Habibnejad-korayem, M., & Takrouri, K.** (2019). Performance of europium in microstructural modification of high strength lightweight aluminum components. International Journal of Lightweight Materials and Manufacture, 2(3), 250-254.

[35] **Mao, F., Yan, G., Xuan, Z., Cao, Z., & Wang, T.** (2015). Effect of Eu addition on the microstructures and mechanical properties of A356 aluminum alloys. Journal of Alloys and Compounds, 650, 896-906.

[36] **Liang, Y. H., Shi, Z. M., Li, G. W., Zhang, R. Y., & Zhao, G.** (2019). Effects of Er addition on the crystallization characteristic and microstructure of Al-2wt% Fe cast alloy. Journal of Alloys and Compounds, 781, 235-244.

[37] **Mao, F., Wei, S., Ou, L., Zhang, C., Chen, C., Wang, X., & Cao, Z.** (2019). Different influences of rare earth Eu addition on primary Si refinement in hypereutectic Al–Si alloys with varied purity. Materials, 12(21), 3505.

CURRICULUM VITAE

Name Surname : **Hayati ŞAHİN**

EDUCATION :

- **B.Sc.** : 2016, Istanbul University, Enginerring Faculty, Metallurgical and Materials Engineering

PROFESSIONAL EXPERIENCE AND REWARDS:

Nov 2022 – Present	**Project Manager**, R&D Center Foseco, Enschede, Netherlands
July 2022 – Present	**R&D Scientist**, R&D Center Foseco, Enschede, Netherlands
Feb 2019 – Nov 2021	**Researcher**, Critical and Functional Material Technologies Application and Research Center at Istanbul Technical University, İstanbul, Turkey
2019 – 2021	**Researcher**, Research and development of next-generation aluminum alloys for aviation applications. Gravity and Low Pressure Sand Casting, İstanbul, Turkey
2018 – 2021	**Researcher**, Production of hypoeutectic Al-Si alloys for cylinders. Die casting, İstanbul, Turkey
2018 – 2021	**Researcher**, Alternative Filling Technique Design and Application for Alloy Wheels, Low Pressure Die casting, İstanbul, Turkey
2018 - 2021	**Researcher** ,Improvement of Metal Quality and Increase the Usage of Recycled Aluminum Alloys Low Pressure Die casting

PUBLICATIONS, PRESENTATIONS AND PATENTS ON THE THESIS:

- **H. Sahin,** D. Dispinar, 2022. Effect of Erbium and Europium Addition in Microstructure and Mechanical Properties of A356 and A201 Alloy, *The 74th World Foundry Congress*, October 16-20, 2022, Busan, Korea.
- **H. Sahin,** D. Dispinar, 2021. Effect of erbium addition on microstructure and mechanical properties of A356, *International Hight Tech Die Casting (HTDC) Conference 2021*, 22-25 June 2021, Online, Italy.

OTHER PUBLICATIONS, PRESENTATIONS AND PATENTS:

- Aydogan, F., Dizdar, K. C., **Sahin, H.,** Mentese, E., & Dispinar, D. Mechanical Property Comparison of Al11Si Wheels Grain Refined by Ti, Nb and MTS. *Archives of Foundry Engineering*.
- Tigli, A., **Sahin, H.,** Dizdar, K. C., & Dispinar, D. 2022. Determination of effect of hydrogen on strength of aluminum by MD simulation. *Applied Physics A*, 128(9), 1-12.
- Dizdar, K. C., **Sahin, H.,** Tezer, F., & Dispinar, D. 2022. Characterization of Casting Properties of Rare-Earth Modified A356. Aluminium Alloys: Design and Development of Innovative Alloys, *Manufacturing Processes and Applications*, 71.
- Aydogan, F., Dizdar, K. C., **Sahin, H.,** Mentese, E., & Dispinar, D. 2022. Weibull analysis evaluation of Ti, B, Nb and MTS grain refined Al11Si alloy. *Materials Chemistry and Physics*, 126264.
- Ernam, O., Sekban, T., Tugan, O., Dizdar, K., **Sahin, H.,** & Dispinar, D. 2022. Effect of Heat Treatment on Mechanical Properties of Er-, Dy-, and Eu-Modified A356 Alloy. *In Light Metals 2022* (pp. 785-789). Springer, Cham.
- Dizdar, K. C., **Sahin, H.,** Ardicli, M., & Dispinar, D. 2022. Flaw Detection of Cast-Steel Safety Parts in Automotive Application. *Archives of Foundry Engineering*, 22(1), 13.
- Nemutlu, B., Kahraman, O., Demirel, K. B., Erkul, I., Cicek, M., **Sahin, H.,** ... & Dispinar, D. 2022. Processing of Boron Nitride Nanotubes Reinforced Aluminum Matrix Composite. *Archives of Foundry Engineering*, 22.
- **Sahin, H.,** Atik, M., Tezer, F., Temel, S., Aydin, O., Kesen, O., ... & Dispinar, D. 2021. Prediction of Fracture Stress with Regard to Porosity in Cast A356 Alloy. *Archives of Foundry Engineering*, (3).
- Aydogan, F., Dizdar, K. C., **Sahin, H.,** Mentese, E., & Dispinar, D, 2022. Statistical Analysis of Mechanical Property Comparison of Ti, B, Nb and MTS Grain Refined Al11Si Alloy, *The 74th World Foundry Congress*, October 16-20, 2022, Busan, Korea.
- Aydogan, F., Dizdar, K. C., **Sahin, H.,** Mentese, E., & Dispinar, D, 2022. Mechanical Property Comparison of Ti, Nb, and MTS Grain Refined Al11Si Alloy Wheels, *The 74th World Foundry Congress*, October 16-20, 2022, Busan, Korea.
- Aydogan, F., Dizdar, K. C., **Sahin, H.,** Mentese, E., & Dispinar, D. 2022. Mechanical Property Comparison of Al11Si Wheels Grain Refined By Ti, Nb and MTS. *11th International Foundry Congress by Tudoksad Academy*, 6-8 October, 2022, İstanbul – Turkey.
- O. Ernam, T. Sekban, O. Tugan, K.C. Dizdar, **H. Sahin,** D. Dispinar, 2022. Effect of heat treatment on mechanical properties of Er, Dy and Eu modified A356 Alloy, 2022 TMS Annual Meeting & Exhibition, Light Metals 2022: Cast Shop Technology, 27 February – 3 March 2022, California, USA.
- Ö. Kesen, O. Aydin, S. Temel, F. Tezer, **H. Sahin,** M. Atik, D. Dispinar, 2021. Th eeffect of bifilm size, location and orientation on thetensile propertiesof A356

alloys , *International Hight Tech Die Casting (HTDC) Conference 2021*, 22-25 June 2021, Online, Italy.

- Kesen, Ö. Aydin, O., Atik, M. Tezer, F., Temel, S. **Şahin, H.,** Dizdar, K.C., Dispinar, D., 2020. Optimization of tensile test mold design for reliable mechanical properties characterization in Al cast alloys, *60th International Scientific Conference Solidification and Crystallization of Metals 2020*, 28-20 September 2020, Krakow, Poland.
- Kesen, Ö. Aydin, O., Atik, M. Tezer, F., Temel, S. **Şahin, H.,** Dizdar, K.C., Dispinar, D., 2020. Grain refinement and mechanical properties of Sc, V, Er, Y modified A356", 60th International Scientific *Conference Solidification and Crystallization of Metals 2020, 28-20 September 2020*, Krakow, Poland.
- Kesen, Ö., Aydin, O., Atik M., Temel S., Tezer F., **Sahin H.,** D. Dispinar, 2019. Prediction of fracture stress with regard to porosity in A356 cast alloy, *II International Conference of Casting and Materials Engineering ICCME*, 8th November 2019, Krakow, Poland
- **Sahin H.,** Gursoy Ö., Emik S., Dispinar D. 2019. Boşluk Yapıcılar Kullanılarak A356 Alüminyum Köpük Üretimi, *9th Inernational Aluminium Symposium*, 10 – 11 October 2019, Istanbul, Turkey
- **Sahin H.,** Gursoy Ö., Emik S., Dispinar D. 2019. Döküm Yöntemiyle Boşluk Yapıcılar Kullanılarak A356 Köpük Üretimi, *2nd National Foundry Congress by Tudoksad Academy*, 30 November - 1 December 2019, Izmir, Turkey